Modelling of hydraulic fracturing in unconventional reservoirs

Submitted by Davood Mahdavian to the University of Exeter as a thesis for the Degree of Doctor of Philosophy in Engineering in November 2019

I certify that all material in this thesis which is not my own work has been identified and that no material has previously been submitted and approved for the award of a degree by this or any other University.

Signature: ……..

TO MY MOTHER AND MY FATHER

ACKNOWLEDGEMENTS

I would like to express my sincere appreciation to my supervisor Professor Akbar Javadi for his continued encouragements and guidance during this research. This work has been completed from the continual supervision, insight, constructive comments provided by Professor Javadi. Without his leadership, support, time and energy I would not be able to accomplish this research.

Finally, I would like to thank my family and my friends for their support during the entire period of this study.

ABSTRACT

Hydraulic fracturing (HF) is a process of fluid injection into the well in order to create tensile stresses in the rock to overcome the tensile strength of the formation. In this study, the development and application of a fuzzy model to predict the efficiency of hydraulic fracturing is presented with application in a coal mine as an unconventional reservoir. The most important parameters affecting the HF process of a coal seam are: dip, thickness, seam uniformity, roof and floor conditions, reserve of coal seam and coal strength. In the developed model, the efficiency of hydraulic fracturing of coal seams is calculated as a dimensionless numerical index within the range 0-100. The suggested numerical scale categorizes the efficiency of HF of seams to very low, low, medium, high and very high, each one being specified by a numerical range as a subset of the above range (0-100). HF in the coal bed in PARVADEH 4 Tabas mine in Iran is investigated as a case study. The results show that the developed model can be used to identify seams that have high potential for HF

Moreover, a three-phase hydro-mechanical model is developed for simulating hydraulic fracturing. The three phases include: porous solid, fracturing fluid and reservoir fluid. Two numerical simulators (ANSYS Fluent for fluid flow and ANSYS Mechanical for geomechanical analysis) are coupled together to model multiphase fluid flow in hydraulically fractured rock undergoing deformations, ranging from linear elastic to large, nonlinear inelastic deformations. The two solvers are coupled, using system coupling in ANSYS Workbench. The coupled problem of fluid flow and fracture propagation is solved numerically. The fluid flow model involves solving the Navier-Stokes equations using the finite volume method. The flow model is coupled

with the geomechanics model to simulate the interaction between fluid flow inside the fracture with rock deformations. For any time step, the pore pressures from the flow model are used as input for the geomechanics model for the determination of stresses, strains, and displacements. The strains derived from the gomechanics model are in turn used to calculate changes to the reservoir parameters that are fed as input to the flow model. This iterative process continues until both (fluid and solid) models are converged. The laboratory-scale study of hydraulic fracturing in the Second White Specks (SWS) shale was simulated using the developed model. The numerical and experimental results were compared. Comprison of the results shows that the numerical model can predict the behaviour of the shale under hydraulic fracturing with a good accuracy.

List of publication from this research:

Journal papaers:

- **Mahdavian, D.,** Javadi, A.A. Numerical analysis of fluid-rock interactions in hydraulic fracturing, Engineering and Computational Mechanics (ICE) Journal, December 2018.

- **Mahdavian, D.,** Javadi, A.A. Study of hydraulic fracturing for gas drainage in a coalmine in Iran, Environmental Geotechnics (ICE) Journal, April 2019.

Conference papaers:

- **Mahdavian, D.,** Javadi, A.A. Numerical investigation of hydraulic fracturing, Proceedings of the 24th UK Conference of the Association for Computational Mechanics in Engineering (ACME2016), Cardiff University, 31 March-1 April 2016.

- **Mahdavian, D.,** Javadi, A.A. Numerical analysis of flow parameters in hydraulic fracturing, Proceedings of the 25th UKACM Conference on Computational Mechanics, University of Birmingham, 11-13 April 2017.

List of Contents

List of Tables

List of Figures

List of symbols

I_m	a parameter, to quantify geological disturbances
m	displacement of a seam
t	thickness of the seam
Q_r	roof strength index
σ_c	average uniaxial compressive strength of the core
K_1	a factor to account for decrease in strength
K_2	a factor to account for decrease in strength with creep loading
K_3	a factor to account for decrease in strength with an increase in humidity
m	thickness of the immediate roof
K	swelling coefficient
$L(t)$	fracture length changes with time
A	a fuzzy set
X	universe od discourse
x	an element of set
$fA(x)$	characteristic function of A
$\mu A(x)$	membership function of set A
$\mu B(x)$	membership function for set B
$\mu\overline{\mathrm{A}}(x)$	membership function for complement (NOT) operation
$\tilde{A}$	a fuzzy set
$\tilde{B}$	a fuzzy set
$\tilde{C}$	a fuzzy set
$\mu_{\tilde{C}}\ (c)$	membership function of set $\tilde{C}$
SUP	upper limit of $\mu_{\tilde{C}}(c)$

a	Crack length
$\mathbf{B}$	matrix, which transfers the net pressures into equivalent nodal forces
$\mathbf{H}$	to conclude the contributions of fluid leak-off and fluid injection
h_f	fracture height
$\acute{E}$	plane train modulus of elasticity
$\mathbf{F}$	equivalent global nodal force of net pressure
K	stress intensity factor
$\mathbf{K}_{\mathrm{u}}$	global stiffness of solid elements
$\mathbf{K}_{\mathrm{w}}$	global flux stiffness of fluid elements
$\mathbf{L}$	global length stiffness of fluid elements
$L(t)$	fracture length changes with time
$\acute{\mathbf{L}}$	to determine the contribution of node displacements on fracture surface to fracture width
n	power law model parameter
$\mathbf{P}, \mathbf{P}_{\mathrm{n+1}}$	node net pressure and node net pressure at the n + 1-th step
Δp_{net}	pressure drop
q_0	injection rate per 1−v unit height of the fracture
q_i	injection rate
S	collection of boundary conditions of flow
t	time
$\mathbf{U}_{\mathrm{i}}^{\mathrm{f}}(\mathrm{i} = \mathrm{n}, \mathrm{n}+1)$	node displacement with contribution to fracture width at the i-th step
$\mathbf{U}$	global nodal displacement
u	component of velocity in x axis
v	component of velocity in y axis

v_x	average fluid velocity
w	fracture width
$\mathbf{W}$	a vector formed by the widths on of the nodes on fracture surface
$\mathbf{W}_{\mathrm{i}}(\mathrm{i}=\mathrm{n},\mathrm{n}+1)$	fracture width at the i-th step
$\mathrm{W}_{\mathrm{well}}(t)$	width of fracture
$\overline{w}$	height-averaged fracture width
w	component of velocity in z axis
$\Delta\mathrm{x}$	length
δ_{p}	allowable testing function
σ	stress
ν	Poisson's ratio
μ	fluid viscosity

Chapter 1. Introduction

1.1 HYDRAULIC FRACTURING

The technology of hydraulic fracturing has been widely used for reservoir stimulation, especially for unconventional reservoirs (Economides and Nolte, 2000). The difference between a conventional and unconventional reservoir is migration. The unconventional reservoir has hydrocarbons that were formed within the rock and never migrated. The conventional reservoir is a porous rock formation that contains hydrocarbons that have migrated from a source rock (Beaumont and Foster, 1988). In general, the process of hydraulic fracturing can be defined as initiation and propagation of fractures due to the pressurization of fluid flow within existing fractures. Optimal design of hydraulic fracturing is a fundamental problem in Civil, Mining and Petroleum Engineering and plays a critical role in many applications within the industry. Hydraulic fracturing is a coupled process and it means a change in fluid pressure or fluid mass produce a change in the volume of the porous medium and vice versa. Hydraulic fracturing involves the interaction between four different phenomena:

(1) Porous medium deformation;

(2) Pore fluid flow;

(3) Fracturing fluid flow; and

(4) Fracture propagation (Economides and Nolte, 2000).

Coupled rock deformation and fluid flow in fractured porous media is important for reservoir simulation because rock deformation exerts an important influence on reservoir production (Economides and Nolte, 2000).

The equations and constitutive relations governing these coupled processes are the continuity equation and the Navier-Stokes equation for porous medium, Darcy's law for fracturing fluid flow and the theory of linear elasticity for rock deformation. The focus of this study is the effect of fluid flow and formation properties on hydraulic fracturing process (Economides and Nolte, 2000).

The interaction between fluid and solid processes, commonly known as coupling, arises in geological media due to the presence of deformable, fluid-filled pores and discontinuities. Depending on the type of processes involved, the hydromechanical (HM) response of a rock mass can be fully reversible if associated with elastic deformations only, or irreversible if associated with processes such as yielding, fracturing, and frictional slipping along discontinuities. Advances in theoretical and numerical modelling in coupled HM processes have been driven by several geomechanical applications, including (Yun and Hui, 2011):

- Rock engineering: e.g., landslides and slope instabilities, dam foundation failures, and stability of underground and surface excavations;
- Nuclear waste management: e.g., design and performance assessment of underground nuclear waste repositories;
- Oil and gas exploration and production: e.g., borehole stability, reservoir compaction and subsidence, and hydraulic fracturing and stimulation;
- Geothermal energy extraction: e.g., enhanced geothermal systems;
- Mining: e.g., coal mining and coal methane extraction; and

- Storage of fluid underground: e.g., carbon sequestration, geological storage of natural gas, and liquid waste disposal (Mahabadi, 2012).

The interaction between fluid and structure occurs in a system where flow of a fluid causes a solid structure to deform which, in turn, changes the boundary condition of the fluid system. This can also happen the other way around where the structure makes changes in the fluid flow properties. This kind of interaction occurs in many natural phenomena and man-made engineering systems, hence it becomes a crucial consideration in the design and analysis of different engineering systems (Yun and Hui, 2011).

Hydraulic fracturing is the process of creating a fracture in a formation by means of internal fluid pressure. The fracturing process may happen naturally in the earth's crust, such as with joints, dikes and veins (Pollard, 1987; Pollard and Aydin, 1988; Lacazette and Engelder, 1992) or it can be man-made by pumping a hydraulic fracturing fluid with a high rate and pressure in a borehole. Hydraulic fracturing creates and grows fractures and the stimulation effect is to increase the surface area of the wellbore and to change flow geometry around the well, as a result of which productivity of the well increases. The first hydraulic fracturing job was done during the 1930's when wellbore acidizing was done with the help of pressurized fluid and as a result the well production was enhanced (Gidley et al. 1989).

Hydraulic fracturing is a common technique not just for enhancing hydrocarbon production but also for geothermal energy extraction (Sasaki, 1998; Berumen et

al., 2000). It is widely used for other purposes like hazardous solid waste disposal (Hunt et al., 1994; Hainey et al. 1999), measurement of in-situ stresses (Hayashi et al., 1997; Raaen et al., 2001), fault reactivation in mining (Board et al. 1992) and remediation of soil and ground water aquifers (Murdoch and Slack 2002).

At the present time, hydraulic fracturing is extensively used to improve the productivity of oil and gas wells. Of the production wells drilled in North America since the 1950s, about 70% of gas wells and 50% of oil wells have been hydraulically fractured (Valko and Economides, 1995).

Most models developed for hydraulic fracturing in unconsolidated sands are based on linear elastic fracture mechanics (LEFM), tensile fracture (Mode I fracture), lubrication theory for fluid flow through fracture, and Carter's leakoff model for flow through porous medium (Adachi et al. 2007; Daneshy, 1973; Perkins and Kern, 1961; Geertsma and de Klerk, 1969).

The geometry of the induced fracture is dominated by the rock's mechanical properties, in-situ stresses, the rheological properties of the fracturing fluid and local heterogeneities such as natural fractures and weak bedding planes. In the case of an isotropic and homogeneous medium, the in-situ stress state is the controlling factor on fracture development (Weijers, 1995).

This study presents the development and application of a fuzzy model to predict the efficiency of hydraulic fracturing of a coal seam and a finite element model for production of the behaviour of a shale reservoir. A coal seam is a dark brown or black banded deposit of coal that is visible within layers of rock. These seams are

located underground and can be mined using either deep mining or strip mining techniques depending on their proximity to the surface. These seams undergo normal coal formation and serve as a conventional coal resource and unconventional gas (methane) resource. The reserves of coal are immense, and are the largest of all of the fossil fuels (Boyle et al., 2015). The aim of this study is to investigate various factors affecting hydraulic fracturing, pre-production and post-fracture production in unconventional reservoirs. The main aim of this dissertation is to investigate the pre-production and post-fracture steps of hydraulic fracturing to help improve the production of gas from unconventional reservoirs. A number of numerical poroelastic models have been developed based on two-way coupling of the governing equations of fluid flow and geomechanics (Fung et al., 1992; Koutsabeloulis and Hope, 1998; Settari and Walters, 1999; Tortike and Farouq Ali, 1993) using the finite element method (Chin et al., 2000; Koutsabeloulis and Hope, 1998; Lewis and Schrefler, 1998). A numerical method is developed to simulate the hydro-mechanical evolution of the fracture and the surrounding rock in the finite element analysis framework. The propagation and the exchanges of fluid with the low permeability porous medium are considered. The ability of cohesive elements to model fluid-driven crack propagation in the viscosity-dominated regime is investigated. Hydraulic fractures for reservoir stimulation typically propagate in the viscosity-dominated regime. In this study, we focus on the governing equations of the coupled problem: lubrication equation, pressure continuity and cohesive zone model.

This project also presents the development and application of a fuzzy model to

predict the efficiency of hydraulic fracturing of a coal seam, considering a number of key factors which have been ignored by other researchers. The most important parameters affecting the HF process of a coal seam are: dip, thickness, seam uniformity, roof and floor conditions, coal seam reserve and coal strength (Couch, 2009). The hydraulic fracturing has been investigated numerically through a FEM-based model in different Stree Intensity Factor (SIF), J-integral, elastic modulus, Poisson's ratio, fluid pressure and fluid viscosity. The two models developed in this research can be used to improve the efficiency and production rate of hydraulic fracturing. The outcome of this research can be useful in describing various aspects of behaviour of hydraulic fracturing in unconventional reservoirs.

1.2 Hydraulic Fracturing in Coal Mining

The most important objectives of HF in a coal mine are to achieve: reduced costs; faster development; faster mining; safer mining; concentrating production at fewer locations; achieving higher production rates per shift (each of two or more recurring periods in which different groups of workers do the same jobs in relay); mining with smaller underground crews; smaller capital expenditure per extracted ton of coal; working under protectively supported roofs and more productive crews. To take advantage of HF in a coal seam, a number of factors should be considered. Seam dip, seam thickness, seam uniformity, seam floor condition, seam roof condition and gas concentration are some of the most important factors that affect the potential of coal seam gas to be extracted by HF (Robert 2002). Due to high quantity of methane gas in PARVADEH Tabas coal mine the factor of gas concentration is not considered in this study.

Hydraulic fracturing (HF) is one of the methods to make coal mining operation safer and more economic. One of the hazards in underground coal mining operation is the sudden coal gas emission leading to coal explosion. To reduce the risk of gas emissions to ensure safer mining, it is necessary to pre-drain coal seams and surrounding layers. This study presents the development and application of a fuzzy model to predict the efficiency of hydraulic fracturing, considering the above factors. In the fuzzy model, the efficiency of hydraulic fracturing of coal seams is calculated as a dimensionless numerical index within the range 0-100. The suggested numerical scale categorizes the efficiency of HF of seams to very low, low, medium, high and very high, each one being specified by a numerical range as a subset of the above range (0-100). The model is used to study the potential of hydraulic fracturing in a coal bed in PARVADEH 4 coalmine in Iran, which will be undergoing stress variation due to future mining activities. The mine consists of 5 seams with different characteristics.

1.3. Aim and objectives

The main aim of this study is to develop numerical modelling tools to help improve the production of gas from unconventional reservoirs. Moreover, the mechanisms involved in HF which could help with enhancing gas extraction are studied and the potential design and geological impacts are evaluated. The pre-production and post-fracture steps of hydraulic fracturing were investigated.

The main objectives of this dissertation are as follow:

1. Developing a Fuzzy model considering geological parameters like seam dip,

thickness, uniformity, roof condition, floor condition, strength and reserve to quantify potential of hydraulic fracturing.

2. Developing a coupled model to study the interaction between fluid and rock during fluid injection.
3. Designing appropriate fluid and solid parameters in order to improve production.
4. Propagating fracture within the targeted layer (e.g. Coal or shale) during pumping.

In this study, a numerical approach is developed to evaluate the methane production for various given parameters. This study presents the development and application of a fuzzy model to predict the efficiency of hydraulic fracturing which has been ignored by other researchers. Many researchers have considered only fracture propagation models and ignored geological parameters. In this study, a numerical approach is developed to evaluate the methane production for various given parameters. This study presents the development and application of a fuzzy model to predict the efficiency of hydraulic fracturing which has been ignored by other researchers. The fuzzy model is able to quantify potential of hydraulic fracturing between 0-100 in each targeted layer of rock before starting injection.

The factors affecting the development of coal bed methane extraction by the HF method are examined. As a case study, HF in the coal bed in PARVADEH 4 Tabas mine in Iran, which will be undergoing stress variation due to future mining activities, is investigated. The deformation of coal induced by mining pressure would change the pore volume of matrix, which would lead to the change of coal seam permeability. As a result, mined area will be dangerous for miners due to increasing methane gas presence.

Tabas Coal Mine is located about 60 km South West of Tabas City where the extraction is carried out by longwall mining which is a form of underground coal mining method where a long wall of coal is mined in a single slice. The average coal bed gas content is in the order of 15 m^3/t (cubic meter per ton).

Moreover, the hydraulic fracturing is investigated in a shale reservoir. A numerical method is developed to simulate the hydro-mechanical evolution of the fracture and the surrounding rock in the finite element analysis framework. The propagation and the exchanges of fluid with the low permeability porous medium are considered. The ability of cohesive elements to model fluid-driven crack propagation in the viscosity-dominated regime is investigated. Hydraulic fractures for reservoir stimulation typically propagate in the viscosity-dominated regime. The application of the coupled model to a case study in Canada is presented. In this study, the focus is on the geological parameters (fuzzy model) and the interaction between fluid and solid parameters (coupled model).

1.4 Structure of the Dissertation

Chapter one of this dissertation presented an introduction to hydraulic fracturing, applications of hydraulic fracturing, and hydraulic fracturing models.

Chapter two introduces the governing equations for fracture mechanics analysis, mechanics of fluid flow in the fracture and presents the basics of the numerical tools used in this thesis including: the finite element method, the finite volume method and the fuzzy logic.

Chapter three presents the application of the fuzzy logic model to study the effect

of geological parameters on the efficiency of hydraulic fracturing process. The model is used to study the potential of hydraulic fracturing in a coal bed in PARVADEH 4 coalmine in Iran, which will be undergoing stress variation due to future mining activities.

In Chapter four, a three-phase hydro-mechanical model is developed for simulating hydraulic fracturing. The complexities involved in coupling fracture mechanics and fluid flow simulations are discussed in detail. A parametric study is conducted by changing various model parameters to study their effects on the hydraulic fracturing process. The results show that changes in rock mechanical properties as well as fluid parameters could lead to significant changes in the hydraulic fracture propagation.

The last chapter outlines the results achieved by using these models and suggests further steps to develop the presented methodology. Some applications of this research finding are discussed in more detail. Immediate future works to extend this project are presented.

Chapter 2. Theoretical Foundation and Numerical Modelling

In this chapter, the theoretical foundation of the problems solved in the next chapters will be introduced. The numerical tools to simulate these problems will be explained in detail. Subsequently, the advantages of these methods will be discussed.

2.1: Fracture Mechanics

Fracture mechanics is a field of solid mechanics that deals with the behaviour of crack bodies subjected to stresses and strains. Centre of attention in fracture mechanics is the initiation and propagation of fractures. Theoretical ideas and experimental approaches have been developed, which permit responses to queries like:

- Will a fracture propagate under applied load?
- When a fracture propagates, what is it's speed and direction?
- Will crack growth stop?
- What is the residual strength of a construction (part) as a function of the (initial) crack length and the load?
- What is the proper inspection frequency (time interval between each inspection)?
- When must the part be repaired or replaced?

Several fields of science are involved in responding to these queries: material science, chemistry, theoretical and numerical mathematics, experimental and theoretical mechanics (Schreurs, 2012). Therefore, the field of fracture mechanics

can be subdivided into several specializations, each with its own concepts, theory and terminology (Schreurs, 2012).

Rocks in reservoirs tend to fracture if loaded with stress above some critical level. Rock and fracture mechanics can provide a fundamental understanding of this process and is thus crucial to analyzing the hydraulic fracturing process. Variations in geomechanical conditions such as elastic modulus of the rock mass, in-situ stresses, fracture deformation and failure mechanisms, directly impact the fracture geometry (Warpinski et al., 1982; Warpinski et al., 2012).

To study the mechanical characteristics of rock and fracture, some initial studies were carried out to better understand the behaviour of intact rock under uniaxial stress. These studies involved analyzing laboratory experiments on samples under homogeneous and isotropic conditions (Hoek and Martin, 2014). Kirsch (1898) analyzed the problem of an infinite elastic plate with a circular hole subjected to uniform tensile stress (Figure 2.1). During hydraulic fracturing process, when the elevated fluid pressure exceeds the sum of the tensile strength of the rock and the minimum principal stress, tensile failure can occur and propagate the initiated fracture (Zhao, et al. 2019).

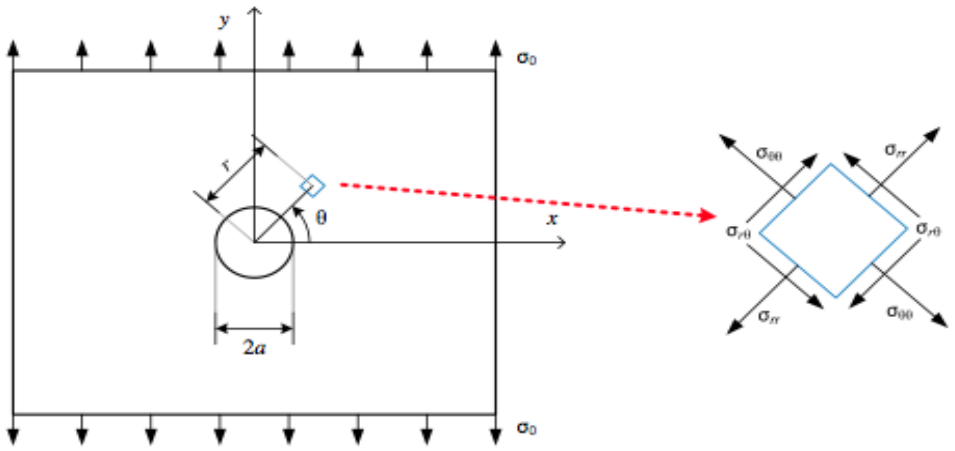

Figure 2.1: Infinite tensile plate with a circular hole (Kirsch, 1898)

where:

σ_0= normal tensile stress,

Θ= loading direction,

A= radius of the hole,

R= radial coordinate,

$\sigma_{\Theta\Theta}$= hoop stress,

$\sigma_{r\Theta}$= shear stress,

σ_{rr}= radial stress and

x and y= two axes of two-dimensional Cartesian coordinates.

The stress distribution within the plate, as indicated by Equations (2.1-2.3), was examined using polar coordinate systems near the circular hole (Grekov and

Yazovskaya, 2014; Bochkarev and Grekov, 2014).

$$\sigma_{rr} = \frac{\sigma_0}{2}\left(1 - \frac{a^2}{r^2}\right)\left\{1 - \left(1 - 3\frac{a^2}{r^2}\right)\cos 2\theta\right\} \quad (2.1)$$

$$\sigma_{\theta\theta} = \frac{\sigma_0}{2}\left\{\left(1 + \frac{a^2}{r^2}\right) + \left(1 + 3\frac{a^4}{r^4}\right) cos\ 2\theta\right\} \quad (2.2)$$

$$\tau_{r\theta} = \frac{\sigma_0}{2}\left\{\left(1 - \frac{a^2}{r^2}\right)\left(1 + 3\frac{a^2}{r^2}\right) sin\ 2\theta\right\} \quad (2.3)$$

Various kinds of geometric discontinuity, such as a sharp change in geometry, opening, hole, notch, crack, and so on are known to be the main source of failure in a large number of catastrophic failures of structures. Such discontinuities generate substantial stress concentrations which reduce the overall strength of material.

2.2. Linear Elastic Fracture Mechanics (LEFM)

Linear elastic fracture mechanics (LEFM) is based on the analysis of cracks in linear elastic materials. It provides a tool for solving most practical problems in engineering mechanics, such as safety and life expectancy estimation of cracked structures and components. The main success of the theory is based precisely upon linearity, which makes it possible to combine very simply the theoretical, numerical, and experimental analyses of fracture. Today, stress analyses of the complex geometry of structures as well as of test specimens are provided by powerful computers using finite element methods (Bui et al., 2011).

A regular planar crack includes two surfaces (top and bottom), and the tip of the crack is a sharp connecting point of these surfaces. If the fractured solid is

subjected to external loads, the fracture surfaces move with respect to each other. Using a local Cartesian coordinate system located at the fracture tip, the relative fracture displacement can be explained by three independent crack modes (Irwin, 1957). These modes are typically called Mode I, Mode II, and Mode III, showing opening, sliding, and tearing of the fracture respectively as shown in Figure 2.2.

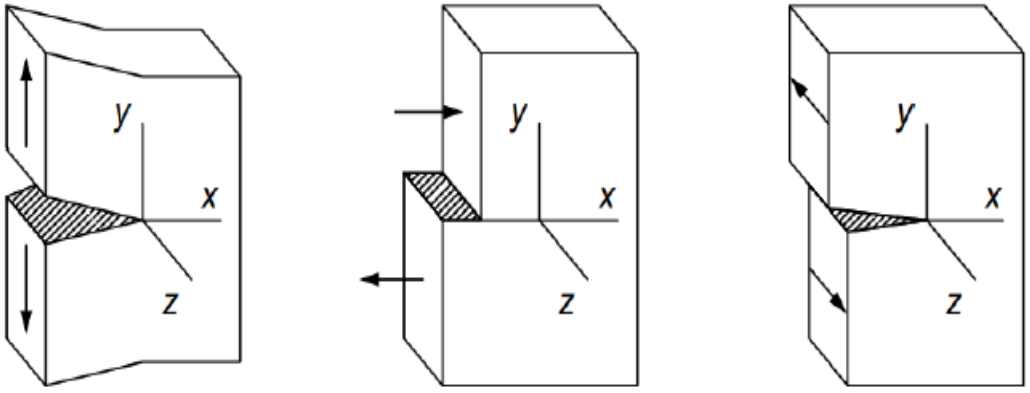

(a) Mode I (b) Mode II (c) Mode III

Figure 2.2: Fracture modes (Sun and Jin, 2012)

In addition, the stresses acting near the fracture tip explain the crack deformation modes. In two-dimensional cases, the stress states corresponding to these three modes are defined by Equations (2.4)-(2.6) (Westergaard, 1939).

$$\sigma_{yy} = \frac{K_I}{\sqrt{2\pi x}} + O\left(\sqrt{x}\right), \qquad \tau_{xy} = \tau_{yz} = 0 \quad for\ Mode\ I \qquad (2.4)$$

$$\tau_{xy} = \frac{K_{II}}{\sqrt{2\pi x}} + O\left(\sqrt{x}\right), \qquad \sigma_{yy} = \tau_{yz} = 0 \quad for\ Mode\ II \qquad (2.5)$$

$$\tau_{yz} = \frac{K_{III}}{\sqrt{2\pi x}} + O\left(\sqrt{x}\right), \qquad \sigma_{yy} = \tau_{xy} = 0 \quad for\ Mode\ III \qquad (2.6)$$

where K_I , K_{II} , K_{III} are the stress intensity factors corresponding fracture modes I, II, and III, respectively and $O\sqrt{x}$ is second term of the stress which is negligible. These equations were introduced by Irwin (1957) for the first time in order to estimate the stress state and the level of singularity at the crack tip. The following stress intensity factor equations were derived from the Westergaard functions (equation 2.7) (1939):

$$\sigma_{xx} = \sigma_{yy} = \frac{\sigma_\infty}{\sqrt{1 - \left(\frac{a}{x}\right)^2}} \qquad (2.7)$$

where:

σ_{xx} and σ_{yy}= stresses along y=0 and x>a

σ_∞= infinite stress at the crack tip

a= crack length

x= distance to crack tip

Westergaard expressed the rectangular coordinates as complex numbers, z=x+iy. This allows stress to be expressed as a function of x and y, $\sigma = f(x, y)$.

2.3 Computational analysis

The analysis of hydraulic fracturing has received a broad interest from the petroleum engineering community. Due to the significant increase in the importance of hydraulic fracturing, some modelling tools have been developed to

study the progressive failure phenomenon in unconventional reservoirs. The finite element method (FEM) is the most widely used numerical tool in fracture mechanics. Various developments, such as singularity or interface elements have been recommended to refine the linear elastic fracture mechanics modelling in the FEM. In the FEM, individual elements are linked together by a topological mapping, and local polynomial representation is employed for the fields within the element. The solution of FE model is a function of the quality of mesh, and the mesh has to conform to the geometry. As a result, by refining the mesh locally (Chan et al, 1975), the displacement near the fracture tip can be captured.

The FEM is an efficient method to calculate the stress intensity factor due to the complexity of the geometry and boundary conditions. In this study the finite element software ANSYS is used to simulate the hydraulic fracturing process. In ANSYS, there are 3 main ways to evaluate fracture mechanics parameters:

- Stress intensity factors (K): is the magnitude of stress singularity at the crack tip
- J-integral JINT (J): represents a way to calculate the strain energy release rate.
- Energy release rate VCCT (G): indicates that the work required to propagate a crack is the same as the energy to close the crack.

2.3.1-Stress Intensity Factors (SIF)

Crack propagation analysis requires the evaluation of the parameters such as the energy release rate and stress intensity factors (SIF) to determine the length,

velocity and orientation of the crack propagation. The stress intensity factor, K, is used in fracture mechanics to predict the stress state near the tip of a crack caused by loads. The stress intensity factor is the magnitude of stress singularity at the crack tip (Anderson 1994).

It is a parameter to characterize the stress field ahead of a sharp crack in a test specimen or a structural member. The parameter, K, is related to the stress level (σ) in the structural member and the size of the crack, and has the unit of ($MPa.mm^{0.5}$). In general, the relationship is represented by:

$$K = \sigma\sqrt{a}\ p \qquad (2.8)$$

where p is a geometrical parameter that depends on the structural member and crack size, and *a* is the crack length. All structural members or test samples that have flaws can be loaded to different levels of K. This is similar to the situation where unflawed structure can be loaded to different levels of stress (σ) (Barsom and Rolfe, 1999).

The magnitude of stress intensity factor depends on sample geometry, the size and location of the crack, and the magnitude and the modal distribution of loads on the material.

The energy release rate for crack growth or strain energy release rate is the change in elastic strain energy per unit area of crack growth. The well-known criteria for crack propagation are maximum circumferential (hoop) stress (Erdogan and Sih 1963), maximum energy release rate (Nuismer 1975), and maximum strain energy density (Sih 1974). Both the orientation of crack growth and the stress at which the growth would take place are predicted by the above criteria. They predict

slightly different angles for the initial kink, but they all predict kink initiation. Cracks with direction change are defined as kinked cracks. Due to the sudden change in tangent orientation at the kink points, the orientation would be the one that locally releases the maximum energy or satisfies some other mixed mode criteria. But these do not necessarily occur with K_{II} = 0 for the developing kink (Cotterell and Rice 1980). Cotterell and Rice (1980) indicated that the Erdogan and Sih (1963) criterion is a more practical basis at the developing kinks. Thus, the Erdogan and Sih (1963) measure could be employed to calculate fracture propagation direction,

$$\theta = 2\arctan\left(\frac{1}{4}\left(\frac{K_I}{K_{II}} \mp \sqrt{\left(\frac{K_I}{K_{II}}\right)^2 + 8}\right)\right) \qquad (2.9)$$

where θ is the crack growth angle in the crack-tip local coordinate system. Equation (2.9) gives two directions for crack propagation; the one with positive tensile stress is acceptable.

2.3.2- J-integral JINT (J)

The J-Integral evaluation is based on the domain integral method proposed by Shih. The domain integration formulation applies area integration for 2-D problems and volume integration for 3-D problems. Area and volume integrals offer much better accuracy than contour integral (contour integration is a method of evaluating integrals along paths in a complex plane) and surface integrals (a surface integral is a generalization of multiple integrals to integration over surface), and are easier to implement numerically (Shih et al., 1986).

J-integral is described as a path-independent line integral that determines the

strength of the singularities for stresses and strains near a fracture tip. J-integral, also known as J, was established by Rice[14].

$$J = \lim_{\Gamma \to 0} \int_{\Gamma} n.H.qd\Gamma \qquad (2.10)$$

$$H = WI - \sigma \frac{\partial u}{\partial x} \qquad (2.11)$$

where, W is strain energy density, Γ is the contour path, n the normal on the path, H is potential energy, I is dimenetionless integral , x is coordinate direction , u is corresponding displacement vector, and q is the virtual crack extension direction.

The J-integral is normally employed in rate-independent quasi-static crack analysis to determine the energy release associated with crack propagation. If the material response is linear, it can be associated to the stress intensity factor. This relationship for homogeneous, isotropic materials is as follows:

$$J = \frac{1}{\bar{E}}(K_I^2 + K_{II}^2) + \frac{1}{2G}K_{III}^2 \qquad (2.12)$$

where $\overline{E}$=E for plane stress and $\overline{E}$=E/(1-υ^2) for plane strain, axisymmetric and three dimensional conditions (Hasanpour, and Choupani, 2009).

Asumptions, such as defining the geometry of the crack, constitutive models of rocks and fluids and fluid flow differ in many models which have been proposed to study hydraulic fracturing. The standard method of energy release rate from the fracture mechanics theory is used to define the criteria for the crack growth(Courtin et al, 2005).

Because of the singularity of strain field in edges, modelling of the crack as a discontinuity has always been considered as a challenge in numerical approaches. In addition, complexity arises while modelling HF specially when a force like fluid pressure generates the fracture.

In the modelling process, fluid pressure was considered as a uniform pressure on the injection hole shell and the fracture. Stress intensity factor and Rice's released elastic energy (J-Integral), which are the fracture mechanics variables, were studied under plane strain conditions. In this work modelling was carried out in Ansys using quadratic elements in 2D and 3D. The mesh was refined around fracture tip and a linear elastic finite element analysis was carried out under a 3D stress condition (Courtin et al, 2005).

2.3.3- Energy release rate VCCT (G)

Energy release rate is based on the assumption that the energy needed to separate a surface is the same as the energy needed to close the same surface. The approach for evaluating the energy-release rate is based on the virtual crack-closure technique (VCCT). The VCCT is applied to partition the fracture modes, i.e. to determine the energy release rate contributions related to fracture modes I, II, and III (Delorenzi, 1982).

2.4. Hydraulic fracturing models

The first simplified theoretical models for hydraulic fracturing were developed in the 1950s (Crittendon 1950, Harrison et al. 1954 and Hubbert and Willis 1957).

One of the most important papers published in this area was by Perkins and Kern who adapted the classic Sneddon plane strain crack solution to develop the so-called PK model (Figure 2.3) (Perkins and Kern, 1961). Later, Nordgren adapted the PK model to formulate the PKN model, which included the effects of fluid loss (Nordgren, 1972). Khristianovic and Zheltov (1995), and Geertsma and de Klerk (1969) independently developed the so-called KGD (plane strain) model (Figure 2.3). The radial or penny-shaped model (Figure 2.4) with constant fluid pressure was solved by Sneddon. The problem of a flat elliptical crack under constant loading was studied by Green and Sneddon (Adachi et al, 2007).

The PKN and KGD models differ in one major assumption: the way in which they convert a three-dimensional solid and fracture mechanics problem to a two-dimensional plane strain model. Khristianovic and Zheltov (1995) assumed plane strain in the horizontal direction i.e. all horizontal cross sections act independently or equivalently, which is equivalent to assuming that the fracture width changes much more slowly vertically along the fracture surface from any point on the fracture surface than it does horizontally. In practice this is true if the fracture height is much greater than the length or if free slip occurs at the boundaries of pay zone (a pay zone is a reservoir or part of a reservoir that contains hydrocarbons that can be extracted economically). Perkins and Kern (1961), on the other hand, assumed that each vertical cross section acts independently (Figure 2.3), which is equivalent to assuming that the pressure at any section is dominated by the height of the section rather than the length of the fracture. This is true if the length is much greater than the height. This difference in one basic assumption has led to two

different ways of solving the problem. In the case of the PKN model, the effect of the fracture tip is not considered; the concentration is on the effect of fluid flow and the corresponding pressure gradients (Dahi, 2009). In the KGD model, however, the tip region plays a much more important role (Dahi, 2009).

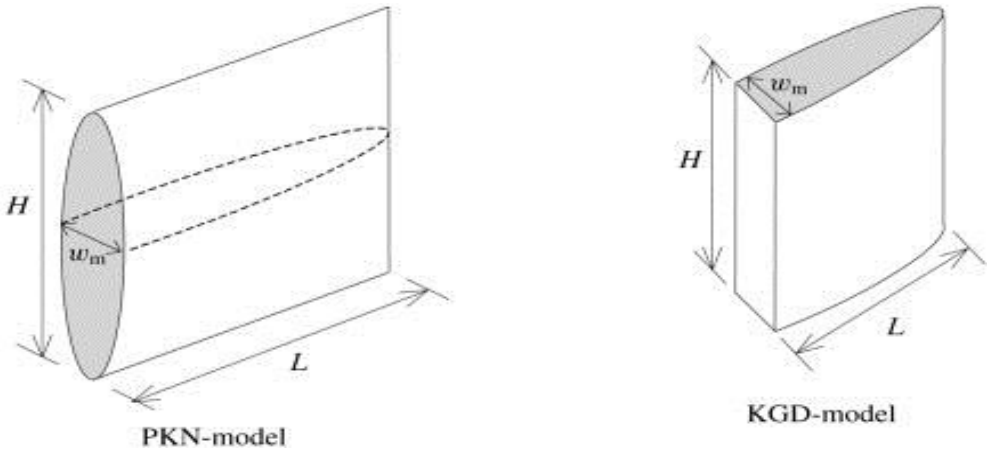

Figure 2.3: PKN and KGD fracture Geometry (Adachi et al, 2007)

In Figure 2.3, L is the fracture length, H is the frature hight and w_m is the fracture width. Review of the literature indicates that there is a lack of 3 dimensional models for simulating of hydraulic fracturing and this area needs more research effort.

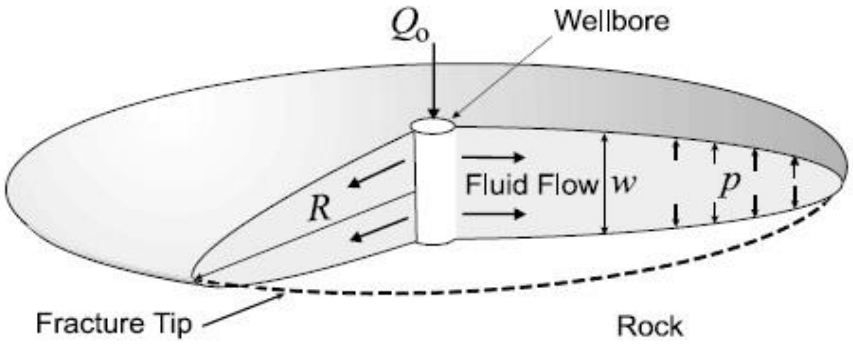

Figure 2.4: Penny-shaped fracture geometry (Adachi et al, 2007)

In the figure 2.4, P is pressure, R is radius of the frature, Q_o is fluid injection rate and w is the fracture width.

2.5. Fracture Initiation

Reservoir rocks are mainly subjected to three principal in-situ stresses, namely the vertical stress, the maximum horizontal stress, and the minimum horizontal stress. The in-situ stresses should be transformed into cylindrical coordinates due to the shape of wells in order to define the fracture initiation criteria (Figure 2.5). Assuming isotropic, homogeneous, and linearly elastic formation, stresses acting on the wall of a cylindrical well are derived from Kirsch's equation as (Dieley and Owens, 1969; Bradley, 1979; Aadnoy et al. 1987; Aadnoy, 1988):

$$\sigma_{rr} = P_w \qquad (2.13)$$

$$\sigma_{\theta\theta} = (\sigma_h + \sigma_v) - 2(\sigma_h - \sigma_v)\cos 2\theta - P_w \qquad (2.14)$$

$$\tau_{r\theta} = 0 \qquad (2.15)$$

where P_W is the fluid pressure acting on the cylindrical wall, σ_v is the vertical stress, σ_h the minimum horizontal stress, and $\theta$is the fracture angle. Considering the fracture direction is perpendicular to the minimum principal stress (θ=90°) (where there is minimum resistance to fracture initiation), the tensile stress, $\sigma_{\theta\theta}$ is simplified as (Hossain et al. 2000):

$$\sigma_{\theta\theta} = 3\sigma_h - \sigma_v - P_w \qquad (2.16)$$

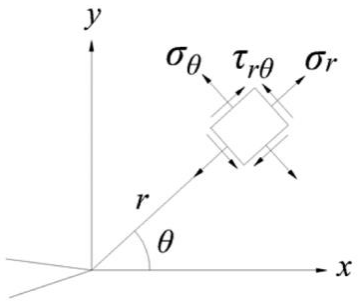

Figure 2.5: Stress transformation on crack tip

Incorporating the tensile strength of the rock, σ_t , Hubbert and Willis (1957) defined the fracture initiation pressure, p_{wf} . The fracture is initiated when the tensile stress exceeds the sum of the fracture initiation pressure and the tensile strength of the rock.

$$P_{wf} = 3\sigma_h - \sigma_v - P_w + \sigma_t \qquad (2.17)$$

Equation (2.16) assumes that there is no fluid exchange between the well and the surrounding formation. Therefore, the fracture initiation pressure is an upper bound solution. If fluid penetrates the formation, the resulting increase in pore pressure decreases effective stress and thus the fracture initiation pressure. Schmidt and Zoback (1989) added poro-elasticity and derived Equation (2.18) as a lower bound pressure for the fracture initiation (Valko and Economides, 1995).

$$P_{wf} = 3\sigma_h - \sigma_v - 2\eta_{pe}P_w + \sigma_t \qquad (2.18)$$

where η_{pe} is the poro-elasticity parameter defined as Equation (2.19) with Biot coefficient, α_{biot} and ν is the Poisson's ratio.

$$\eta_{pe} = \frac{\alpha_{biot}(1-2\nu)}{2(1-\nu)} \qquad (2.19)$$

When low viscosity fluids are used with low pumping rates, it is expected that more fluid transfers to the formation, and thus fracture initiations takes place at lower pressure (Hossain et al. 2000).

2.6. Fracture propagation

The fracture propagation criterion is derived from Linear Elastic Fracture Mechanics (LEFM), which was established based on the Griffith's concepts of crack stability (Griffith, 1920; Griffith, 1924). The stress field around an elliptical crack and a criterion for crack propagation were proposed in Griffith (1924). The load bearing capacity of a material containing a fracture is proportional to the square root of the fracture length (According to LEFM). Therefore the linear elastic solution is singular at the fracture tip. The intensity of the singularity is represented by stress intensity factor, which depends on the geometry and the loading condition. This concept was developed by Irwin (1957) in three elementary modes; Mode I (opening mode), mode II (shearing or sliding mode) and mode III (tearing mode).

The opening mode occurs in symmetrical extension and bending of fractured materials where movement is perpendicular to the plane of fracture. The sliding mode is experienced in skew-symmetric plane loading of fractured materials where, at the leading edge of the fracture, the movement is in the plane and parallel

to the orientation of the fracture. The tearing mode occurs in skew-symmetric bending (twisting) or skew-symmetric loading in which the movement is perpendicular to the plane of the material and in the plane of fracture surface. In LEFM, each of the crack extension modes are related with a corresponding fracture tip stress intensity factor K_I, K_{II} and K_{III}.

The asymptotic displacement along y-axis at the crack tip for mode I can be determined as (Irwin, 1957):

$$u_y = \frac{K_I}{2G}\left(\frac{r}{2\pi}\right)^{1/2} \sin\frac{\theta}{2}\left(k - 1 - 2cos^2\frac{\theta}{2}\right) \qquad (2.20)$$

where:

u_y=displacement discontinuity along y axis

G=shear modulus

r, θ= polar coordinates with origin at fracture tip

K_I=stress intensity factor for mode I and

$k = 3 - 4\nu$ for plane strain with ν being Poisson's ratio.

Based on Griffith's ideas for fracture stability, fracture propagation can be simulated through a cycle of steps. Firstly stress intensity factor is computed for a given geometry and loading condition. Then the crack growth criterion is used to check if the fracture is stable or not. In the third step, if fracture is unstable, propagation occurs to a certain distance (Clifton and Abou-Sayed, 1979). The

fracture is extended if the stress intensity factor is equal or greater than a critical value known as fracture toughness, K_{IC}, or critical stress intensity factor which is a material property (Clifton and Abou-Sayed, 1979).

Henshell and Shaw (1975) and Barsoum (1976) proposed special crack tip singular elements for the finite element modelling of linear elastic media containing fractures. In these 8-noded isoparametric elements, the mid-side nodes which are close to the crack tip, are moved to their quarter point. It has been proved that such a shift of nodes results in required stress singularity at the fracture tip (Barsoum, 1976; Henshell and Shaw, 1975). The quarter point crack tip elements have been successfully applied in modelling fracture problems both in finite element method (Ingraffea, 1977a; Murti and Valliappan, 1986; Owen and Fawkes, 1983) and boundary element method (Blandford et al., 1981; Smith and Mason, 1982).

Using the displacement correlation method, numerical results of displacements field at the crack tip are used to determine the stress intensity factor. The stress intensity factor at the fracture tip for mode I (crack opening) can be determined as follows (Ingraffea, 1977a; ingraffea and Manu, 1980; Murti and Valliappan, 1986):

$$K_I = \frac{G}{(k+1)}\sqrt{\frac{2\pi}{L}}\{4(u_{yB} - u_{yC}) + u_{yD} - u_{yA}\} \qquad (2.21)$$

where u_{y_A},u_{y_B},u_{y_C},$u_{yD}$are the nodal displacements at different nodes and L is the length of fracture tip element. The above technique has been found to provide very good accuracy when compared with existing analytical solutions providing that

following guidelines are abided by (Ingraffea, 1977a; Murti and Valliappan, 1986):

- A reduced numerical integration scheme for fracture tip elements
- An aspect ratio of close to one for fracture tip elements
- The length of fracture tip elements about 15-25% of the fracture length
- The angle of fracture tip elements at the fracture tips less than 90 degrees.

In poroelastic materials, diffusion process at the crack tip region controls the behaviour of the crack. This is the characteristic feature of fracture mechanics problems related to poroelastic media. Craster and Artinkson (1996) showed that the pore pressure is nonsingular in the case of poroelastic fracture problems. The pore pressure field at fracture tips only experiences a temporal singularity during undrained phase and becomes non-singular after dissipation of the undrained response. However, they showed that the pore pressure gradient at the tip is singular, if permeable fracture faces are considered. The fracture propagation problems in poroelastic media are classified into two groups of transient (Boone and Ingraffea, 1990; Detourney and Cheng, 1991) and steady state (Yoffe, 1951) problems.

In this study, Eq. 2.21 is used to determine stress intensity factor at the crack tip. In order to take advantage of symmetry of the geometry of the model, Eq. 2.21 can be expressed in the following form (to avoid complexity) (Boone and Ingraffea, 1990; Detourney and Cheng, 1991):

$$K_I = \frac{G}{(k+1)}\sqrt{\frac{2\pi}{L}}\{8u_{yB} - 2u_{yA}\} \qquad (2.22)$$

Once K_I is numerically equal to the fracture toughness of the material K_{IC}, the hydraulic fracture propagates to the following node and the numerical model advances to the next time step (Boone and Ingraffea, 1990; Detourney and Cheng, 1991).

2.7. Mechanics of fluid flow in the fracture

The major fluid flow parameters are the fluid viscosity μ and injection rate q_i. Consider a Newtonian fluid flowing laterally through a narrow slit (Fig. 2.6). In the case of laminar flow (the general case for flow inside hydraulic fractures), the pressure drop along some length Δx of the slit is (Economides, 2000):

$$\frac{\Delta p_{net}}{\Delta x} = \frac{12\mu q}{h_f w^3} \qquad (2.23)$$

where h_f is fracture height, Δp_{net} is pressure drop and w is fracture width.

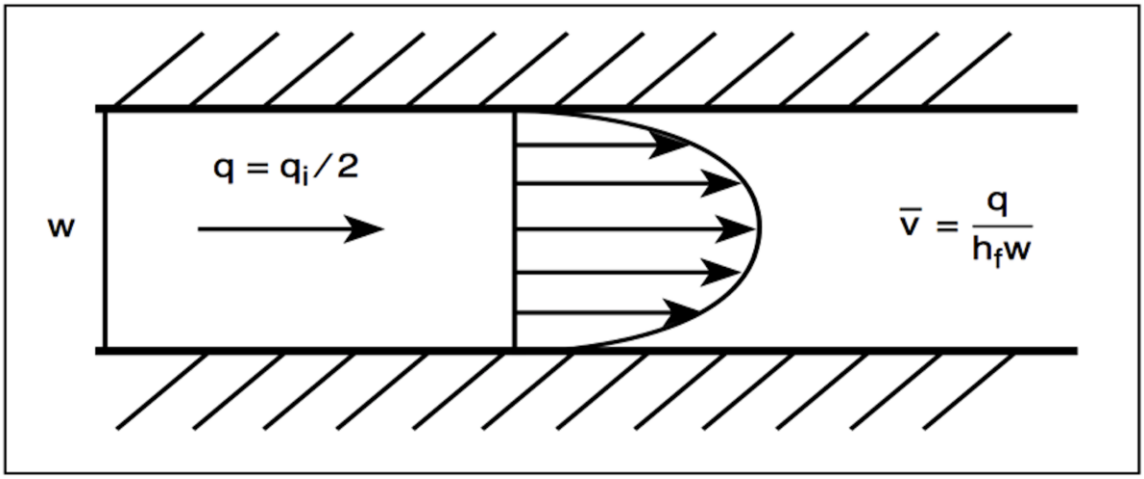

Figure 2.6: Fluid flowing laterally through a narrow fracture (Economides, 2000)

The fracture is essentially a channel of varying width over its length and height. The local pressure gradient within the fracture is determined by the fracturing fluid rheology, fluid velocity and fracture width. Equations governing fluid flow within the fracture can be derived using the principle of conservation of momentum and lubrication theory applied to a fluid travelling in a narrow conduit. The rheology of fracturing fluids is generally represented by a power law model that incorporates two parameters *K* and *n*. In recognition that fluid flow within a fracture is laminar for most fracturing applications (Perkins and Kern, 1961), the global pressure gradient along the length of a fracture can be expressed as:

$$\frac{dp}{dx} \propto \frac{K v_x^n}{\overline{w}^{1+n}} \qquad (2.24)$$

where v_x is the average fluid velocity along the length of the fracture and is defined in terms of the volumetric injection rate q_i, fracture height h_f and height-averaged fracture width $\overline{w}$. Material balance or conservation of mass suggests that v_x is proportional to $qi/\overline{w}h_f$. Equation 2.24 then becomes

$$\frac{dp}{dx} \propto \frac{K}{\overline{w}^{1+2n}} \left(\frac{q_i}{h_f}\right)^n \qquad (2.25)$$

In the special case of a Newtonian fluid (n = 1 and K = μ, where μ is the fracturing fluid viscosity), Eq. 2.25 reduces to (Economides, 2000)

$$\frac{dp}{dx} \propto \frac{\mu}{\overline{w}^2} \left(\frac{q_i}{\overline{w}h_f}\right) \qquad (2.26)$$

where the term $\bar{w}h_f$ is readily recognized as the average fracture cross-sectional area. Equation 2.26 is essentially Darcy's law with the permeability proportional to $\bar{w}^2$. Equations 2.24 and 2.25 are formulated in terms of the average velocity and implicitly ignore change in the fracture width over its height. The varying width profile has an effect on the flow resistance relative to the case of a constant-width channel. The increase in the flow resistance is accentuated during periods of fracture height growth into barriers at higher stress. The varying width profile affects other physical phenomena that are highly sensitive to the velocity (Economides, 2000).

2.8. Numerical Tools

2.8.1. Fuzzy logic in hydraulic fracturing of coal seam

Fuzzy logic is a powerful tool for the analysis of systems that work with vague parameters and receive qualitative inputs, and uncertain and simple analytical information of the conditional IF-THEN type. These IF-THEN rule statements are used to fotmulate the conditional statements that comprise fuzzy logic in an algorithm in shortest time and with suitable results. A fuzzy set is an extension of the concept of crisp set. While a crisp set only allows full membership or no membership to every element of a universe of discourse, a fuzzy set permits for partial membership (Dubois and Prade, 2010).

Over the past decades, the Fuzzy Set Theory (FST) has been employed in geotechnical engineering problems to address the problem of uncertain data due to lack of accuracy, incompleteness, vagueness and randomness of the

information as well as incorporating subjective expert judgment into problem analyses. Introduced by Zadeh in 1965, FST provides a means for representing epistemic uncertainty using set theory (Dubois and Prade, 2010).

The fuzzy set theory includes fuzzy variables or fuzzy functions, fuzzy logic, fuzzy inference system, fuzzy probability, and hybrid fuzzy set. Fuzzy inference has been used in this study. Fuzzy inference system defines relationships between input and output variables of a system by using linguistic labels in a collection of IF-THEN rules, Mamdani and Takagi-Sugeno systems being the most commonly used. Details on the FST can be found in e.g., Zimmermann, (1991) and Celikyilmaz and Turksen, (2009).

Since early 80's when the first applications of FST in geotechnical engineering appeared, it has been developing intensively and currently it is employed in wide variety of problems for instance, slope stability, rock engineering, tunnelling, project management, and even constitutive modelling of geomaterials. In this study, the potential of HF in coal mining is studied using the fuzzy logic. The effects of different parameters on the potential of HF are defined. This definition is subjective. When the results are evaluated in terms of geotechnical parameters, qualitative words are usually employed such as excellent, favourable, poor, etc. These terms are ambiguous and vague (Chen and Pham, 2000).

Fuzzy logic refers to the study of approaches and principles of human reasoning. The classical logic deals with propositions (e.g., conclusions or decisions) that are either true or false. Each proposition has an opposite. The classical logic, thus, deals with mixtures of parameters that represent propositions (Chen and Pham,

2000). As each parameter stands for a hypothetical proposition, any combination of them assumes a value. The main content of classical logic is the study of rules that permit new logical parameters to be generated as functions of certain existing parameters (Chen and Pham, 2000).

2.8.1.1. Fuzzy logic

A fuzzy set can be described as a set with fuzzy boundaries. Let X be the universe of discourse and its elements be denoted as x. In classical set theory, a crisp set A of X is defined as function $fA(x)$ called the characteristic function of A

$$fA(x): x \rightarrow [0,1] \qquad (2.27)$$

where

$$fA(x) = \begin{cases} 1, & if\ \ x \in A \\ 0, & if\ x \notin A \end{cases}$$

This set maps universe X to a set of two elements. For any element x of universe X, characteristic function $fA(x)$ is equal to 1 if x is an element of set A, and is equal to 0 if x is not an element of A. In the fuzzy theory, a fuzzy set A of universe X is defined by function $\mu A(x)$ called the membership function of set A (Zadeh, 1992)

$$\mu A(x): x \rightarrow [0,1] \qquad (2.28)$$

where

$$\mu A(x) = 1\ if\ x\ is\ totally\ in\ A$$

$$\mu A(x) = 0 \; if \; x \; is \; not \; in \; A$$

$$0 < \mu A(x) < 1 \quad if \; x \; is \; partly \; in \; A$$

This set permits a continuum of feasible options. For any element x of universe X, membership function $\mu A(x)$ equals the degree to which x is an element of set A. This degree, a value between 0 and 1, represents the degree of membership, also called membership value, of element x in set A (Zadeh, 1992). The evaluations of the fuzzy rules and the combination of the results of the individual rules are performed using fuzzy set operations. The operations on fuzzy sets are different than the operations on non-fuzzy sets. Let μA and μB be the membership functions for fuzzy sets A and B. Table 3.7 contains possible fuzzy operations for OR and AND operators on these sets, comparatively. The mostly used operations for OR and AND operators are max and min, respectively. For complement (NOT) operation, Eq. (2.29) is used for fuzzy sets (Mendel, 1995).

$$\mu\bar{A}(x) = 1 - \mu A(x) \qquad (2.29)$$

Table 2.1: Fuzzy set operations

OR (Union)		AND (intersection)	
MAX	Max{μA (x), μB (x)}	MIN	Min{μA (x), μB (x)}
ASUM	μA(x) + μB(x) − μA(x)μB(x)	PROD	μA(x)μB(x)
BSUM	Min{1,μA(x) + μB(x)}	BDIF	Max{0,μA(x) + μB(x) − 1}

After evaluating the result of each rule, these results should be combined to obtain a final result. This process is called inference. The results of individual rules can be combined in different ways. Table (3.8) contains possible accumulation methods that are used to combine the results of individual rules. The maximum algorithm is generally used for accumulation. x' is the sum of elemens in fuzzy sets in Table 3.8 (Mendel, 1995).

Table 2.2: Accumulation methods

Operation	Formula
Maximum	Max{μA (x), μB (x)}
Bounded sum	Min{1, μA (x) + μB (x)}
Normalized sum	μA (x)+μB (x) Max{1,Max{μA (x′),μB (x′)}}

In order to design a fuzzy system we need to creat membership functions and fuzzy rule bases which will be discussed in the next chapter.

2.8.1.2. Fuzzy inference

After constructing the rule bases, an inference engine is needed. A fuzzy inference system (FIS) is a system that employs the fuzzy set theory to map inputs to outputs. The most frequently used fuzzy inference method is known as Mamdani approach, which was introduced, by Mamdani and Assilian in 1957. It was the first attempt to control a steam engine and boiler combination by synthesizing a set of

linguistic control rules acquired from experienced human operators. An equally influential publication by Zadeh (Zadeh, 1973) was inspired by Mamdani method. Interest in fuzzy control has persisted and the literature on the subject has mushroomed quickly. A survey of the field with fairly extensive references may be found in Lee (1990) or, more recently, in Sala et al., (2005). The rule of Mamdani inference is as follows:

$$If \quad x \ is \tilde{A} \ \ And \ \ y \ is \tilde{B} \ then \ z \ is \tilde{C}$$
$$\mu_{\tilde{C}}(c) = SUP_{z=F(x,y)} \left\{ \min(\mu_{\tilde{A}}(x), \mu_{\tilde{B}}(y)) \right\}$$

In fuzzy sets the SUP is upper limit of $\mu_{\tilde{C}}(c)$.

Mamdani's fuzzy inference system can be used as a decision making model to categories geotechnical sites based on water, soil, support, infrastructure, input, and risk factor related information.

Many inferences can be used in fuzzy logic. For instance, techniques of inference when the IF part is invoked, are GAMMA, MIN-AVG, MIN-MAX and approaches of inference of the THEN part are MAX, BSUM. In this study, MAX-MIN operator is used. The reason of this choice is less membership degree in the IF part and maximum membership degree in the THEN part (Ataee, 2009). The last step of designing a fuzzy system is defuzzification which will be discussed in the next chapter.

2.8.2. Numerical modelling in rock mechanics

In the past three decades, numerical techniques have become widely available, due to the rapid develpments in computer hardware and software. The suitability of these methods for analysis and design of very complex geotechnical systems is another reason for their popularity. Several analytical methods are applicable in rock mechanics to circumstances similar to the ones for which they were developed; although, there are numerous issues for which no past experience is available (Pande and Beer, 1990). In such cases, numerical approaches are the first choice to solve the design issues. Furthermore, numerical techniques should be employed as a supportive technique together with analytical and experimental approaches.

According to Jing and Hudson (2002), numerical approaches in rock mechanics can be categorized into continuum, discontinuum and hybrid techniques as explained below:

Continuum methods are:

- The finite element method (FEM)
- The finite difference method (FDM)
- The boundary element method (BEM)
- The finite volume method (FVM)

Discontinuum methods are:

- Discrete (or Distinct) elements method (DEM)

- Discrete fracture network (DFN)

Hybrid methods are:

- Hybrid FEM/BEM
- Hybrid DEM/BEM
- Hybrid FEM/DEM

The choice of continuum or discontinuum approaches relies on the problem scale and the fracture system geometry. Discontinuum techniques are acceptable for moderately fractured rock masses where large-scale displacements of individual blocks are feasible (Jing, 2003).

There is no absolute guide on which approach is better than another and when one or another should be employed. (Bobet et al., 2009).

FEM is a systematic numerical approach which can be applied for rock mechanics and geomechanical design issues. It has the potential to deal with material heterogeneity, anisotropy, non-linearity, complex boundary conditions, in-situ stresses and gravitational stresses (Jing and Hudson, 2002). Consequently, in this work, FEM will be employed as the major numerical technique to carry out the numerical analysis.

2.8.3. Finite Element Method

FEM is a common numerical approach, which can be used for rock and soil mechanics problems (Singiresu, 2004). FEM is the numerical solution of the mathematically weak form of a problem in engineering, which mainly consists of

six steps as explained briefly below (Singiresu, 2004):

Step 1: Discretization of the domain

The domain is splitted into small elements. Elements are linked at points called nodes. The specific arrangement of elements is called a mesh (Figure 2.4).

- Step 2: Selection of a proper shape function

The unknown variable is interpolated with certain shape functions that are localized to those finite elements (Singiresu, 2004).

- Step 3: Calculating the element stiffness matrices

In the finite element method for the numerical solution of partial differential equations, the system of linear equations represented by the stiffness matrix, is solved in order to ensure an approximate solution to the differential equation.

- Step 4: The assemblage of elements (global stiffness matrix)

Element stiffness matrices are assembled in this step to give the global stiffness matrix or the stiffness matrix of the structure. With this, the overall equilibrium equations are obtained. The element stiffness of all the elements need to be determined and then assembled together in a systematic manner.

- Step 5: Finding the displacement for each node

- Step 6: Computation of element stresses and strains

Steps 5 and 6 will be discussed later through an example (Singiresu, 2004).

FEM produces an estimated solution. The solution can be improved by using a finer mesh (more elements) to represent the structure (Cook et al., 2001).

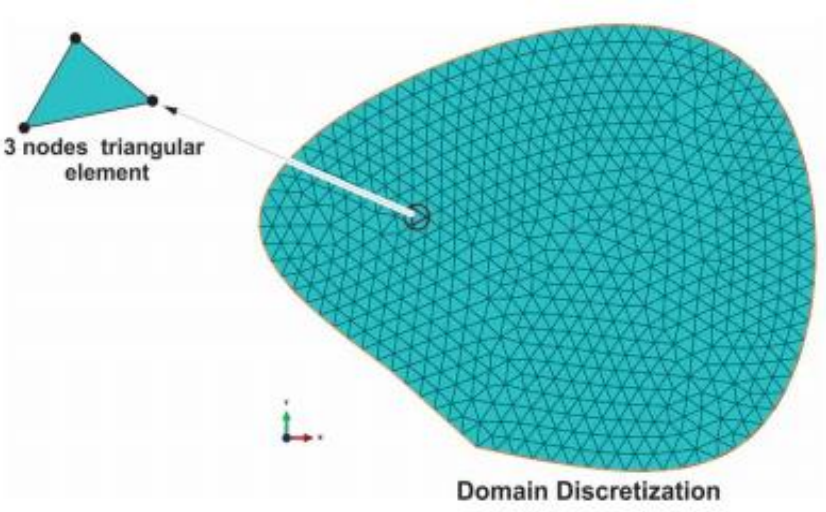

Figure 2.7: Finite elements and meshing for discretization of the domain (Singiresu, 2004)

To illustrate the abovementioned steps, an example is given below. Assuming a 2D problem, the domain is discretised with a number of triangular elements (step 1), as indicated in Figure 2.7. A typical linear triangular element is shown in Figure 2.8 (Singiresu, 2004).

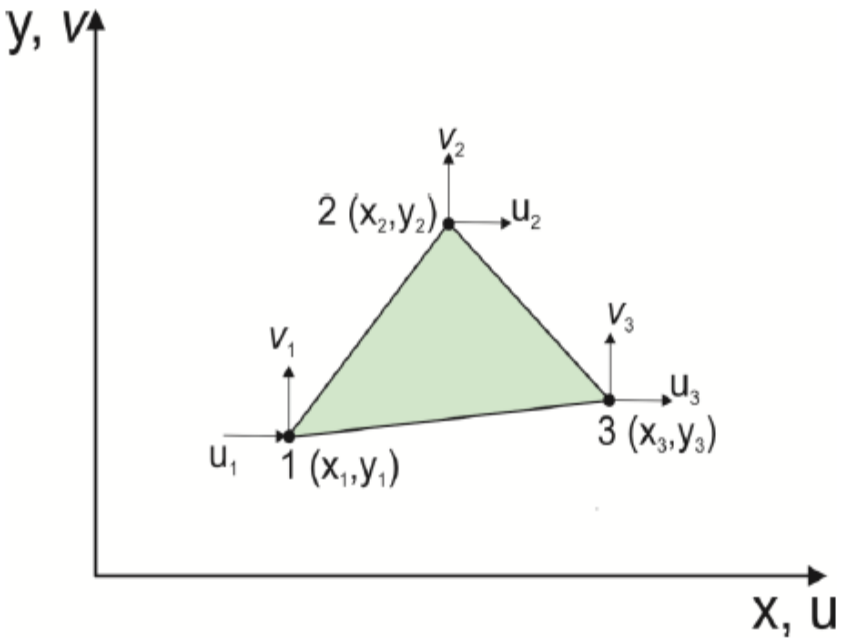

Figure 2.8: A linear triangular element(Singiresu, 2004)

The process to find the interpolation functions (shape functions, step 2) is described below (Adeeb, 2010).

To compute the shape functions, normally there are two approaches: the intuitive method and rigorous structured method. Both are the same, but the rigorous structured method is most acceptable for higher order elements. For this example, the latter method is only discussed.

According to the number of degrees of freedom, the interpolation functions based on the Pascal triangle are chosen as below (Adeeb, 2010):

$$\mathbf{u}(x,y) = a_1 + a_2 x + a_3 y \qquad (2.30)$$

$$\mathbf{v}(x,y) = b_1 + b_2 x + b_3 y \qquad (2.31)$$

where, **u**, **v** are displacement functions and *x*, *y* are point coordinates. The displacement function must be capable of rigid body displacements of the element. The constant terms used in the polynomial (a to a_3 and b to b_3) ensure this condition (Adeeb, 2010).

$$\begin{Bmatrix}\mathbf{u}\\ \mathbf{v}\end{Bmatrix} = \begin{pmatrix}1 & 0 & x & 0 & y & 0\\ 0 & 1 & 0 & x & 0 & y\end{pmatrix}\begin{Bmatrix}a_1\\ b_1\\ a_2\\ b_2\\ a_3\\ b_3\end{Bmatrix} \qquad (2.32)$$

$$\mathbf{u} = Xa \qquad (2.29)$$

$$\begin{Bmatrix}\mathbf{u_1}\\ \mathbf{v_1}\\ \mathbf{u_2}\\ \mathbf{v_2}\\ \mathbf{u_3}\\ \mathbf{v_3}\end{Bmatrix} = \begin{pmatrix}1 & 0 & x_1 & 0 & y_1 & 0\\ 0 & 1 & 0 & x_1 & 0 & y_1\\ 1 & 0 & x_2 & 0 & y_2 & 0\\ 0 & 1 & 0 & x_2 & 0 & y_2\\ 1 & 0 & x_3 & 0 & y_3 & 0\\ 0 & 1 & 0 & x_3 & 0 & y_3\end{pmatrix}\begin{Bmatrix}a_1\\ b_1\\ a_2\\ b_2\\ a_3\\ b_3\end{Bmatrix} \qquad (2.33)$$

$$\mathbf{u_e} = Aa \qquad (2.34)$$

$$a = A^{-1}u_e \qquad (2.35)$$

$$\mathbf{u} = Xa = XA^{-1}u_e \qquad (2.36)$$

Therefore, the shape function $\mathbf{N_i}$ is equal to (Adeeb, 2010):

$$\mathbf{N} = XA^{-1} \qquad (2.37)$$

$$\mathbf{N} = \begin{bmatrix}N_1 & 0 & N_2 & 0 & N_3 & 0\\ 0 & N_1 & 0 & N_2 & 0 & N_3\end{bmatrix} \qquad (2.38)$$

After computing the shape functions, the stiffness matrix of the element is

calculated (step 3). The elemental stiffness matrices are assembled to give the global stiffness matrix. The global stiffness matrix is employed to calculate the global force and displacement. To determine the element stiffness matrix, the following steps are taken (Adeeb, 2010):

As shown in equation (2.36), the complete element displacement (u) is:

$$\mathbf{u} = \mathbf{N}.u_e \qquad (2.39)$$

Therefore, the stiffness matrix is equal to:

$$\mathbf{K} = \int B^T.C.B.dv = t\int B^T.C.B.dA = t\int_{-1}^{1}\int_{-1}^{1} B^T.C.Bdydx \qquad (2.40)$$

where *t* is the thickness of the element and the constitutive matrix [**C**] contains elastic constants. The dimension of the [**C**] matrix relies on on the strain components. For example in 2D problems, strain has three components (ε_{xx}, ε_{yy}, γ_{xy}) so the dimension of [**C**] is 3×3. For 3D problems, the strain components are 6 so the dimension of [**C**] is 6×6.

For plane stress conditions (Adeeb, 2010):

$$\mathbf{C} = \frac{E}{1-\nu^2}\begin{bmatrix} 1 & \nu & 0 \\ \nu & 1 & 0 \\ 0 & 0 & \dfrac{1-\nu}{2} \end{bmatrix} \qquad (2.41)$$

and for plane strain:

$$\mathbf{C} = \frac{E}{(1+\nu)(1-2\nu)}\begin{bmatrix} 1-\nu & \nu & 0 \\ \nu & 1-\nu & 0 \\ 0 & 0 & \frac{1-2\nu}{2} \end{bmatrix} \qquad (2.42)$$

The matrix [**B**] also known as the strain-displacement matrix, is defined as (Adeeb, 2010):

$$[\mathbf{B}] = [\mathbf{O}].[\mathbf{N}] \qquad (2.43)$$

The [**O**] matrix is the operation matrix. For this example, it can be defined as (Adeeb, 2010):

$$[\mathbf{O}] = \begin{bmatrix} \frac{\partial}{\partial x} & 0 \\ 0 & \frac{\partial}{\partial y} \\ \frac{\partial}{\partial y} & \frac{\partial}{\partial x} \end{bmatrix} \qquad (2.44)$$

Therefore,

$$\mathbf{B} = \begin{bmatrix} \frac{\partial N_1}{\partial x} & 0 & \frac{\partial N_2}{\partial x} & 0 & \frac{\partial N_3}{\partial x} & 0 \\ 0 & \frac{\partial N_1}{\partial y} & 0 & \frac{\partial N_2}{\partial y} & 0 & \frac{\partial N_3}{\partial y} \\ \frac{\partial N_1}{\partial y} & \frac{\partial N_1}{\partial x} & \frac{\partial N_2}{\partial y} & \frac{\partial N_2}{\partial x} & \frac{\partial N_3}{\partial y} & \frac{\partial N_3}{\partial x} \end{bmatrix} \qquad (2.45)$$

Now the stiffness matrix of this element can be calculated:

$$\mathbf{K} = \int B^T.C.B.dv = t\int B^T.C.B.dA = t\int_{-1}^{1}\int_{-1}^{1} B^T.C.B dydx \qquad (2.46)$$

where t is the thickness of the element (Adeeb, 2010).

After computing the element stiffness matrices, they are assembled to create the global stiffness matrix (step 4). In this case, the global equilibrium equations are (Reddy, 1984):

$$\mathbf{K}.\mathbf{U} = \mathbf{F} \qquad (2.47)$$

where **K** is the global stiffness matrix, **U** is the vector of global displacements and **F** is the global vector of loads. From equation (2.45), displacements for each node can be computed as follows (step 5):

$$\mathbf{U} = \mathbf{K}^{-1}.\mathbf{F} \qquad (2.48)$$

Eventually, from the displacements, the strains and stresses for elements can be computed (step 6) (Reddy, 1984).

A piecewise implementation of the variational approaches describes the finite element technique. In these methods, the approximation functions are algebraic polynomials and the unknown coefficients indicate the values of the solution at a finite number of preselected points, called nodes. The variational approaches include the Ritz technique, the least-squares technique, the collocation technique, the Petrov-Galerkin and the Galerkin method (Reddy, 1984). All these approaches seek an approximate solution in form of a linear mixture of suitable functions. Among them, the Galerkin method has proved to be superior, mainly due to its simplicity and wider range of applicability (Reddy, 1984).

2.8.4. Discretization with Finite Elements

Discretizing the equivalent model with finite elements, as shown in Fig. 2.9, we can achieve a finite element equation for the solid medium as

$$\boldsymbol{K_u U} = F \qquad (2.49)$$

where $\boldsymbol{K_u}$ is the global stiffness of the solid elements, $\boldsymbol{U}$ is the global nodal displacement, and F is the equivalent global nodal force of the net pressure.

As only net pressure has contribution to F, Eq. (2.49) can be rewritten as

$$\boldsymbol{K_u U} - \boldsymbol{BP} = 0 \qquad (2.50)$$

where $\boldsymbol{P}$ is a vector of nodal net pressure, and matrix $\boldsymbol{B}$ transfers the net pressures into equivalent nodal forces. The conservation of the incompressible fluid in the fracture leads to its weak form as (Bao et al, 2014)

$$\int_{l_t}\left[-\nabla(\delta p).q + (\delta p)\frac{\partial w}{\partial t} + (\partial p)g\right]dl + \delta pq|_S = 0 \qquad (2.51)$$

where Δ is the gradient operator, δp is any allowable testing function, q is the fluid flux, l_t is the half fracture length at time t, and S is the collection of boundary conditions of flow. Therefore, a finite element equation for fluid flow within the fracture is cast as

$$\boldsymbol{K_w}(\boldsymbol{W})\boldsymbol{P} + \boldsymbol{LW} + \boldsymbol{H} = 0 \qquad (2.52)$$

where $\boldsymbol{W}$ is a width vector formed by the nodes on the fracture surface, $\boldsymbol{K_w}$ is the assembly of the flux stiffness of the fluid elements and is a function of $\boldsymbol{W}$, $\boldsymbol{L}$ is the assembly of the length of the fluid elements, and $\boldsymbol{H}$ includes the contributions of the fluid leak-off and the fluid injection (Devloo et al, 2006).

Taking time integration with Eq. (2.52), we have

$$\int_{tn}^{tn+1}[\boldsymbol{Kw}(\boldsymbol{W})\boldsymbol{P} + \boldsymbol{LW} + \boldsymbol{H}]dt = 0 \qquad (2.53)$$

The backward Euler scheme for time difference is used in this research. So according to Eq. (2.53) we have

$$\boldsymbol{K_w}(\boldsymbol{W_{n+1}})\boldsymbol{P_{n+1}}t - \boldsymbol{L}(\boldsymbol{W_{n+1}} - \boldsymbol{W_n}) + \boldsymbol{H}D_t = 0 \qquad (2.54)$$

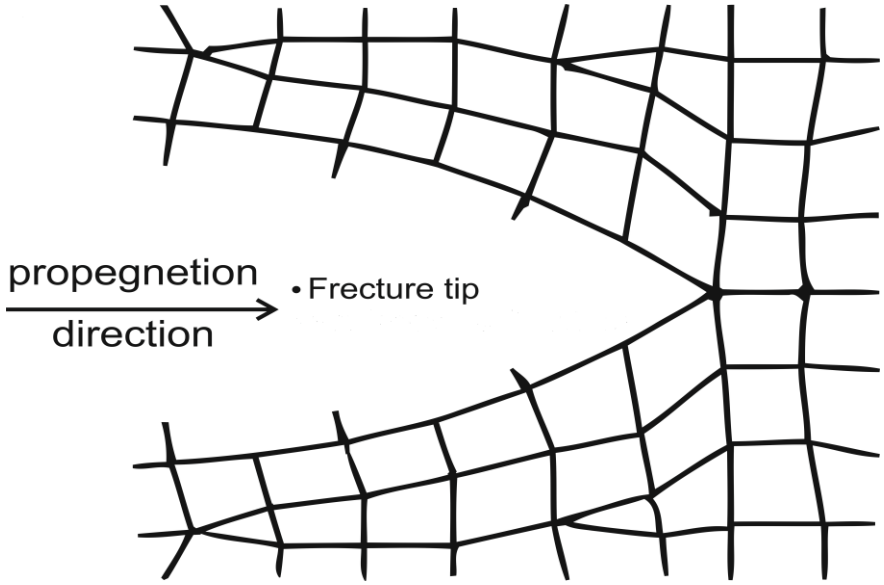

Figure 2.9: Discretization with finite elements

where $\boldsymbol{W_{n+1}}$ and $\boldsymbol{P_{n+1}}$ are the unknown fracture width and net fluid pressure at the $(n + 1)^{th}$ step, respectively, W_n is the known fracture width at the n^{th} step, and D_t is the time step between the n^{th} step and the $(n + 1)^{th}$ step.

Eq. (2.54) can be rewritten in an alternative way as (Garagash , Detournay, 2005)

$$\boldsymbol{K_w}(\boldsymbol{U_{n+1}})\boldsymbol{P_{n+1}}\Delta_t + \boldsymbol{L'}(\boldsymbol{U^f_{n+1}} - \boldsymbol{U^f_n}) + \boldsymbol{H}\Delta t = 0 \qquad (2.55)$$

where $\boldsymbol{U^f_{n+1}}$ and $\boldsymbol{U^f_n}$ are the displacements of the nodes on the fracture surface at the $(n + 1)^{th}$ step and n^{th} step, respectively, and $\boldsymbol{L'}$ determines the contribution of nodal displacements on the fracture surface to fracture widths. Note that $\boldsymbol{U^f_{n+1}}$ is a subset of $\boldsymbol{U_{n+1}}$, and $\boldsymbol{U^f_n}$ is known a priori (Bao et al, 2014).

In every step, Eq. (2.55) leads to a new equation written as

$$\boldsymbol{K_u U_{n+1} - B P_{n+1}} = 0 \qquad (2.56)$$

$\boldsymbol{U_{n+1}}$ and $\boldsymbol{P_{n+1}}$ can be obtained by solving the coupled Eqs. (2.55) and (2.56) (Bao et al, 2014).

2.8.5. Finite Volume Method

The finite volume method is a discretization method, which is well suited for the numerical simulation of various types (elliptic, parabolic or hyperbolic, for instance) of conservation laws. It has been extensively used in several engineering fields, such as fluid mechanics, heat and mass transfer and petroleum engineering. Some of the important features of the finite volume method are similar to those of the finite element method (Odeon, J.T, 1991).

In the early 1970's, the finite volume method was introduced. Exceptionally, in the Weighted Residual Method, the weighting function takes the form of the following (Sayma, 2009):

$$\bar{W}^i = 1 \qquad (2.57)$$

In the finite volume method, several weighted residual equations are generated by splitting the solution domain into sub-domains known as 'control volumes'. The weighting function is set as unity over the control volumes one at a time, and zero elsewhere. This entails that the residual over each volume must become zero.

A finite volume discretization is derived by starting from the integral form of the flow equations. The integral form (Sayma, 2009) is another way of representing the flow equations. For instance, the continuity equation for a control volume Ω with a surface boundary Γ can be stated as (Sayma, 2009):

$$\frac{\partial}{\partial t}\int_{\Omega}\rho d\Omega + \oint_{\Gamma}\rho\vec{U}d\vec{\Gamma} = 0 \qquad (2.58)$$

where $\vec{U}$= $\vec{u}$+ $\vec{v}$+ $\vec{w}$, **u**,**v**, **w** are the flow velocity vectors, *t* is the time and ρ is density (Sayma, 2009).

The above equations states that the rate of accumulation of fluid within domain Ω equals to the rate of the flux through its boundaries.

Similarly, integral formulations can be acquired for the momentum equations. For instance, the integral form of the momentum equation can take the form (Sayma, 2009):

$$\frac{\partial}{\partial t}\int_{\Omega}\rho u d\Omega + \oint_{\Gamma}\left(\rho u\vec{U} + p - \tau\right)d\Gamma \qquad (2.59)$$

where τ is the viscous flux given by:

$$\tau = \mu\left(\frac{\partial u}{\partial x} + \frac{\partial u}{\partial y} + \frac{\partial u}{\partial z}\right) \qquad (2.60)$$

The integral forms can be expressed for the y and z momentum equations in a similar way.

The finite volume formulation can initiate from this integral form. The basis of the Finite Volume formulation is shown by the fact that the variation of any quantity within a volume relies completely on the surface values of the fluxes.

The Finite Volume formulation begins by subdividing the solution domain into small volumes. Afterwards, the integral form of the conservation laws for each volume can be individually written. The global conservation can be recovered by adding up the fluxes of the sub-volumes (Sayma, 2009).

Let's take for instance the volume in Figure 2.10, which is splitted into 4 sub-volumes (Sayma, 2009).

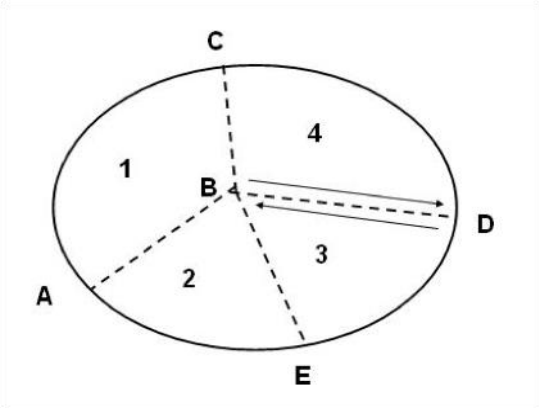

Figure 2.10: Finite volume subdivisions (Sayma, 2009)

The flux through the internal subdivisions cancels out. For intance the flux going through boundary BD of volume 3 is equal in magnitude and opposite in sign to the flux going through boundary DB of volume 4. A system of algebraic equations is formulated by working out the fluxes through all the boundaries on each sub-volume in terms of the field variable either at the volume center point or at the vertices. These equations are then solved for the unknown parameters (Sayma, 2009).

In this study finite volume approach was employed to discretize fluid flow equations. The theoretical and numerical tools to simulate the hydraulic fracturing problem in this study, including fracture mechanics, fluid mechanics, finite element method, finite volume method and fuzzy logic, were introduced in this chapter.

Chapter 3. Fuzzy model for hydraulic fracturing in Tabas coal mine

3.1 Introduction

In underground coal mines, the gas content of coal seam increases with depth and mining intensity and is a primary factor in mining safety and efficiency. Coal is a complex porous medium that consists of primary pores and fissures that result from tectonic movement, thus, it has a large amount of free space and multiple pore surfaces. Coal seam gas exists in adsorbed and free states. Only free gas can flow to a working face or be extracted. Coal bed methane is one of the main causes of underground coalmine explosions. Regardless of the negative financial and environmental impacts of coal bed gas, it is still considered as a fuel source (MacDonald, 1990).

Methane is present within the natural pores of coal and micro pores of coal matrix. Some of this methane is absorbed by coal molecules and bonded to them (Holditch, 1989). If underground coal seams are pressurized, coal molecules will be trapped within the seams. If there is a pressure drop (due to mining, construction of a front or gas drainage drilling), coal molecules will begin to move towards the low pressure area. As coal has high potential for absorbing methane, coal layers will accumulate a considerable amount of gas (Sereshki, et al, 2003).

Coal is of a porous nature with low permeability, its pore structure is far more complex than ordinary layers of other rocks (Soeder, 1991). Natural fractures, coal permeability and hydraulic fractures generate a path for gas and water to flow into coal seams from the cleats. Cleats in a coal seam are natural systematic fractures similar to those of sedimentary rocks (Kendall & Briggs, 1993). Cleat systems are

among the features of gas reservoirs that influence the economic feasibility of gas drainage from coal layers. This affects the success or failure of such projects, and is influential in the progress of gas drainage operations (Dhir, 1991).

Hydraulic fracturing is routinely applied to stimulation of coalbed methane wells around the world. Hydraulic fracturing can improve the permeability of coalbed methane reservoirs effectively, which is of great significance to the commercial production of coalbed methane. The basic task of mining engineers is to generate more coal and methane gas at a given level of labour input and material costs, ideal quality and maximum efficiency. To make these goals attainable, it is required to automate and mechanize mining operations. HF can result in significant cost reduction and higher levels of profitability for coalmines. Hence, mining engineers are continuously looking for different ways to mechanize mining procedures, especially gas drainage of coal mines that provides a great potential for reduced cost of ventilation, increased safety and improved profitability (MacDonald, 1990). Methane drainage operation is carried out in underground coalmines to prevent sudden gas and coal outbursts and to improve safety. Normally, coal beds possess low gas recovery. When the coalface is mined, a pressure difference is generated between the faces and somewhere deep inside the coal bed layer. This results in methane emission into the working face. Gas emission is further facilitated by horizontal and vertical fractures induced by the changing ground stress conditions (Sereshki, et al, 2003).

In this study, the development of an incremental mehtod to assess the methane production for different variables is investigated. The parameters affecting the

development of coal bed methane extraction by the HF technique are examined. As a case study, HF in the coal bed in PARVADEH 4 Tabas mine in Iran, which will be undergoing stress variation due to future mining activities, is investigated. Tabas Coal Mine is located about 60 km South West of Tabas City where it will be mined by longwall mining. The average coal bed gas content is in the order of 15 m^3/t (MacDonald, 1990).

3.2 Hydraulic Fracturing of Coal

Hydraulic fracturing is the process of creating fractures in rock and placing proppants into the fractures. Hydraulic fracturing is regularly used for stimulation of oil, gas, and coalbed methane wells around the world. The stimulation effect is achieved in coal seams as in other reservoirs, by producing conductive fractures, connecting the well to the coal reservoir. The conductivity of the fracture is commonly maintained by placing round and sieved sand proppant in the fracture channel. The proppant prevents the fracture faces from closing back completely on one another after the treatment (Jeffrey, 2012).

The coalbed methane (CBM) industry began after the realization that large methane contents of coals could often be produced profitably if the seams were dewatered and if a permeable path to the wellbore could be established for the gas.

Although hydraulic fracturing had been highly developed for conventional gas reservoirs of low-permeability, adjustments to the process were necessary for the coal because of the following phenomena (Jeffrey, 2012):

• The surface of the coal adsorbs chemicals of the fracturing fluid.

• The coal has an extensive natural network of primary, secondary, and tertiary fractures that open to accept fluid during hydraulic fracturing but close upon the removal of the fluid pressure, which is followed by damage, fluid loss, and treating pressures higher than expected (Jeffrey, 2012).

• Fracturing fluid can leak deep into natural fractures of coal without forming a filter cake.

• Multiple, complex fractures develop during treatment.

• High pressures are often required to fracture coal.

• Young's modulus for coal is much lower than that for conventional rock.

• Induced fractures in some vertical CBM wells may be observed in subsequent mine troughs.

• Horizontal fractures take place in very shallow coals.

• Fines and rubble result from fracturing brittle coal.

• Coal seams to be fractured may be multiple and thin, perhaps only 0.3 or 0.6 meter thick, requiring a strict economical method to the operations (Jeffrey, 2012). To produce the water and gas from the coal seam, holes are introduced that penetrate the casing, cement and a short distance into the coal. These holes are normally generated using perforating guns that consist of a string of shaped explosive charges that, when set off, shoot an explosively generated jet through the steel, cement and rock to a distance of 200 to 400 mm into the coal. On the other hand, a high pressure water and sand slurry can be directed at the casing to cut a hole or slot through the casing and into the coal (Jeffrey, 2012). Hydraulic

fracturing is then done by isolating the perforated section, generally by installing a plug inside the casing that presses against the casing to hold itself in place. Pumping fluid down the well then pressurizes the section perforated. The fluid pressure increases until the in situ stress and strength of the rock are exceeded, resulting in formation of a fracture. This fracture is extended as a hydraulic fracture by continuing to pump the fracturing fluid into it as it grows in size into the reservoir. The rate of growth of the fracture relies on the fluid injection rate, its overall shape and a number of other rock properties and fluid characteristics (Jeffrey, 2012).

The rate of fracture propagation diminishes with time and, generally after 15 to 20 minutes, growth has slowed to a few meters per minute. Hydraulic fracture treatments in coal would typically generate fractures extending to between 100 and 300 m, but smaller and larger fractures can be formed depending on the injection rates, seam thickness, fracturing fluid type and volume, and other features of the coal, surrounding rock, in situ stress and treatment execution. Volumes used per fracture treatment range from a few hundred liters for test fractures up to up to around one million liters. Average treatments might be approximately 250,000 liters in volume. Injection pressures rely on the depth of the interval being fractured and generally range from 10 MPa to 40 MPa. Average pressures might be 25 MPa. Both the volume injected and the pressure responses are dependent on the features of the site and the stimulation design (Jeffrey, 2012). Figure 3.1 demonstrates hydraulic fractures in a horizontal production well and a coal seam which is commonly isolated by thick shale and claystone, acting as natural barriers to vertical movement of groundwater. A fracking fluid unit, wastewater ponds,

borehole casing, gas bearing formation, pre-existing fault and location of induced seismicity were shown in the figure.

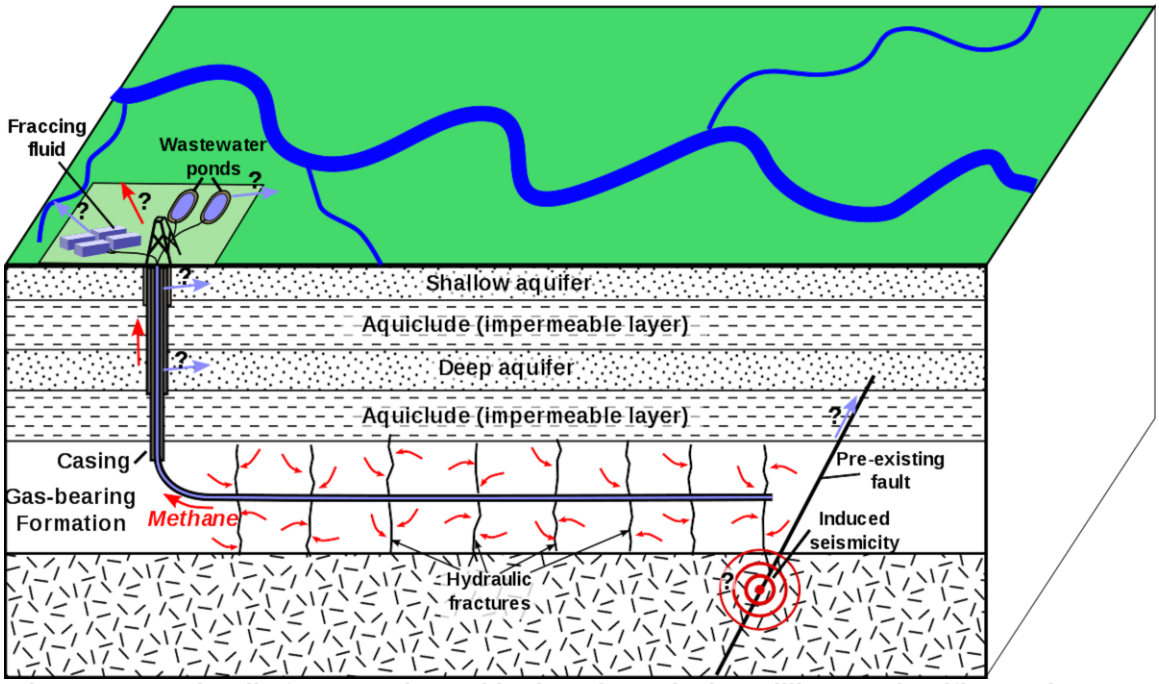

Figure 3.1: Hydraulic fractures in coal bed methane (John Williams Scientific Services Pty Ltd, 2012)

3.3 Injection of fluids and proppants in hydraulic fracturing

In general, it is necessary to inject fluids and proppant into the well to initiate fracturing in the coal seam and to keep the fractures open so that gas and water can flow to the well. Injection takes from tens of minutes to a few hours (Taleghani 2009).

The fracture faces expose a large area of the seam to the lower producing pressure, allowing the water and gas to drain directly into the propped fractures at an accelerated rate (Economides & Martin 2007). Hydraulic fracture treatments

are designed to place a propped conductive fracture in the coal seam that will efficiently stimulate production from the seam. The stimulation effect achieved relies both on the conductivity and size (length and height) of the fracture and on the permeability and thickness of the coal seam. Effective stimulation of a low-permeability seam needs longer moderate conductivity hydraulic fractures, while stimulation of a high-permeability seam demands shorter high-conductivity fractures (Economides & Martin 2007).

The fluids and particles should only be injected into the target coal layer and not the units above and below. This can be achieved through accurate subsurface characterisation so that perforation and subsequent injection only happens at the target coal layer. Nevertheless, some fracture treatments are designed to generate a fracture that propagates vertically through several adjacent thin layers because stimulating each layer individually would not be cost effective. The fracturing fluid is mainly made up of water, with the next largest component being the proppant, which is transported into the fractures to hinder them from closing once the high fluid pressure is removed. Proppant is generally sand but can also be nut shells, ceramics or bauxite (Beckwith 2010).

Some hydraulic fracturing fluids also contain either a gel mixed in with the water to increase viscosity or a friction-reducing additive. Viscosity is a measure of a fluid's resistance to flow. The main difference between fracturing with water or 'slickwater', which is water with a friction reducing additive, or a water-gel mixture, is that the increase in viscosity from the addition of gel allows more proppant to be moved into the fractures (APLNG 2013b). Fracturing with gel may need a volume

of up to 1.2 percent of additives, compared to water fracturing which generally holds a 0.1 percent volume of additives (APLNG 2013b). Most operators in Australia use water-gel mixtures (APLNG 2013b; Golder Associates 2010b).

A range of other chemicals are employed including acid, biocides, stabilisers, pH buffers and breakers. A summary of the fracturing fluids and proppants utilized is provided in Table 3.1. The fluid composition and volume changes during injection are tailored to suit the site-specific condition at each well. The usual order of operations involves the following considerations (Economides & Martin 2007):

If there is significant calcium carbonate present in the coal, then a dilute mix of acid and corrosion inhibitors is injected to dissolve it. Acid is also employed to stabilise pH and to clean the perforation tunnels. Injection of high pressure water to initiate fracturing using corrosion inhibitors, clay stabilisers, biocides and optionally gelling agents continues until a drop in pressure is recorded that signifies initiation of fracturing. If a gelling agent is utilized then ‘breaker’ chemicals are progressively added to the slurry to breakdown the gel and decrease the viscosity close to that of water to make it easier to extract the injected fluid back. A small volume of water or uncrosslinked gel is injected at the end of the treatment to flush the last slurry to the perforations so that no proppant is left in the well. The typical gelling agents are natural polymers such as guar gum derived from the pods of the guar bean (Economides & Martin 2007).

Table 3.1: Summary of the fluids and particles used in hydraulic fracturing fluid in Australia (Economides & Martin 2007; Golder Associates 2010b; APLNG 2011; AGL 2011; Santos 2011; QGC 2011; Arrow Energy 2012b).

Injected substance	Purpose and notes	Used materials
Water	Fractures the coal when injected under high pressure. Volume of water required is ~0.2 to 1.3 ML per well.	Bore water, farm pond water or groundwater previously extracted from coal seams is often used
Proppant	Keeps the fractures open once the high pressure fluid is removed. The latest technology advances in proppants include high strength ceramics and sintered bauxite	Sand, Resin-coated sand, Ceramics, Bauxite
Acid	Dissolves calcite in the coal prior to fracturing. Not all wells require this treatment because coal seams do not always contain calcite	Hydrochloric acid, Muriatic acid, Acetic acid
Gelling agent or Clay stabilisers	Increases the viscosity of the fluid, to allow more proppant to be carried into fractures. Not all hydraulic fracturing uses a gel; gel-free fracturing is termed 'slickwater'	Guar gum, Starches, Cellulose derivatives Polydimethyldiallylammonium chloride (Claytrol) Tetramethylammonium chloride (Claytreat 3C)
Crosslinker	Increases the viscosity of gelling agents. There are different crosslinkers for different gelling agents	Borate salt , Ethyl glycol, Isopropanol Disodium octaborate tetrahydrate Boric acid, Boric oxide

Injected substance	Purpose and notes	Used materials
Biocide	Limits or prevents growth of bacteria that could damage the gelling agent. The natural polymer gelling agents are good food for bacteria so they encourage bacterial growth - biocides kill these bacteria	Glutaraldehyde, Boric acid, Caustic soda 2,2-Dibromo-2-cyanoacetamide, bronopol Tetrakis(hydroxymethyl)phosphonium sulfate Sodium hypochlorite, Sodium thiosulfate
pH buffer	Keeps the pH of the fluid in a specified range. Required for the stability of crosslinked polymers	Acetic acid, Sodium hydroxide Potassium carbonate, Sodium carbonate,
Breaker	Chemically breaks the bonds of the gel in order to reduce the viscosity back to that of water. Only required if a gel is used	Hydrogen peroxides, Sodium persulfate Diammonium peroxidisulphate
Friction reducers	Reduce fluid surface tension	Oxyalkylated alcohol

3.4 Vertical and horizontal wells for gas drainage in HF

Vertical wells drilled in advance of mining to drain seam gas need stimulation to speed up the drainage process and to permit fewer wells to successfully drain the area targeted. A particular distance between wells might be 200 to 400 m. Hydraulically fractured wells at this spacing might need five years or more to drain 50 percent of the gas in place (Jeffrey, 1999). Closer spaced wells drain the gas more rapidly, but the total costs of drilling, completion and operating promptly

increase. Thus, employing vertical wells to drain gas before mining needs important lead-time and upfront investment. There is good scope for mines to partner with a coal seam methane producers to reduce the cost to the mine significantly. Hydraulic fracturing is regularly applied to stimulate coal seam methane boreholes (Jeffrey et al., 1997, Jeffrey et al., 1998, Diamond and Oyler, 1987).

Horizontal boreholes are drilled and hydraulically fractured in oil and gas reservoirs. The fracture treatments are undertaken to stimulate production and connect the horizontal well into layered reservoir formation. The horizontal layering in the reservoir invariably imparts a permeability anisotropy to the rock. Usually, the vertical permeability is significantly lower than the horizontal permeability. Furthermore, hydraulic fractures bypass the near wellbore damage zone, which can be an important factor in reducing the productivity of any horizontal well or drainage borehole. Hydraulic fractures can be placed in horizontal drain holes by running inflatable straddle packers on an injection string. Fluid bypass or even fracturing of the coal under the packers may take place (Jeffrey, 1999).

Several trials of placing hydraulic fractures in coal layers have been carried out (Croft, 1980, Kravits, 1993, Jeffrey, 1999) with some success reported by Kravits. Special pumps and blenders are required if sand is included in the treatment, but some stimulation effect can be attained by employing only water. Fracturing horizontal wells have been developed in the petroleum industry and might be adapted to fracturing horizontal drain wells in coal seams (Croft, 1980, Kravits, 1993, Jeffrey, 1999). Potential of hydraulic fracturing, as a stimulating technique,

in the Parvade4 Tabas coal mine in Iran will be studied in the next sections. Vertical wells as an access way to the coal seam and horizontal well as a production well can be used in the Tabas coal seams.

3.5 Tabas Coal Mine

Tabas coal region is one of the most comprehensive coal resources in Iran. Tabas coal mine is located in the central part of Iran near the city of Tabas in Yazd Province and situated 75 km from southern Tabas. The mine area is a part of Tabas-Kerman coalfield. The coalfield is splitted into 3 parts in which PARVADEH region, with the extent of 1200 km² and 1.1 billion tones of estimated coal reserve, is the largest and main part for excavation and exploitation for future years (IMPASCO 2005). The coal seam has eastern-western expansion with reducing trend in thickness toward east. Its thickness ranges from 0.5 to 2.2 m but in most places it has a consistent 1.8 m thickness. The large volume of coal reserve and appropriate geometry of coal seams in Tabas have created an ideal condition for application of HF. The most important coal seam in the Tabas region is C1 with the average thickness of 1.8 m. Figure 3.2 shows Parvadeh 1, 2, 3, 4, central and east Parvadeh coal mine in the Parvadeh region, which are major resource of coking coal in central Iran (IMPASCO 2005).

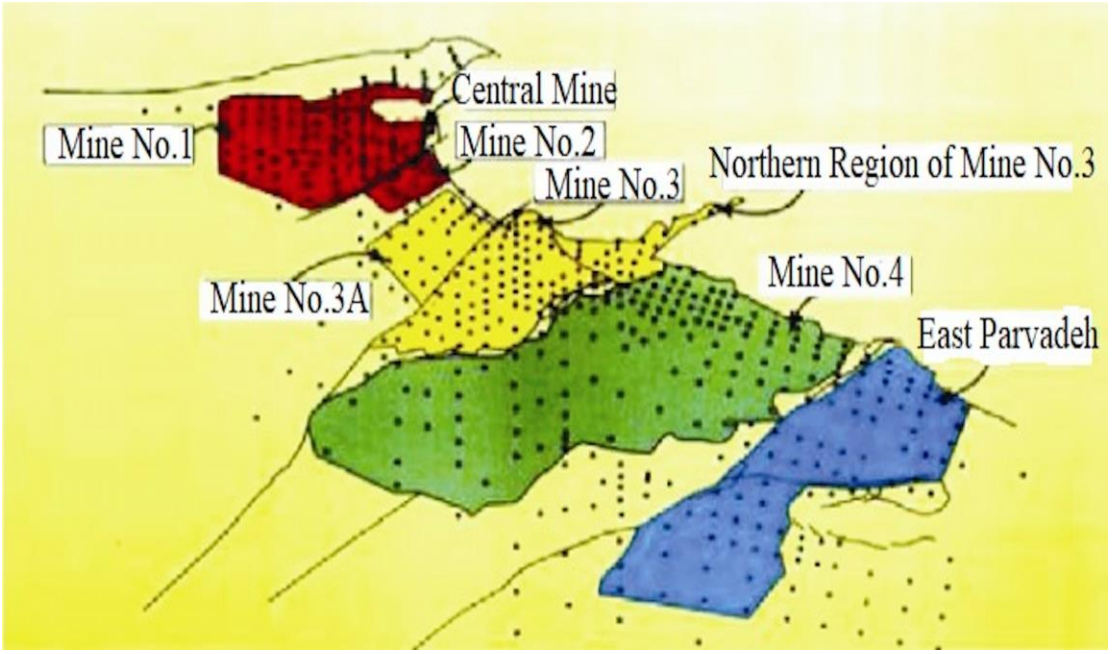

Figure 3.2: PARVADEH 4 Coal mine in PARVADEH Region (IMPASCO 2005)

In this region, the longwall mining technique has been employed for a section of the C1 seam in the mine No 1. The development and opening of the orebody have been carried out through inclined openings. Table 3.2 shows the average geomechanical parameters of the coal and the overburden rocks of PARVADEH 4 Tabas coal seam (IMPASCO 2005).

Table 3.2: PARVADEH 4 Tabas coal seams data (IMPASCO 2005)

Seam	B1	B2	C1	C2	D
Thickness (m)	0.4-0.9	0.5-1	0.8-1.1	0.4-0.8	0.4-0.7
Dip (degree)	9	8	7	9	11
Uniformity	Semi-uniform	Uniform	Semi Uniform-Uniform	Un-uniform	Un-uniform
Roof Type	Claystone	Siltstone	Siltstone	Siltstone	Siltstone
Floor Type	Siltstone	Claystone	Sandstone	Siltstone	Siltstone
Strength (MPa)	4.7	4.5	4.4	4.4	4.4
Reserve (ton)	29785000	72877000	64936000	30862000	7753000

3.6 Objectives of HF and the parameters affecting HF

The most important objectives of HF in a coal mine are to achieve: reduced costs; faster development; faster mining; safer mining; concentrating production at fewer locations; achieving higher production rates per shift; mining with smaller underground crews; smaller capital expenditure per extracted ton of coal; working under protectively supported roofs and more productive crews.

To take advantage of HF in a coal seam, a number of parameters should be considered. Seam dip, seam thickness, seam uniformity, seam floor condition, seam roof condition and gas concentration are some of the most important parameters that affect the potential of coal seam gas to be extracted by HF (Robert 2002). Due to high quantity of methane gas in PARVADEH Tabas coal mine the factor of gas concentration is not considered in this study.

3.6.1 Seam dip

Coal seam's dip is the angle at which coal deposits are inclined to the horizontal plane. Most coal gas drainage activities occur in flat or nearly flat seams. Usually, seams with low slope are more amenable for HF. Seams with slope of over 35 degrees have low potential for hydraulic fracturing. The application of HF turns out to be more complex with increase in seam slope. The best operational conditions are level layers (Ataee, 2009) .

3.6.2 Seam thickness

The thickness of the seam and its regularity are key parameters in coal seam hydraulic fracturing and great irregularities cannot be accommodated. The thickness that can be worked, at present, ranges from 0.5m and 5m. Where coal

seams are limited in thickness and the individual seams within the coal measures are normally less than 0.5 m thick, hydraulic fracturing may be utilized to link separate seams over a target horizon of 2 to 5 m (Ataee, 2009).

3.6.3 Seam uniformity

The effect of faulting on the geomechanics of HF is one of the most difficult issues to estimate. In some cases, the presence of faults or jointing can have a dominant effect on the geomechanics of a retreating mining operation. If there are complex geological conditions such as faults and seam pinch-outs, the applicability of HF will be minimized. The amount of coal seam displacement and the number of faults present over the length of a seam are very important parameters that affect the condition of the working face and the decision to mechanize the operation of the seam. In this study, the displacement index (I_m) as a factor to measure geological disturbances has been used as follows:

$$I_m = \frac{m}{t} \qquad (3.1)$$

where m is the displacement of a seam by faults and t is the thickness of the seam.

Table 3.3 indicates the level of seam uniformity with respect to the displacement index. In this classification, seam uniformity ranges from 0 to 1, where seams with an index I_m =0 are completely uniform and seams with a displacement index of more than 1.5, are considered to be non-uniform (Unrug and Szwilski, 1982).

Table 3.3: Seam uniformity classification (Unrug and Szwilski, 1982)

Seam uniformity Condition	Seam Uniformity Score	Seam Displacement index
Uniform	1-0.6	0-0.05
Semi-uniform	0.6-0.35	0.5-1
	0.35-0.2	1-1.5
Non-uniform	0.2-0.13	1.5-2
	0.13-0.08	2-2.5
	0.08-0.04	2.5-3
	0	3

3.6.4 Roof conditions

During the hydraulic fracturing process, the fractures should be kept open in order to extract the methane gas but if the roof of coal seam is not strong enough, it will push the fractures and close them. Also after hydraulic fracturing in coal seam, due to cutting coal seam by shearer machines, strong roof is unavoidable. Both operational experience and research results have demonstrated that roof stability is relative (Unrug and Szwilski, 1982). For an unstable roof, certain methods are necessary to monitor and change the factors contributing to the unstable conditions and to upgrade its stability after HF.

Quantitative techniques are available to evaluate the propensity of roofs to cave in. These techniques use different parameters such as lithological sequences, amount of roof convergence at the gob edge, lack of support over a time period before caving, seismic wave velocity, drill core strength, average frequency of bedding plane and rock strength and bed separation resistance. The following empirical equation is used to determine the roof strength index (Unrug and Szwilski, 1982).

$$Q_r = 0.016 \times \sigma_c \times K_1 \times K_2 \times K_3 \times \frac{m}{K-1} \qquad (3.2)$$

where Q_r is the roof strength index, σ_c is the average uniaxial compressive strength of the core (kg /cm^2), K_1 is an factor that considers the reduction in strength from the laboratory to a field, K_2 is a factor to consider the reduction in strength with creep loading, K_3 is a factor to consider for reduction in strength with rise in humidity, m is the thickness of the immediate roof (cm) and K is a swelling coefficient with a value between 1.3–1.5. The roof strength index represents several design parameters which are based on a roof classification system (see Table 3.4). Table 3.5 indicates the values of various factors for different kinds of roofs (Unrug and Szwilski, 1982).

Table 3.4: Roof strength and time exposure classification (Unrug and Szwilski, 1982)

Roof type	Roof strength index	Description
Unstable	$0 \le Q_r \le 18$	After exposure, roof caves in immediately or after a short delay
Low stablility	$18 \le Q_r \le 35$	Roof very difficult to control. Full of cavities, fractures and fissures, caves in easily
Medium stability	$35 \le Q_r \le 60$	Easily to be caved. From fractured roof with local falls to fairly good roof
Stable	$60 \le Q_r \le 130$	Good roof with excellent caving properties to hardly any caving
Very stable	$Q_r \ge 130$	Very strong and very stable. Artificial caving is necessary

Table 3.5: K value for different rocks (Unrug and Szwilski, 1982)

Rock type	Sandstone	Mudstone	Siltstone
K_1	0.33	0.42	0.5
K_2	0.7	0.6	0.6
K_3	0.6	0.4	0.4

3.6.5 Floor conditions

The floor should be sufficiently strong to withstand intrusions. Intrusion of soft floors can perturb advancing and also make the roof conditions complex to control due to high convergence. During mining operations, some coal may be left as support. Stability of strata is remarkably influenced by the reaction of floors to any type of support, installed along or behind mining faces. If the design of the support is to be determined by a satisfactory rate of closure or deformation along a mining face and its ends, then, in order to ensure support balance and stability, the stratum pressure within the face area should be monitored. This necessitates: (a) constant pressure and deformation distribution along the face; (b) a floor bearing capacity beyond the effective stratum pressure applied on it through the supports. Where footwall rocks are delicate, support systems may fail by punching into the peripheral rock of ore bodies. The failure mode is equivalent to bearing capacity failure of a foundation and may be analysed as such. The floor rock bearing capacity is directly related to the uniaxial compressive strength of rocks. Generally, a higher strength would lead to a greater bearing capacity and a wider potential for HF of the coal layer (Hartman, 1987).

3.6.6 Seam reserve

Coal reserve is measured tonnage of coal that has been calculated to occur in a coal seam. The coal reserve should be adequately large to utilize hydraulic fracturing. It takes 15–20 days to drill the wellbore and install the equipment in order to begin the hydraulic fracturing. In case a coal seam is not thick and does

not accomodate sufficient gas to be a feasible target for production by itself, the HF will not be economical. A large coal reserve would result in lower installation cost per cubic meter of extracted coal bed methane (Ataee, 2005).

3.6.7 Coal Strength

Coal strength is one of the important factors that can affect in initiation and propagation of fractures in HF. As seen in Table 3.6, by increasing uniaxial compressive strength of coal, more shear force is required to overcome the coal strength (Peng and Chiang, 1984).

Table 3.6: Shear stress and uniaxial compressive strength of coals by considering stiffness (Peng and Chiang, 1984)

Coal Type	Uniaxial Compressive Strength (MPa)	Shear Stress (MP)
Soft	9.81	14.7
Medium	9.81-19.61	14.7-29.4
Hard	19.61-29.42	2.94-44.1

3.7 Membership degrees of effective parameters in hydraulic fracturing

A membership function is a curve that defines how each point in the input space is mapped to a membership value (or degree of membership) between 0 and 1. The membership degree quantifies the grade of membership of each element in the fuzzy set.

Seam dip is one of the major parameters that determine the HF potential of coal seams. A fuzzy membership grade of seam dip has been developed, as shown in Figure 3.3. It should be noted that “very low” is allocated a membership grade of 1.0 at a seam dip $\leq$8 degrees after which it gradually declines to 0. On the other

hand, “very high” means a membership grade of 0 for a seam dip ≤45 degree and gradually increases to 1.0 at a seam dip ≥50 degree. Other qualitative legends (low, medium and high) are defined as shown in Figure 3.3.

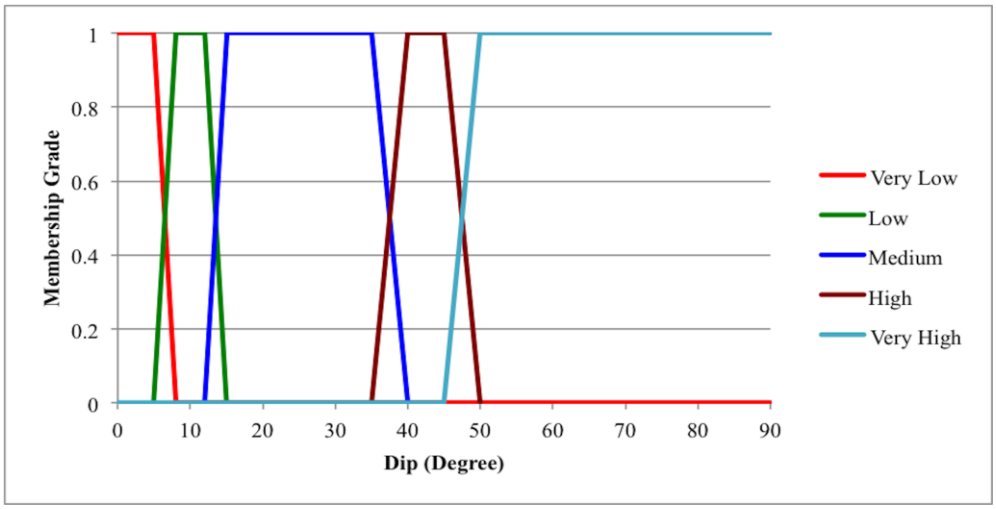

Figure 3.3: Membership function diagram for seam dip

Seam thickness is defined between 0 and 6 m. Figure 3.4 describes five qualitative legends ‘‘very low’’, ‘‘low’’, ‘‘medium’’, ‘‘high’’ and ‘‘very high’’. ‘‘Low’’ is allocated a membership grade of 1.0 when the thickness of the seam is between 0.8 and 1 m and 0.0 when the seam thickness is ≥1.4 m or ≤0.4 m. Other qualitative legends are defined as shown in Figure 3.4.

For seam uniformity three qualitative legends (low, medium and high) are defined as shown in Figure 3.5. For roof and floor conditions, qualitative legends are defined as shown in Figures 3.6 and 3.7 respectively. There are three qualitative legends (low, medium and high) for seam strength also, as shown in Figure 3.8. For seam reservoir, qualitative legends are defined as Figure 3.9. Seam

membership grades of hydraulic fracturing potential are defined by five qualitative legends (very low, low, medium, high, very high) are shown in Figure 3.10.

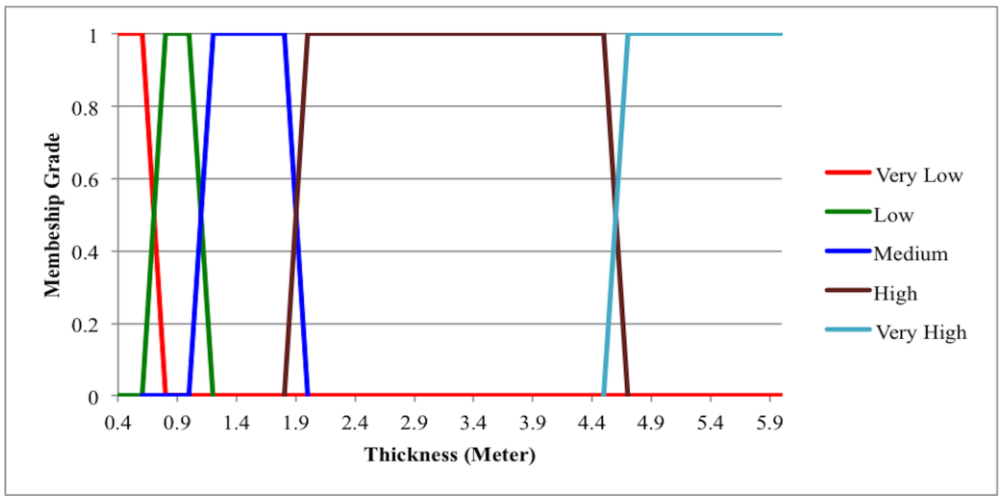

Figure 3.4: Membership function diagram for seam thickness

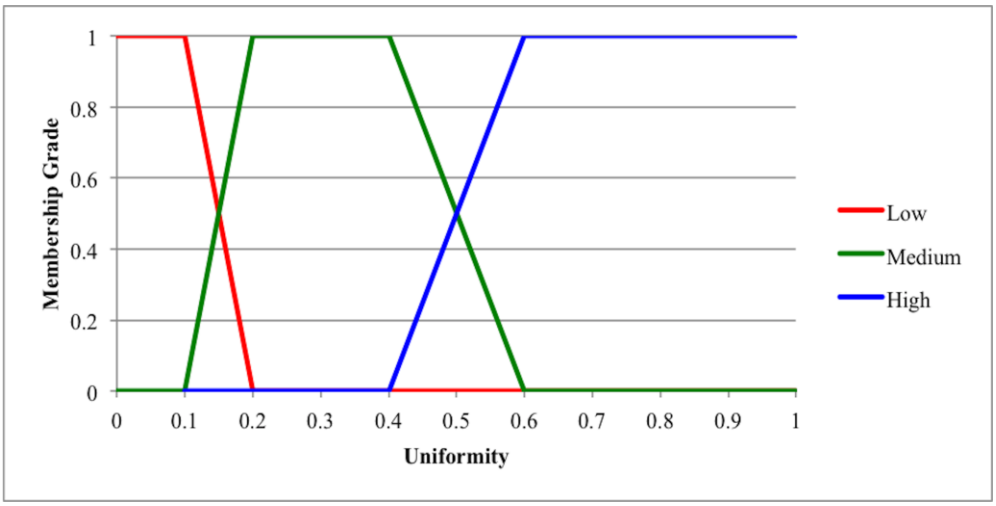

Figure 3.5: Membership function diagram for seam uniformity

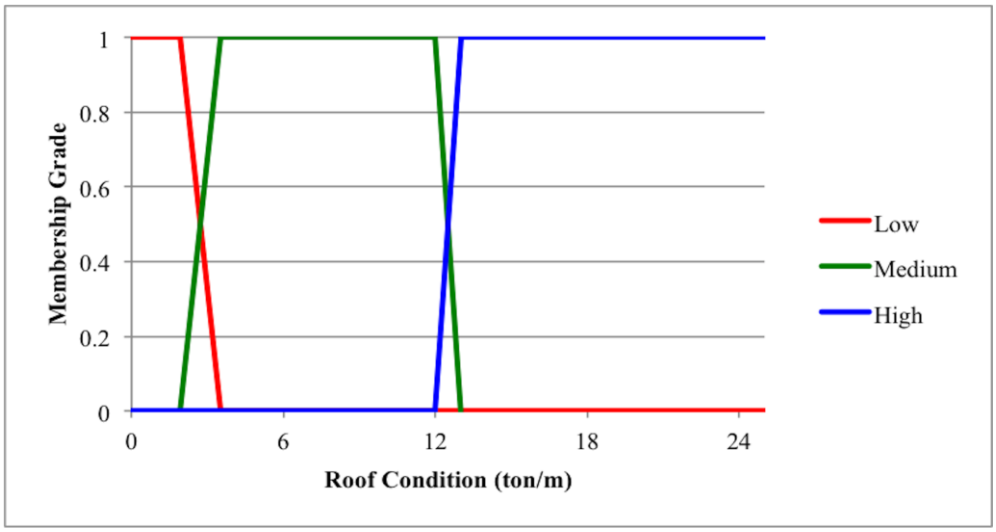

Figure 3.6: Membership function diagram for seam roof conditions

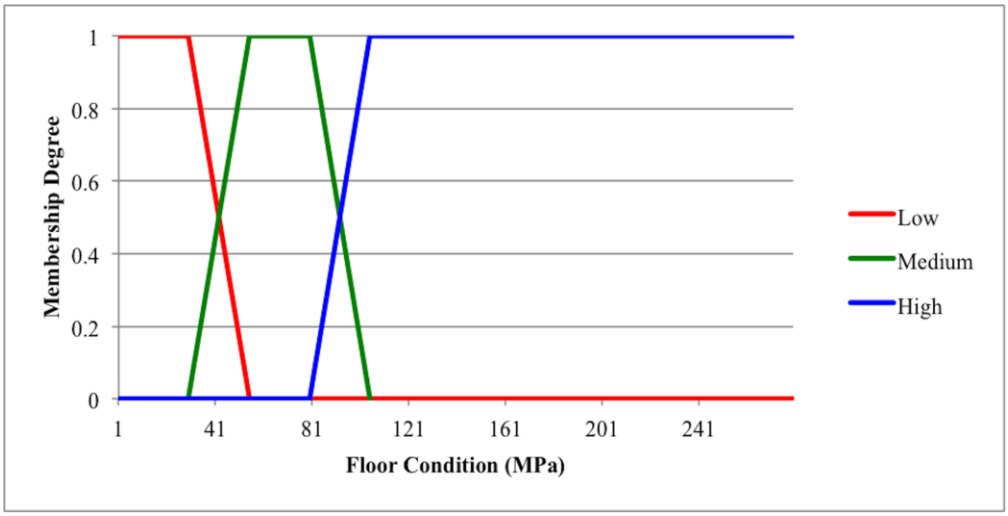

Figure 3.7: Membership function diagram for seam floor conditions

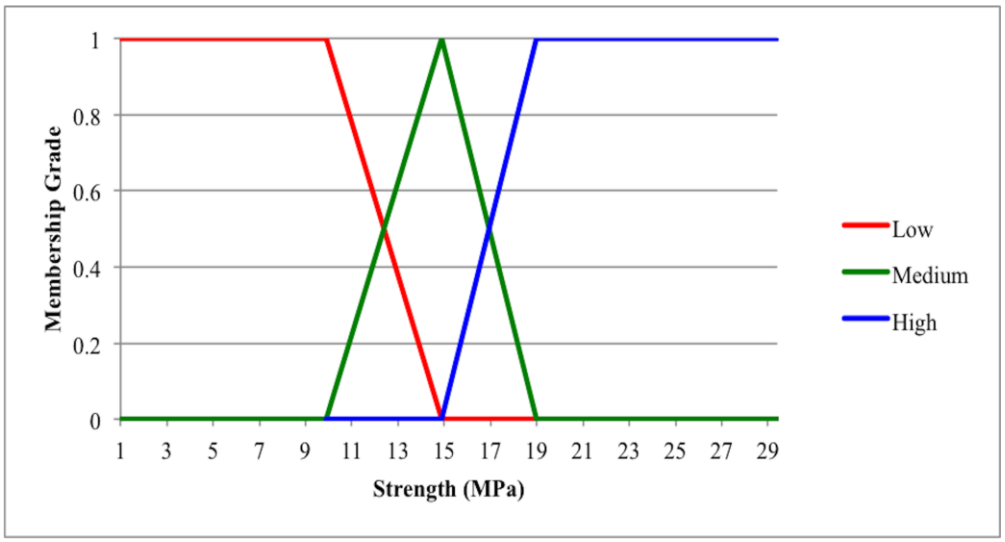

Figure 3.8: Membership function diagram for seam strength

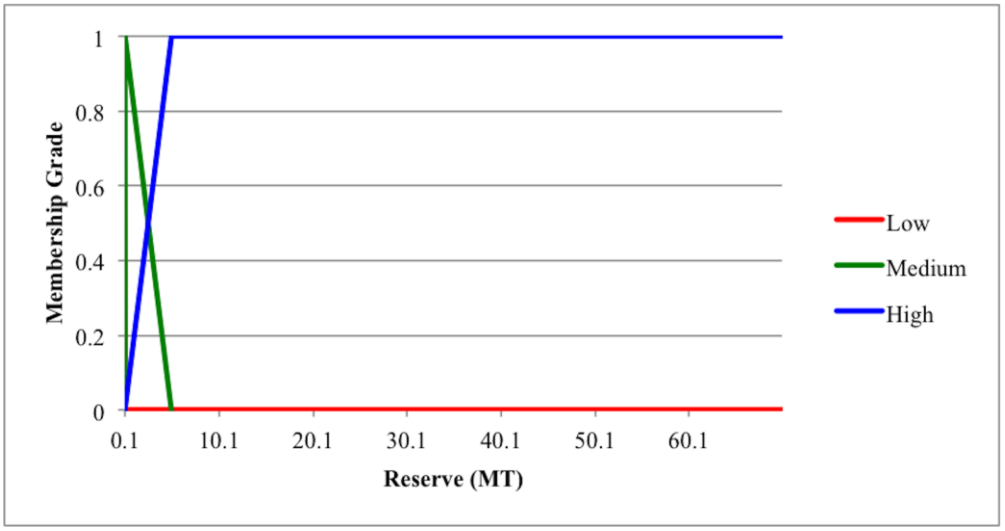

Figure 3.9: Membership function diagram for seam reserve

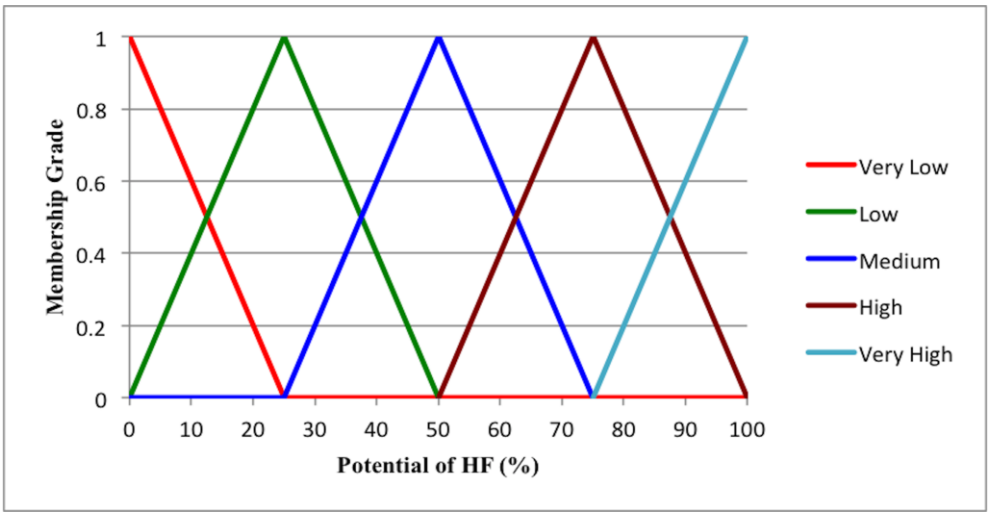

Figure 3.10: Membership function diagram for HF

Figure 3.10 shows the potential of hydraulic fracturing in the coal seam of Parvadeh 4 Tabas coal mine in percent and describes five qualitative legends ‘‘very low’’, ‘‘low’’, ‘‘medium’’, ‘‘high’’ and ‘‘very high’’. The horizontal axis shows the variation of hydraulic fracturing potential and the vertical axis shows the variation of membership grade. The classifications presented in Figures 3.3-3.10 are based on engineering judgment and current literature. The work of Ataee (2009) is a good example of coal mine mechanization using fuzzy logic.

3.8 Fuzzy rule-base

The main way to control a fuzzy logic system is to define the fuzzy rule–base in order to set up rules, which can combine different cases related to effective parameters in HF and the interaction of parameters with one another and eventually the overall effect on HF potential. At this stage, all input, intermediate and output variables and their interactions in a fuzzy logic system are determined. In order to predict the potential of hydraulic fracturing based on available inputs, a

number of simple rules in the form of IF-THEN statements are needed to relate inputs to suitable results.

In this study 7 input variables, 5 intermediate variables, 6 rule bases and 104 fuzzy rules are used. Seam dip and uniformity variables which are the most effective physical parameters in the structure of coal seam in one side and roof, floor and coal quality which are mechanical (strength) parameters in the other side and the coal reserve which is an economical parameter, are classified separately (Figure 3.11). The intermediate variables are used in fuzzy logic system in order to simplify the analysis of fuzzy rules and eventually predict the impact of effective parameters on HF potential. The rule base of seam structure is divided into two parts. The first part is related to seam dip and thickness as seam structure1 and the second part by considering seam structure1 and seam uniformity as seam structure2 was investigated. The rule base of strength parameters is also studied in two parts. The first part considers the quality of seam roof and floor as coal seam surrounding layers and second part considers the coal strength parameter and coal seam surrounding layers as strength factor. Fuzzy rule bases of the developed fuzzy model in this study were shown in tables 3.7-3.12.

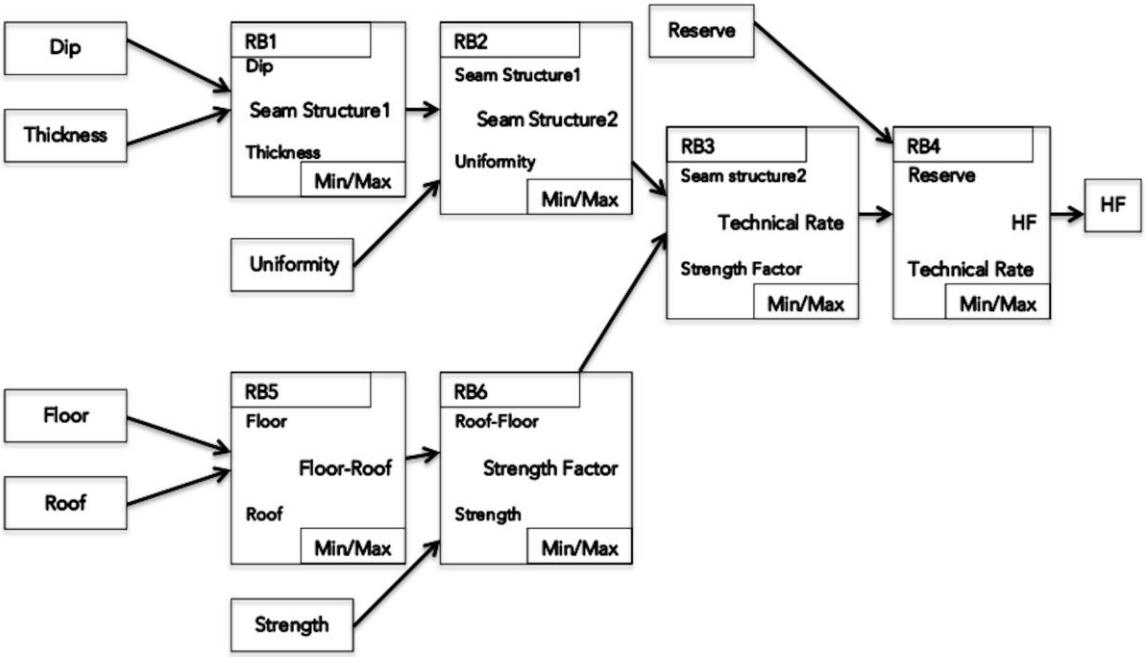

Figure 3.11: Fuzzy rule bases for determining the HF potential

Table 3.7: Fuzzy rule base of seam structure1

IF		THEN
Dip	Thickness	Seam structure1
Very low	Very low	Low
Very low	Low	Medium
Very low	Medium	Very high
Very low	High	Very high
Very low	Very high	Medium
Low	Very low	Low
Low	Low	Medium
Low	Medium	Very high
Low	High	Very high
Low	Very high	Medium
Medium	Very low	Low
Medium	Low	Medium
Medium	Medium	Very high
Medium	High	Very high
Medium	Very high	Medium
High	Very low	Very low
High	Low	Medium
High	Medium	Medium
High	High	Medium
High	Very high	Very low
Very high	Very low	Very low
Very high	Low	Very low

Very high	Medium	Low
Very high	High	Low
Very high	Very high	Low

Table 3.8: Fuzzy rule base of floor-roof

IF		THEN
Floor	Roof	Floor-Roof
Low	Low	Very low
Low	Medium	Very low
Low	High	Very low
Medium	Low	Low
Medium	Medium	Medium
Medium	High	Low
High	Low	Low
High	Medium	Very high
High	High	Low

Table 3.9: Fuzzy rule base of seam structure2

IF		THEN
Seam structure1	Uniformity	Seam structure2
Very low	Low	Very low
Very low	Medium	Very low
Very low	High	Very low
Low	Low	Very low
Low	Medium	Low
Low	High	Low
Medium	Low	Very low
Medium	Medium	Low
Medium	High	Medium
High	Low	Very low
High	Medium	Low
High	High	High
Very high	Low	Very high
Very high	Medium	Medium
Very high	High	Medium

Table 3.10: Fuzzy rule base of strength factor

IF		THEN
Roof-Floor	Strength	Strength factor
Very low	Low	Very low
Very low	Medium	Very low
Very low	High	Very low

Low	Low	Low
Low	Medium	Low
Low	High	Low
Medium	Low	Medium
Medium	Medium	Medium
Medium	High	Low
High	Low	Very high
High	Medium	High
High	High	Medium
Very high	Low	Very high
Very high	Medium	High
Very high	High	Medium

Table 3.11: Fuzzy rule base of technical factors

IF		THEN
Seam structure 2	Strength factor	Technical factor
Very low	Very low	Very low
Very low	Low	Very low
Very low	Medium	Very low
Very low	High	Very low
Very low	Very high	Very low
Low	Very low	Very low
Low	Low	Low
Low	Medium	Low
Low	High	Low
Low	Very high	Low
Medium	Very low	Very low
Medium	Low	Low
Medium	Medium	Medium
Medium	High	Medium
Medium	Very high	Medium
High	Very low	Very low
High	Low	Low
High	Medium	Medium
High	High	High
High	Very high	High
Very high	Very low	Very high
Very high	Low	Medium
Very high	Medium	Medium
Very high	High	High
Very high	Very high	Very high

Table 3.12: Fuzzy rule base of hydraulic fracturing potential

IF		THEN
Technical factor	Reserve	HF
Very low	Low	Very low
Very low	Medium	Very low
Very low	High	Very low
Low	Low	Low
Low	Medium	Low
Low	High	Low
Medium	Low	Very low
Medium	Medium	Medium
Medium	High	Medium
High	Low	Low
High	Medium	Medium
High	High	High
Very high	Low	Very low
Very high	Medium	Medium
Very high	High	Very high

Fuzzy rule-based systems are one of the most significant areas of implimentation of fuzzy sets and fuzzy logic. Constituting an extension of classical rule-based systems, these have been successfully used in a wide range of issues in various domains for which uncertainty and vagueness emerge in several ways. A fuzzy rule is described as a conditional statement in the form: IF x is A. THEN y is B. where x and y are linguistic variables; A and B are linguistic values determined by fuzzy sets on the universe of discourse X and Y, respectively. The seam structure and the strength can be considered as technical factors of a coal layer, which have a very important role in determining the potential of HF in a coal seam. The classifications presented in Tables 3.11 and 3.12 are based on engineering judgement and fuzzy logic.

3.9 Defuzzification

After determination of fuzzy output, a certain level of defuzzification of the potential of hydraulic fracturing must be executed (Figure 3.12). During this phase, a choice

of various techniques, such as the center of maximum (COM) and the mean of maximum (MOM) is available. The COM method was selected in this study.

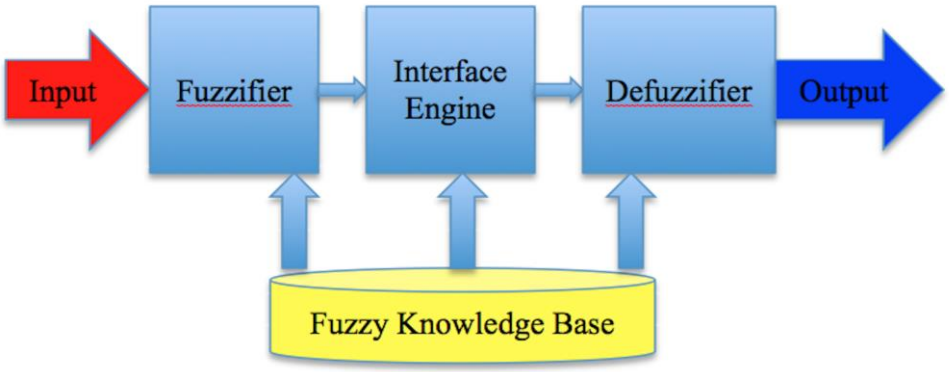

Figure 3.12: A Fuzzy Logic System

3.10 Results and Discussion

Due to productivity of the HF method, this technique is used as a process of gas drainage in this study in order to calculate the possibility of gas drainage in Tabas coal seams. The numerical value of HF potential is calculated by considering the technical restrictions. The main restrictions are, seam gradient, thickness, uniformity, roof and floor conditions, quantity of the reserve and coal strength. According to the fuzzy logic, the membership functions and then rule bases were established and eventually the numerical value of HF potential in coal seam of PARVADEH 4 Tabas coal seam was calculated.

The dominant natural conditions in coal seams are the most effective parameters in the determination of the potential of HF. According to the table 3.13 seam thickness and dip has great impact on the potential of hydraulic fracturing in each individual coal seam. Moreover, coal seams with higher uniformity have higher

potential of hydraulic fracturing. In this study, a fuzzy logic system was designed using the Fuzzy Tech 5.54 software. FuzzyTECH is the world leading family of software development tools for fuzzy logic and neural-fuzzy solutions (user's manual of the fuzzyTECH). All fuzzyTECH Editions contain all editors, analysers and tools to design a complete fuzzy logic system. Table 3.13 shows the result of the potential of HF in PARVADEH 4 Tabas coal seams.

Table 3.13: Potential of hydraulic fracturing in PARVADEH 4 Tabas Coal Mine

Seam	Dip (degree)	Thickness (m)	Uniformity	Roof (t/m)	Floor (MPa)	Strength (MPa)	Reserve (Mt)	Potential of HF (%)	
B1	9	0.65	0.3	10.2	83.4	4.7	29.875	31.83	Medium
B2	8	0.75	0.6	7.6	112.5	4.5	72.877	81.27	High
C1	7	0.95	0.58	11.2	273	4.4	64.936	94.6	High
C2	9	0.6	0.15	6.2	83.4	4.4	30.862	7.5	Very Low
D	11	0.55	0.15	7.08	83.4	4.4	7.753	7.5	Very Low

In order to construct a fuzzy system for calculating the potential of HF in coal seam, 7 input parameters, 5 intermediate parameters, 6 rule bases (diagram 3.11) and 104 fuzzy rules (Tables 3.7-3.12) were used. After constructing the fuzzy system, the potential of HF in PARVADEH 4 Tabas coal seam was calculated. The most significant parameter, which reduced the potential of using HF in this coalmine was low thickness of D and C2 seams and apart from thickness, seam uniformity is also very effective.

If a single coal layer is thin and does not consist sufficient gas to be a feasible objective for production by itself, hydraulic fracturing can be utilized to fracture stimulate a medley of seams with one treatment. Successful fracturing of a number of seams depends on the layer thickness, the thickness of the interburden seam between them and the stress acting in the layers and in the interburden seams.

3.11 Conclusion

The PARVADEH 4 Tabas coalmine is one of the largest coal reserves in the Tabas coal basin. Hydraulic fracturing can be utilized to create high conductivity channels in the coal layer. The conductive channels stimulate gas and water drainage rates by bypassing near borehole damage and forming a low pressure drain in the coal. Therefore, gas drainage increases at an increasing rate. Coal has always been a crucial source of energy and it's long-term total demand in the world has not been adversely affected and always shows an upward trend despite temporary fluctuations. Minimising costs, attaining higher production rates per shift and improving safety levels are the most essential issues to tackle in Iranian coalmines. Coal gas drainage plays an important role in exploitation of coal seam reserves. Coal seam gas drainage requires significant investment and detailed studies before making a final decision on the execution of HF.

The findings of this chapter can be summarized as below:

- The most important parameters (seam gradient and thickness, geological disturbances, seam floor conditions and seam roof conditions) that affect the viability of HF in coal seams were studied.
- Using the fuzzy logic theory, membership functions and fuzzy rule-bases were created and used to assess the potential for HF.
- 7 input variables, 5 intermediate variables, 6 rule bases and 104 fuzzy rules were used.
- Seam dip, thickness and uniformity variables (which are the most effective structural parameters of coal seam), and roof conditions, floor conditions

and coal quality (which are strength parameters), were classified separately.

- The coal reserve was also classified separately as an economical parameter.
- The results show a high potential for HF in B2 and C1 seams and low potential of HF for B1, C2 and D of the PARVADEH 4 Tabas coalmine.

The fuzzy modelling framework developed in this research is applicable in any unconventional gas reservoir, as it includes geological formation that has inclination, thickness, strength, roof, floor, and reserve. However, in each case, special considerations should be given to the geology, rock type and application.

Chapter 4. Coupled Hydro-Mechanical Modelling of Hydraulic Fracturing

4.1 Introduction

In this chapter, the development of a coupled approach to evaluate the hydraulic fracturing in a shale reservoir is investigated. A numerical model is developed to simulate the hydro-mechanical evolution of the fracture and of the surrounding rock in the finite element analysis framework.

4.2 Computational Fluid Dynamics

The Computational Fluid Dynamics (CFD) code, FLUENT, was used for numerical analysis of fluid flow. The code uses a finite volume-based technique to convert the governing mathematical equations to algebraic equations that can be solved numerically. The code is supplemented by a proprietary ANSYS based geometry construction and meshing engine, which allows users to build and mesh complex flow models to be used by the solver (Versteeg and Malalasekara, 1995).

Like most CFD programs, Fluent is based on the finite volume method (FVM). The finite volume method is a generalization of the finite difference method to unstructured meshes. Unlike the finite element method, FVM yields values across the entire volume contained within a cell. This has a particular advantage in preserving the flux of state variables across intercellular surfaces (Wilkes, 1999).

We are interested in using CFD to solve the Navier–Stokes equations or some coherent simplified subset of these. These are the set of equations which, taken together, completely describe continuum hydrodynamics. The momentum conservation equations are (Wilkes, 1999):

$$\rho\left(\frac{\partial u}{\partial t}+u\frac{\partial u}{\partial x}+v\frac{\partial u}{\partial y}+w\frac{\partial u}{\partial z}\right)=\frac{\partial p}{\partial x}+\mu\left(\frac{\partial^2 u}{\partial x^2}+\frac{\partial^2 u}{\partial y^2}+\frac{\partial^2 u}{\partial z^2}\right)$$
$$\rho\left(\frac{\partial v}{\partial t}+u\frac{\partial v}{\partial x}+v\frac{\partial v}{\partial y}+w\frac{\partial v}{\partial z}\right)=\frac{\partial p}{\partial y}+\mu\left(\frac{\partial^2 v}{\partial x^2}+\frac{\partial^2 v}{\partial y^2}+\frac{\partial^2 v}{\partial z^2}\right) \quad (4.1)$$
$$\rho\left(\frac{\partial w}{\partial t}+u\frac{\partial w}{\partial x}+v\frac{\partial w}{\partial y}+w\frac{\partial w}{\partial z}\right)=\frac{\partial p}{\partial z}+\mu\left(\frac{\partial^2 w}{\partial x^2}+\frac{\partial^2 w}{\partial y^2}+\frac{\partial^2 w}{\partial z^2}\right)$$

The the associated continuity equation is

$$\frac{\partial u}{\partial x}+\frac{\partial v}{\partial y}+\frac{\partial w}{\partial z}=0 \quad (4.2)$$

where, *u*, *v*, *w* are *x*, *y*, *z* components of velocity respectively. The continuity equation (equation 4.2), and the Navier-Stokes equations (equation 4.1) completely describe the motion of an incompressible fluid in a continuous medium in 3D (Wilkes, 1999). Fracture permeability can be defined by Darcy's Law for a limited range of low velocity and low flow rate. Typically, the motion of incompressible free fluid is described by the Navier-Stokes equations while Darcy's equation is used to model the filtration process. Darcy's law is a linear flow law, but Navier-stokes equations are nonlinear equations (Discacciati and Quarteroni, 2009).

Broadly, the strategy of CFD is to replace the continuous problem domain with a discrete domain using a grid. In the continuous domain, each flow variable is defined at every point in the domain. Appropriate initial and boundary conditions need to be applied in order to solve the Navier-Stokes and continuity equations (Kriesi, 2018). The boundary conditions in a 2D crack on the wall of a production well, which are used in this study, are as follows:

- No-slip boundary condition is used to bound fluid and solid regions.
- Velocity inlet boundary conditions are used to define the velocity and scalar properties of the flow at inlet boundaries.
- Pressure inlet boundary conditions are used to define the total pressure and other scalar quantities at flow inlets.
- Pressure outlet boundary conditions are used to define the static pressure at flow outlets.

In addition, material properties including density and viscosity for each zone are specified. It is important to accurately represent a boundary layer or fully developed turbulent flow at the inlet but in this study laminar flow is used. Multiple upstream meshes can be used in Fluent, giving users the flexibility to select the most efficient mesh combinations for different applications but tetrahedral mesh, is used in this study. The advantage of using tetrahedral mesh is that it gives an indication of how the mesh is likely to respond to the deformations experienced during simulation. This is in contrast to many traditional methods that may produce an initial mesh with good quality measures, but also with hidden deficiencies that can be revealed during simulation leading to poor accuracy or element collapse (Kriesi, 2018).

4.3 Coupled Hydro-Mechanical Modelling

Multi-physics problems are very difficult to solve by analytical methods and using numerical or experimental methods is the best way to solve them. Advanced techniques and the availability of powerful commercial software tools in both fluid and solid parts have made this numerical simulation possible (Benra et al, 2011). There are three different coupling approaches for solving coupled problems: full

coupling, two-way coupling and one-way coupling (Benra et al, 2011).

4.3.1 One-way Coupling

In one-way coupling, two separate sets of equations are solved independently over the same total time interval. Periodically, output from one simulator is passed as input to the other; however, information is passed in only one direction. For example, pore pressures might be sent from the flow code to the mechanical simulation code as input load to calculate the mechanical responses such as stresses, strains, and displacements. No information would be passed back from the mechanical model to the flow model, however. In most practical applications, the two simulators are in fact run independently. One can often gain valuable insight into the physical situation from one-way coupling, and it is clearly preferable to fluid flow alone (Fredrich et al., 1996, 1998).

4.3.2 Two-way coupling

This type of coupling is applied to problems where the motion of a fluid influences a solid structure and at the same time the flow of fluid is influenced by reaction of the solid structure. During the first time step, converged solutions of the fluid calculation provide the forces acting on the solid body. Then the forces are interpolated to the structural mesh like in one-way coupling and the solution from the structural solver is obtained with those fluid forces as boundary conditions. As a consequence, the mesh is deformed according to the response of structure. These displacement values are interpolated to the fluid mesh, which results in deformation of the fluid domain. This process is repeated until both force and displacement values are converged below the pre-determined limit (Benra et al,

2011).

4.3.3 Full Coupling

To develop a fully coupled simulator, a single set of equations incorporating all of the relevant physics must be solved simultaneously. As an example, the traditional porous flow equations for a rigid matrix would be modified to include terms for mechanical deformation. Full coupling is often the preferred method for simulating multi-physics problems since it would theoretically produce the most realistic results. Unfortunately, deriving a fully coupled multiphase flow simulator that models nonlinear, inelastic mechanical deformations is extremely difficult. Thus with fully coupled models, often the mechanical part is simplified by the assumption of linear elasticity (Lewis and Sukirman, 1993a,b; Lewis and Ghafouri, 1997; Osorio et al., 1999).

The present study describes a two-way coupling approach, which is somewhere between full and one-way coupling. In two-way (loose) coupling, there are two sets of equations, which are solved independently, but information is passed at designated time intervals in both directions between the two simulators. Laminar flow was used in this study. The flow model is coupled with the geomechanics model to simulate the interaction between fluid flow inside the fracture with rock deformations. For any time step, the pore pressures from the flow model are utilized as input for the geomechanics model for the calculation of stresses, strains, and displacements. The strains obtained from the gomechanics model are in turn employed to determine changes to the reservoir vaiables that are fed as input to the flow model. This iterative process continues until both (fluid and solid) models

are converged. The existing crack length and width were 200 mm. The borehole diameter and length were 30 cm and 200 cm respectively and it was drilled in a shale formation. The modelled domain was a cylinder with diameter of 150 cm. Velocity inlet (5 m/s), pressure inlet (9 MPa), pressure outlet (0 MPa) were used as boundary conditions in this model. Density of shale was considered 2.5 t/m^3 and laminar flow and tetrahedral mesh were used in this study. Two fixed supports were applied to the model, one on the input and another one on the output of the model. Figure 4.1 shows the horizontal borehole and the fracture inside a shale reservoir. The curve shows the fracture tip and x,y and z are the dedicated coordinate system for crack position.

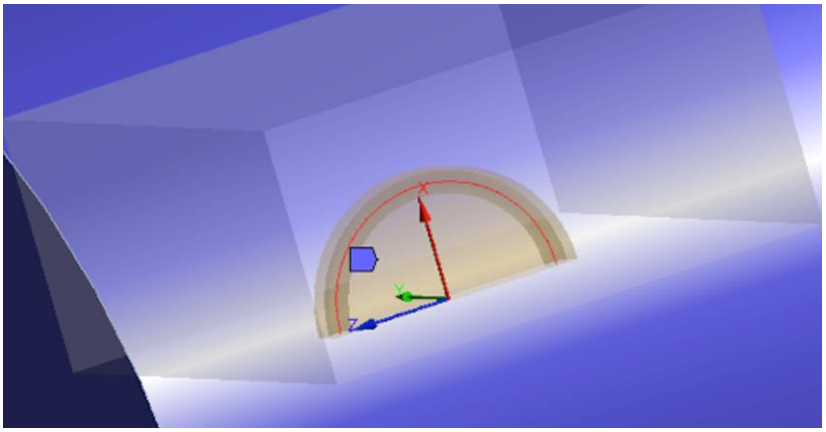

Figure 4.1: Semi-elliptical fracture and horizntal borehole inside a shale reservoire

The Ansys Workbench can be used to perform coupled simulations using two or more systems (ANSYS Mechanical and ANSYS Fluent in this case) using a System Coupling component. One-way or two-way fluid-structure interaction analysis can be set up in the Workbench by connecting a System Coupling component to the Mechanical system and to the ANSYS Fluent fluid flow analysis system. Figure 4.2 shows the hydromechanical coupling procedure in the Ansys

Workbench.

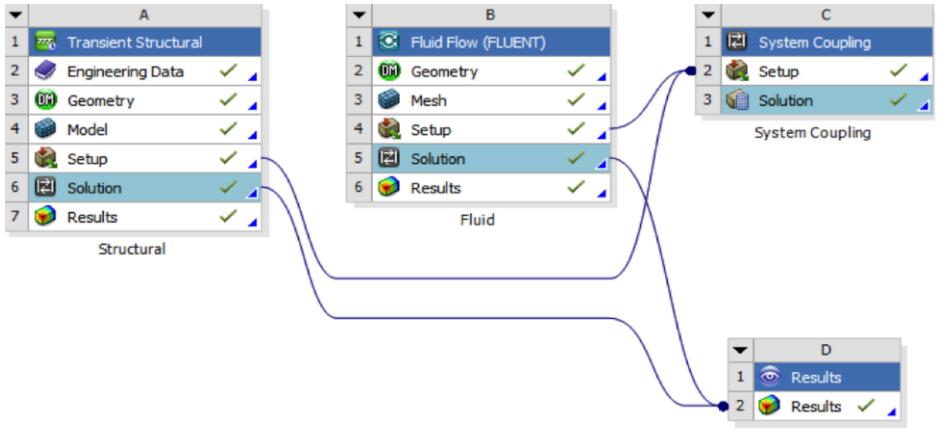

Figure 4.2: System coupling in Workbench

The fluid pressure at the start of pumping was 9 MPa and fluid velocity was 5 m/s. Young's modulus, Poisson's ratio and fluid viscosity were respectively 25 GPa, 0.2 and 0.0003 Pa.s. Figure 4.3 shows the hydraulic fracture after pumping high-pressure fluid and coupling of the two solvers.

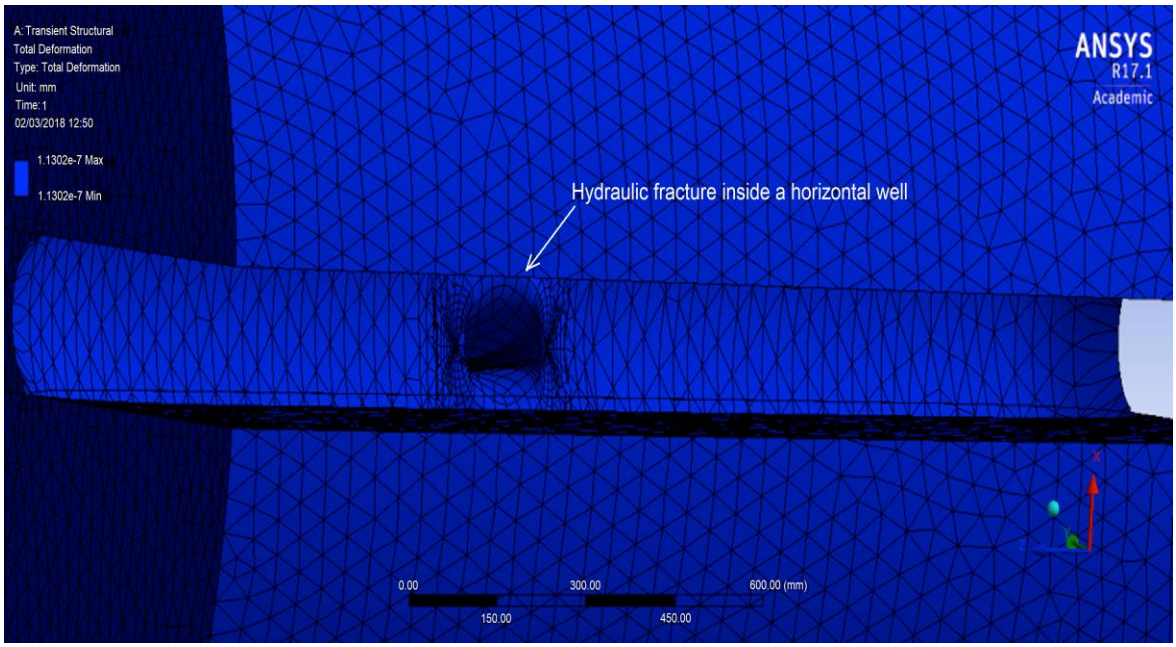

Figure 4.3: Fracture inside borehole after coupling

4.4 Model Validation

The results of the numerical simulations show that the numerical plan is well conducted and keeps a high rate of convergence. During simulation, the data were transferred successfully between the transient structural analysis and fluid flow analysis after the chosen coupling iterations. All simulations were performed by using minimum iteration=1, maximum iteration=5, time step size= 0.01s and total time=10s. The iterative procedure was continued until the convergence was achieved. Figure 4.4 shows the convergence between the fluid flow and static structural analysis in Ansys.

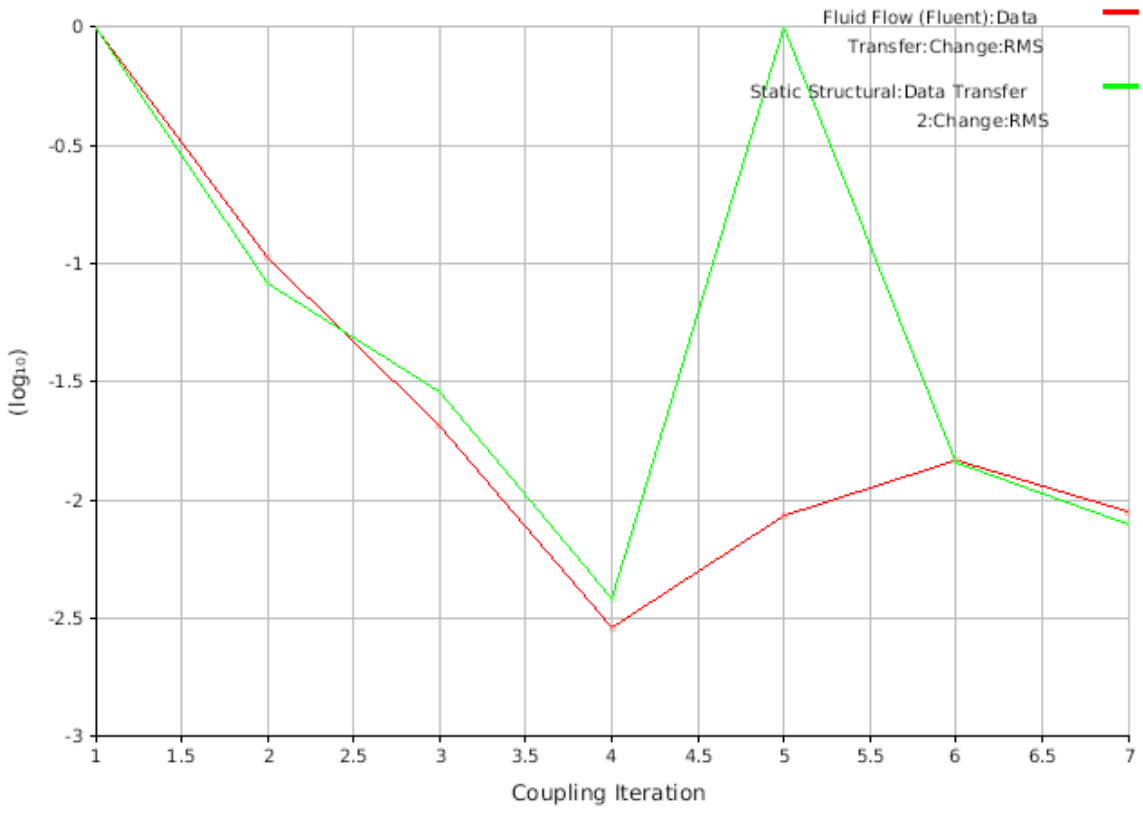

Figure 4.4: Convergence between fluid flow and static structural

In this part, the results for different cases are presented in order to show the validity of the model. There is no accurate solution to verify the model's accuracy beyond easy examples due to the complexity of the hydraulic fracturing problem. Geertsma and de Klerk (1969) presented an estimated solution for a two dimensional fracture with a Newtonian fluid. In this solution, the fracture length, fracture opening at the wellbore, and net pressure can be obtained as:

$$L(t) = 2\left[\frac{16E\acute{q}_0^3}{21\pi^3\mu}\right]^{\frac{1}{6}} t^{\frac{2}{3}} = 2.0 \times 0.539\left[\frac{E\acute{q}_0^3}{\mu}\right]^{\frac{1}{6}} t^{\frac{2}{3}} \quad (4.3)$$

$$W_{well}(t) = \left[\frac{5376\mu q_0^3}{\pi^3 \acute{E}}\right]^{\frac{1}{6}} t^{\frac{1}{3}} = 2.36\left[\frac{\mu q_0^3}{\acute{E}}\right]^{\frac{1}{6}} t^{\frac{1}{3}} \quad (4.4)$$

$$\Delta p_w = \left[\frac{21}{16}\mu \acute{E}^2\right]^{\frac{1}{3}} t^{\frac{-1}{3}} = 1.09\left[\mu \acute{E}^2\right]^{\frac{1}{3}} t^{\frac{-1}{3}} \quad (4.5)$$

where E' is plane-strain modulus of elasticity (E' =2G/(1-ν)), G is the shear modulus (1.6×10^6) and q_0 is the injection rate per unit height of the fracture h_f (q_0 =Q_0 /h_f). Geertsma's solution assumes ~~the~~ smooth closing surfaces as the boundary condition at the fracture tip ($\partial w(L,t)/\partial x = 0$), which is equivalent to Barenblatt's model for cohesive cracks. Hence, the results are not necessarily similar to the results of the model with the zero pressure boundary condition at the tips. The fluid storage in the fracture as the width changes with time is neglected and the flow rate is equal to the injection rate in Geertsma's model. No in situ stress was presumed in this solution to make differentiation simpler as pressure in Geertsma's model is net pressure.

The results of the FEM model are in agreement with those of the analytical solution

(Figures 4.5, 4.6 and 4.7) for a 10 minute constant rate injection of a Newtonian fluid. The fracture length and net pressure results are in close agreement, while the FE model predicts a slightly higher width at later time than the Geertsma's model. This could probably be due to the fact that the storage effect is neglected by the simplifying assumption in Geertsma's model. This inconsistency has also been reported by Yew et al. (1988) and Dahi (2009). The input data for this example is presented in Table 4.1.

Table 4.1: Details of input data

Young's Modulus (E)	Porosity (Φ)	Poisson's Ratio (v)	Injection Rate (Q)	Fluid Viscosity (μ)	Fracture Height (h)
35 GPa	20 %	0.3	5 bbl/min	100 cp	1000 mm

The bottom borehole pressure, plotted in Figure 4.6, deserves further attention. It indicates that the bottom borehole pressure decreases with time while the fracture width grows. This is due to the assumption of infinite height for the fracture (KGD geometry), which implies that longer fractures need less pressure to keep the same opening. Although, the pressure is rarely decreasing because the length of the induced fracture is usually greater than the fracture height, so the fracture height limits the fracture opening. In the KGD model, the net pressure gradient drops quickly with fracture length and reaches nearly a constant value.

The model has been examined with initial assumptions for the pressure distribution, but the solution converged quickly to the accepted range. The model

was able to achieve the results with less than 5% percent error in less than 10 iterations. The model was examined for different initial lengths for the hydraulic fracture to ensure that the results were not sensitive to the initial length of the hydraulic fracture in the model or the location of the initial fracture with respect to the finite element mesh.

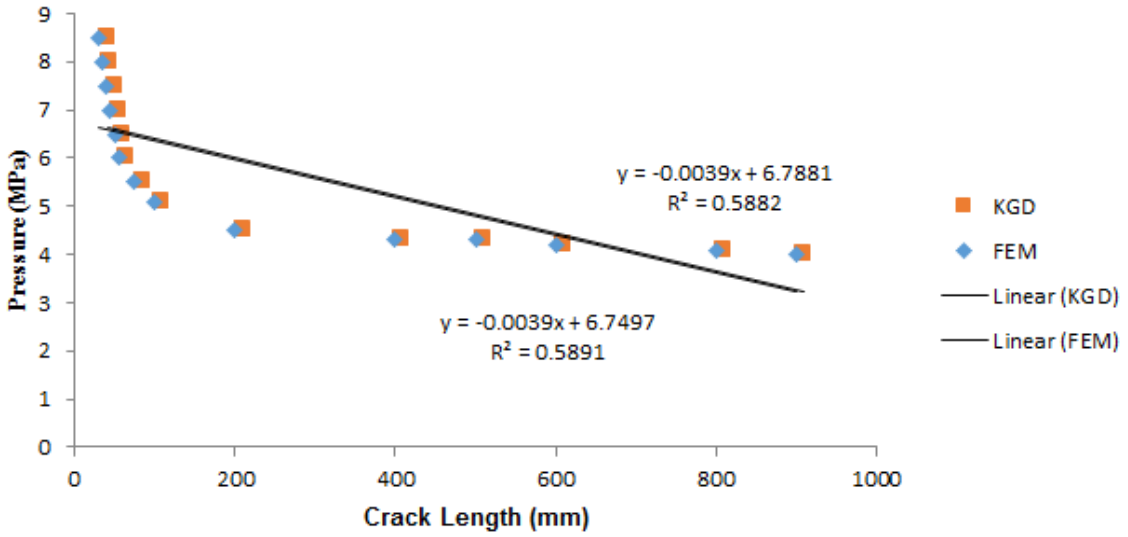

Figure 4.5: Variation of crack length with pressure

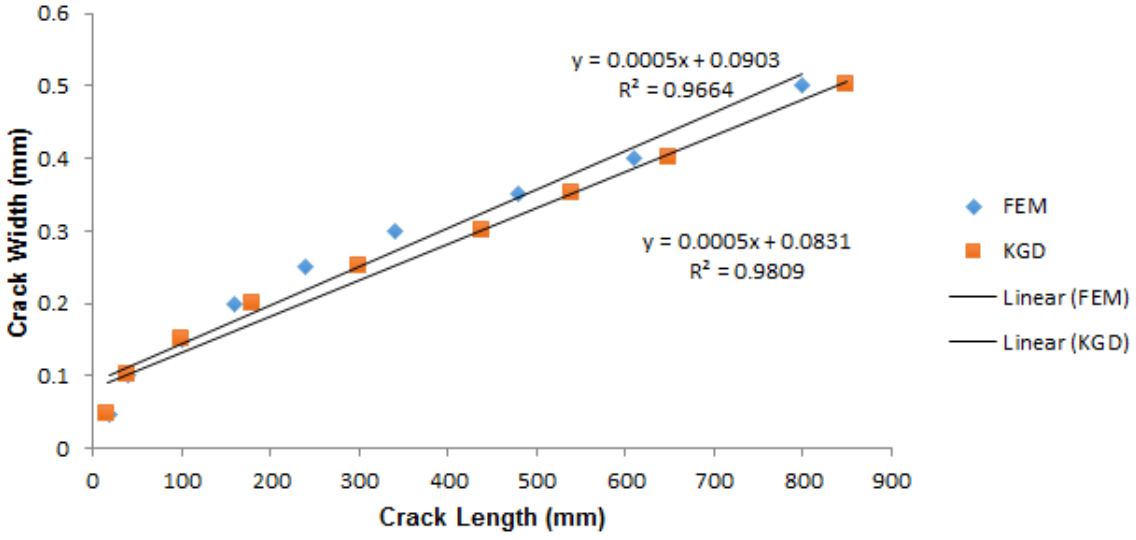

Figure 4.6: Variation of crack length with crack width

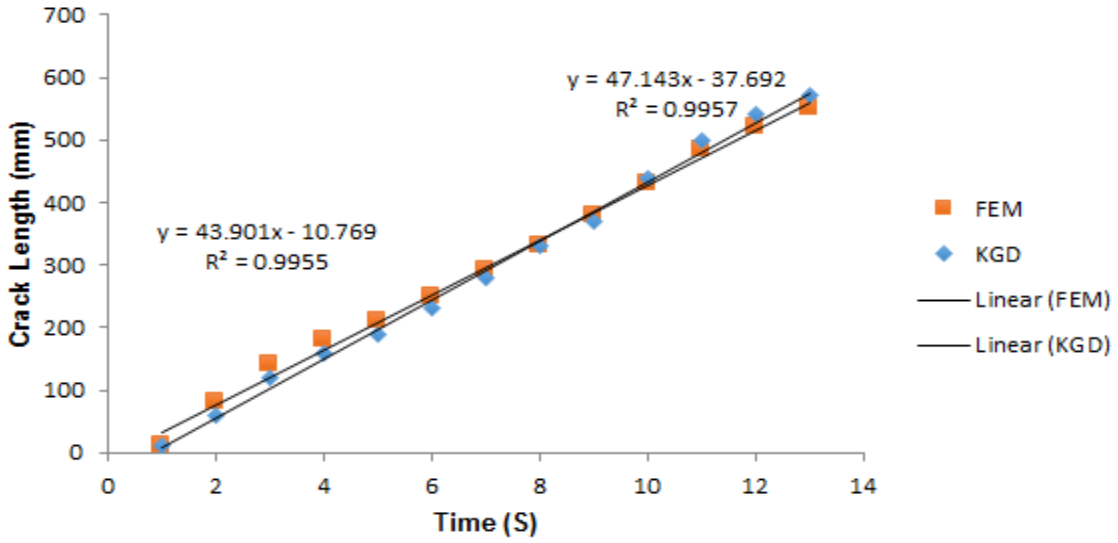

Figure 4.7: Variation of crack length with time

The fracture mechanics solution of Rummel and Winter was used to calculate the stress intensity factor. In this approach, the peak pressure (P_C) is expressed as (Rummel and Winter, 1982):

$$P_C = \frac{1}{h_0+h_a}\left(\frac{K_{IC}}{\sqrt{R}} + S_H f + S_h g\right) \quad (4.6)$$

where S_h and S_H are minimum and maximum in-situ pressures, respectively. P_C is the critical hydraulic pressure, R is the radius of the borehole, and f, g and h, are dimensionless functions of stress intensity factors that are calculated from normalized crack length of a/r, r being diameter of the borehole and *a* crack length.

$$f(b) = -2\left[\frac{(b^2-1)}{\pi b^7}\right]^{0.5} \quad (4.7)$$

$$g(b) = (\pi b)^{0.5}\left(1 - \frac{2}{\pi}\sin^{-1}\frac{1}{b}\right) + 2(b^2+1)\left(\frac{b^2-1}{\pi b^7}\right)^{0.5} \quad (4.8)$$

$$h_0(b) = 1.3\frac{b-1}{1+b^{1.5}} + 7.8\frac{\sin\left[\frac{b-1}{2}\right]}{2b^{2.5}-1.7} \quad (4.9)$$

$$h_a = (\pi b)^{0.5}\left(1 - \frac{2}{\pi}\sin^{-1}\frac{1}{b}\right) \quad (4.10)$$

where b is equal to 1+a/R.

In addition to the confining pressure, the injected fluid pressure is applied on borehole wall and fracture plane. Despite such complex stress conditions, stress intensity factor around the crack tip can be easily formulated using the superposition principle of stress intensity factors.

$$K_I(P_m, P, P_a) = K_I(P_m) + K_I(P) + K_I(P_a) \quad (4.11)$$

In the above equation, K_I specifies the stress intensity factor for mode I. P is the applied pressure and P_a, which is expressed by P_a= P(x,0), determines the pressure distribution in fracture direction from x=(R,-R) to x=(R+a, R-a) (Dos Santos, et al. 2011).

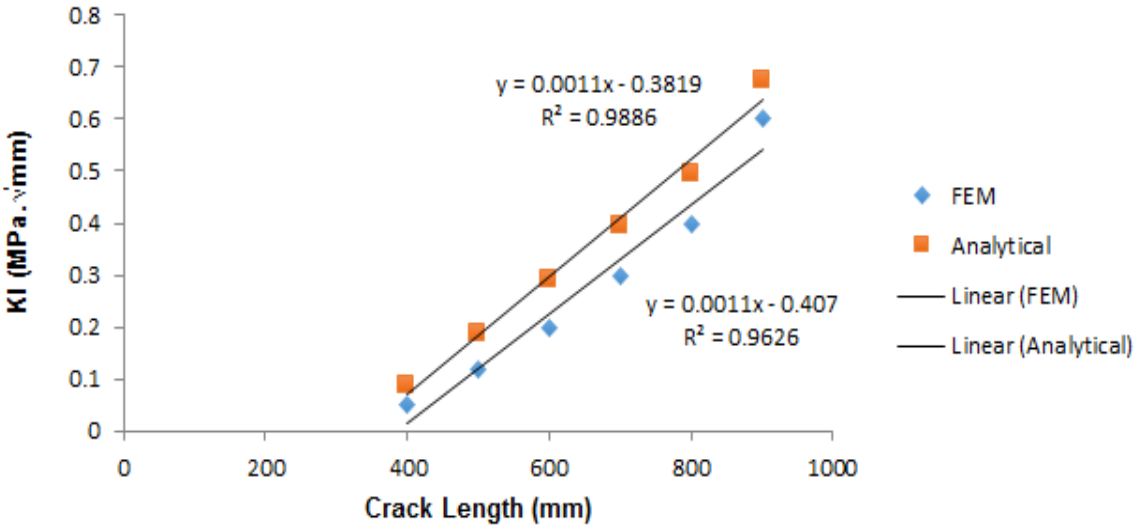

Figure 4.8: Variation of stress intensity factor with crack length

The variations of stress intensity factor as a function of the crack length in the reservoir domain are shown in Figure 4.8. The results show a reasonably good

agreement between the analytical and FEM results. Despite the complex loading conditions and various loads in hydraulic fracturing, stress intensity field in the crack tips, created from any source of loading, can be formulated using the principle of superposition of stress intensity factors.

4.5 Sensitivity Analysis:

In this section the sensitivity analysis of fracturing fluid viscosity is presented. Hydraulic fracturing is a process that is surrounded by uncertainty. The classical KGD model of hydraulic fracturing which is widely used in the Oil and Gas industry to assist in the design of the hydraulic fracturing treatment is considered. The variation of the viscosity in the ranges of 0.1 Pa.s and 0.15 Pa.s was considered. The viscosity values are standard values which are being used in hydraulic fracturing studies.

The viscosity should have a high value to induce a wider crack, and hence a better proppant transport during the hydraulic fracturing process. For this purpose, cross linkers of the polymer chains have been used in industry to increase the viscosity significantly (Taleghani, 2009). Furthermore, for same volume of injected fluid, increasing the fluid viscosity increases the fracture width and decreases the fracture length. Figure 4.9 shows the effects of increasing the viscosity of the injection fluid on the pressure profile.

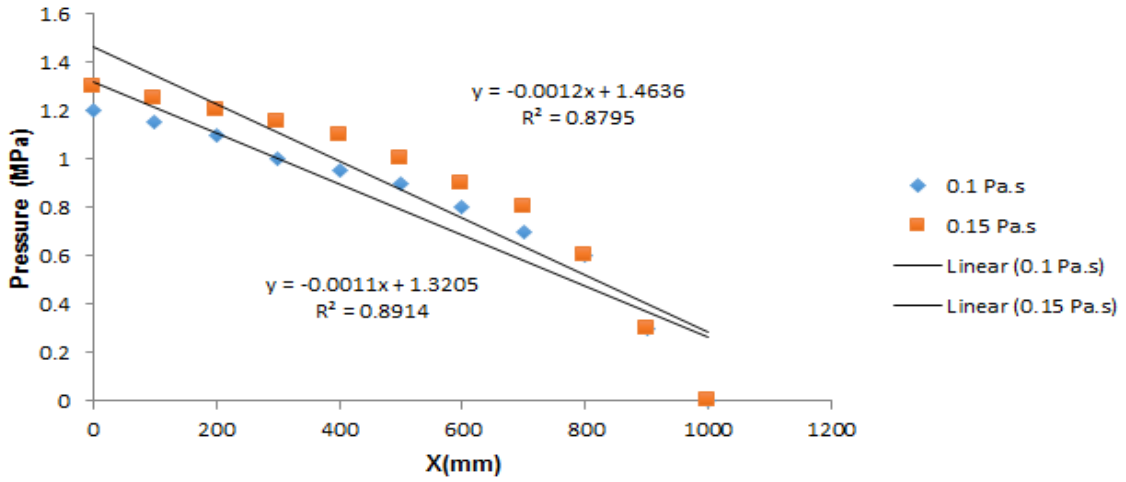

Figure 4.9: Variations of pressure and crack profile with different viscosities

4.6 Results:

The mechanical properties of the rock such as Young's modulus, and Poisson's ratio have significant influences on hydraulic fracturing operation. It is important to note that, these parameters are uncontrollable and are totally dependent to the rock formation properties, which arise from geological conditions. In the meantime, other parameters such as fluid viscosity and leak-off coefficients play important roles in designing a hydraulic fracturing fluid, which can simply change the hydraulic fracture opening.

Figure 4.10 shows the variation of stress intensity factor as a function of the crack length along the cohesive elements in the reservoir domain. The results indicate that increasing stress intensity factor would increase crack propagation. There is a slight deviation from linear relationship beyond crack length of 800 mm. This is likely to be due to sudden change of mesh quality and large deflection in the model. In the cohesive zone model (CZM), the fracture formation is regarded as a gradual phenomenon in which separation of the surfaces involved in the crack, takes place

across an extended crack tip, or cohesive zone, and is resisted by cohesive tractions (Barenblatt, 1962). The trend indicates that the stress intensity factor which is the magnitude of stress singularity at the crack tip increases by the growth of fracture length. Despite complex loading conditions and various loads in hydraulic fracturing, stress intensity field in the crack tips, created from any source of loading, can be formulated using the principle of superimposition of stress intensity factors. The numerical results of stress intensity factor and crack length were compared with the results of Asadi et al. (2013) and Dahi (2009) and showed good agreement.

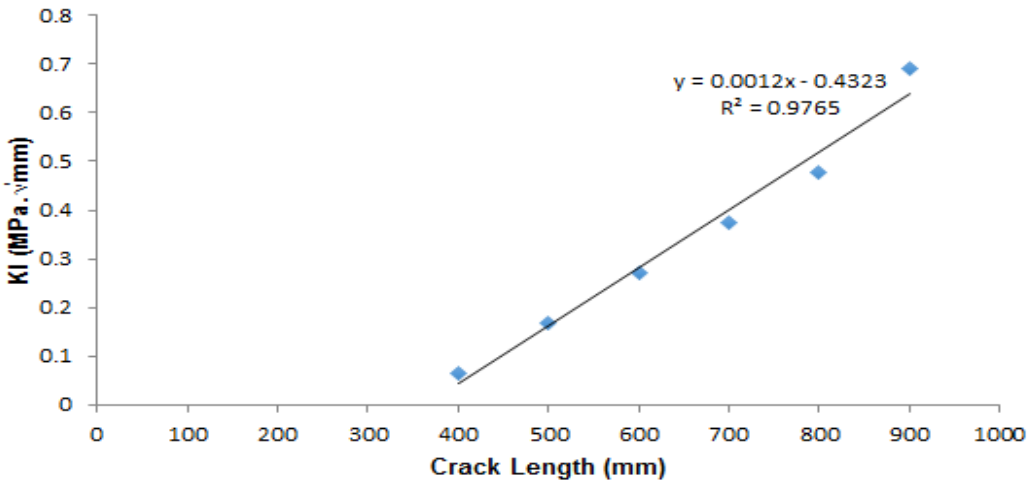

Figure 4.10: Stress intensity factor vs crack length

J-integral is a parameter that can be used for crack propagation analysis. Figure 4.11 shows the variation of J-Integral with crack length. It is seen that J-Integral increases with increasing the crack length. This can be attributed to the concept that with a growth in crack length, the released elastic energy in J-Integral ascends. The figure shows that in the first stage, the rate of variation of J-integral has a descending trend and after reaching a minimum value, the trend changes the

course and adopts an ascending approach. The results of the current study are in good agreement with the results published by Asadi et.al (2013).

The reason for this phenomenon can be explained by the fact that in the initial stages, the released energy is consumed to propagate and develop the cracks and to overcome the surface crack energy. Minimum value of J-integral in this figure shows that the crack has reached its final propagation phase after which, by increasing fluid injection, the crack does not propagate and causes an increase in elastic strain energy in the rock that makes the potential energy to grow up.

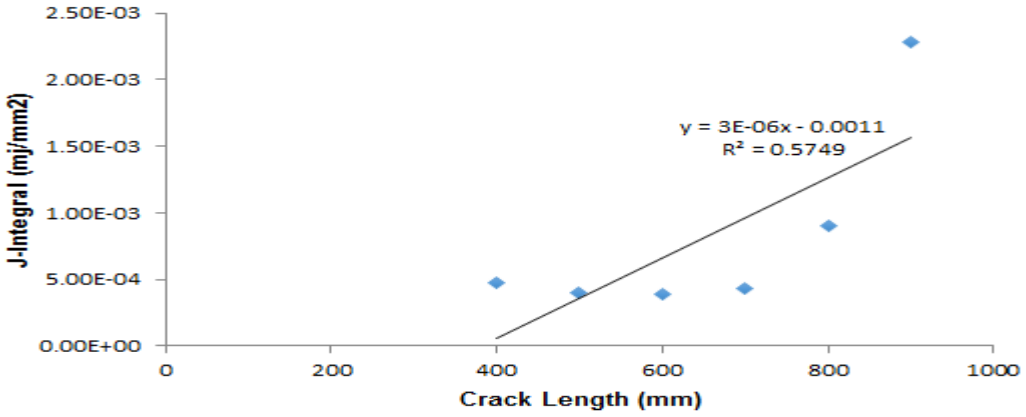

Figure 4.11: J-Integral vs crack length

Figure 4.12 shows the variation of critical pressure of crack propagation with changes in crack length at different pressures. As can be seen, by increasing the crack length, the critical crack propagation pressure decreases. It is shown that the bottom hole pressure drops with time while the fracture length increases. This result is a consequence of assuming an infinite height for the fracture (KGD geometry), which indicates that longer fractures require less pressure to maintain the same opening. The results were compared with the results of Dahi (2009) and

indicated good agreement.

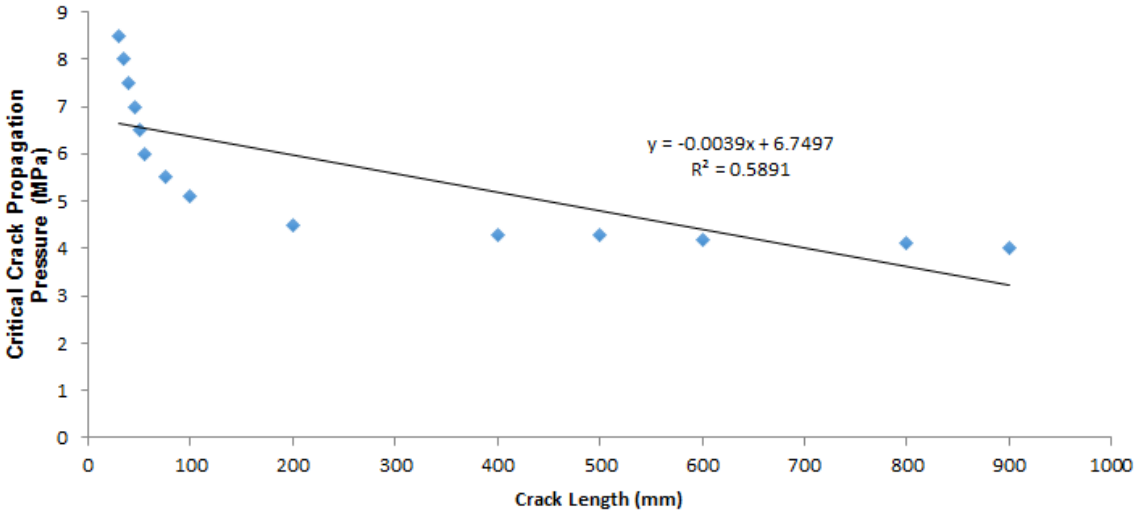

Figure 4.12: Critical crack propagation pressure vs crack length

Figure 4.13 shows the effect of Young's modulus on crack propagation. The results show that, by increasing elastic modulus from 25 to 55 GPa, the stress intensity factor has steeply increased from 0.25 to 0.7 MPa.mm^(0.5). It can be concluded that rocks with higher elastic modulus can be fractured easier. There is a slight no-linearity beyond Young's modulus of 40000 MPa. This is likely to be due to sudden change of mesh quality and large deflection in the model.

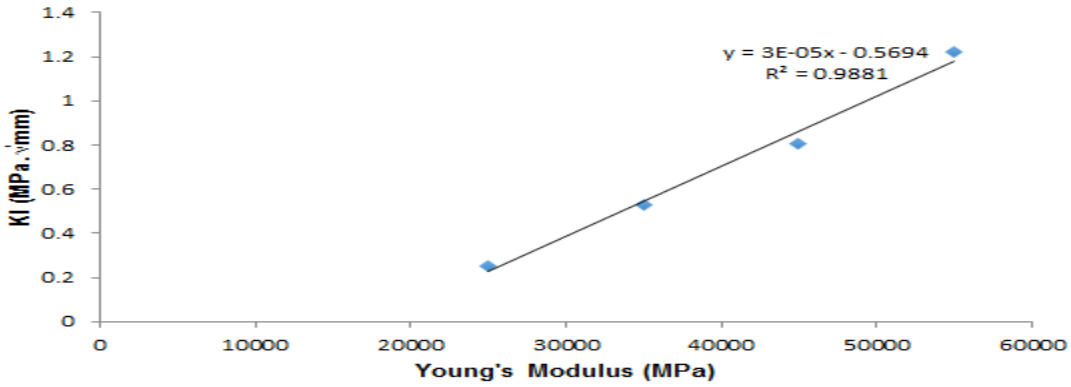

Figure 4.13: Young modulus vs stress intensity factor

Poisson's ratio indicates how much a rock that is shortened in one direction expands in the other two directions. The results show that increasing Poisson's ratio from 0.2 to 0.5, increases the stress intensity factor from 0.5 to 0.75 MPa.mm^(0.5) (Figure 4.14). So, based on the definition of Poisson's ratio, it can be concluded that any increase in this parameter would affect the local stresses as well as the extent of strain level and deformation near the crack tip, which can significantly increase the crack propagation.

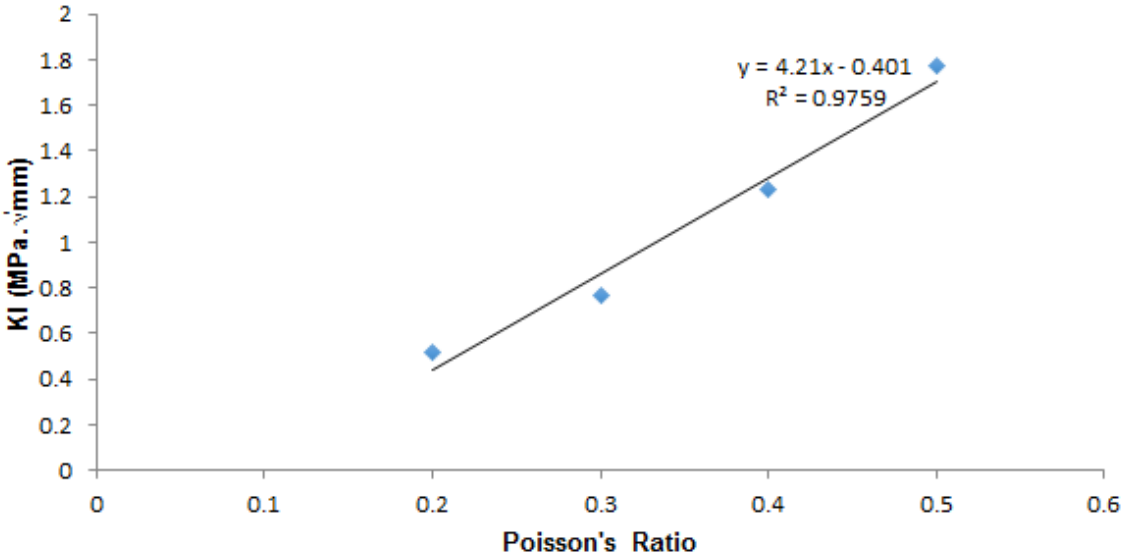

Figure 4.14: Poisson's ratio vs stress intensity factor

Figure 4.15 shows the variations of rock permeability versus confining pressure. As expected, the permeability decreases with the increase of confining pressure at the beginning and curves become less steep when confining pressure exceeds 20~25 MPa. The results of confining pressure versus permeability showed good agreement with the results of Liu et al. (2014).

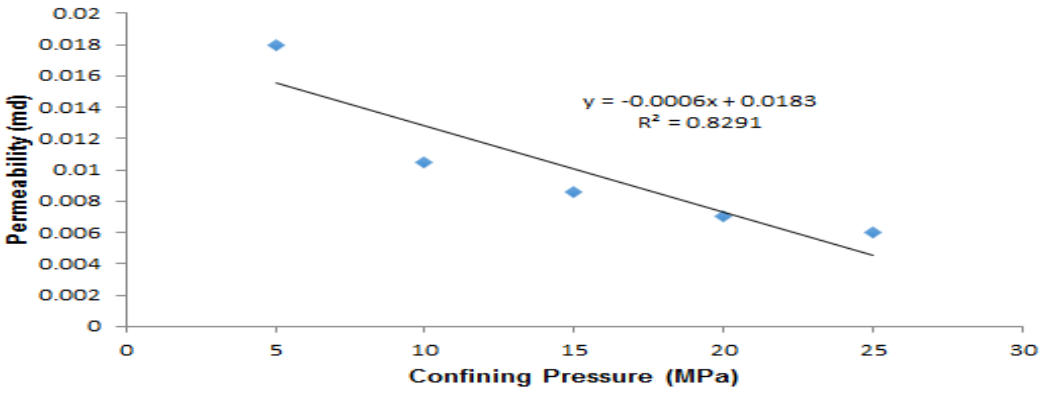

Figure 4.15: Confining pressure vs permeability

The numerical simulation results including stress intensity factor against crack length, J-Integral versus crack length, critical crack propagation pressure against crack length, Young's modulus versus stress intensity factor, Poisson ratio against stress intensity factor and confining pressure versus permeability compared with the current literature and showed good agreement.

4.7 Case study:

4.7.1 Introduction

The Second White Specks formation (SWS) in the Canadian eastern portion of the Western Interior Seaway has been studied in great detail in the outcrops of the Manitoba escarpment by many researchers since Dawson assigned to it a Cretaceous age in 1859 (McNeil and Caldwell, 1981). Other notable papers relevant to the Saskatchewan portion of the escarpment include those by Wickenden (1945) on the Mesozoic of the Eastern Plains and Beck (1974) on the surface economic geology of the Pasquia Hills area, particularly the oil shale and silica sand reservoirs. The report by McNeil and Caldwell (1981) on the Cretaceous of the Manitoba escarpment is the most comprehensive to date; it refines the

stratigraphy utilizing foraminiferal assemblages, detailed outcrop descriptions, and geophysical logs.

The Second White Specks formation has been included in many biostratigraphic studies of the Colorado Group. North and Caldwell's (1975) classic paper on the foraminiferal assemblages of Saskatchewan addresses the entire Cretaceous and refers to a thinning of the Second White Specks in the south-central portion of the province (near Saskatoon), as well as to discontinuities associated with the First and Second White Speckled Shale. Bloch *et al.* (1999) examined the sedimentology, micropaleontology, and geochemistry of the Colorado Group in context of the Western Canadian sedimentary basin from the foothills of Alberta to the Manitoba escarpment. Their study contains numerous hydro-geochemical analyses.

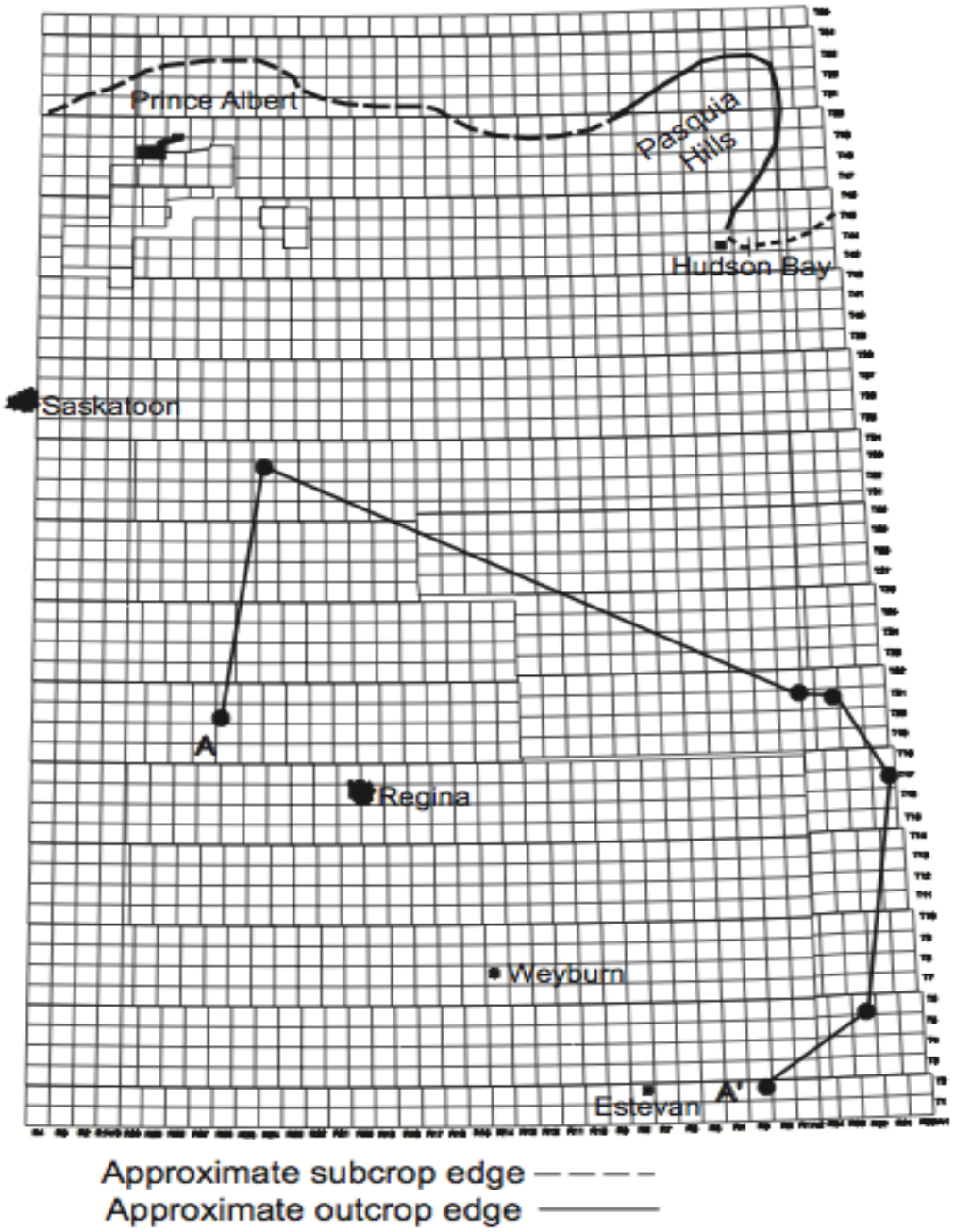

Figure 4.16: Map of eastern Saskatchewan showing the northern limit of the Second White Specks formation; subcrop edge is indicated by a black dashed line, and outcrop edge by a solid line. (modified from Beck, 1974).

4.7.2 Structural and lithological description:

In the study area, the Second White Specks formation crops out in the Pasquia

Hills and subcrops against Quaternary sediments in a west-northwest–striking belt that dips to the south-southwest (Figure 4.16). A structure map on the formation (Figure 4.17) reveals the layout of a tri-partite southwesterly to south-southwesterly dipping monocline, sloping from 367 m (msl) in the northeast to -416 m (msl) at the international border (Manitoba border crossing). Between Tps (Total petroleum system)18 and 36 , the monocline is shaped by the multi-component Punnichy Arch. The latter is made up of the Watrous and Wynyard domes, the graben-like Tabbernor lineament belt and the Yorkton salient protruding west into the Wynyard Dome from the western front of the Moosomin-Hudson Bay structural trend (Christopher, 2003). The monocline east of Rge (canadian mapping unite) 20W2 dips more steeply southward into the central part of the Williston Basin. West of Rge 20W2, the surface of the Second White Specks is more flat lying and may in places be structurally influenced by the escarpment along the Middle Devonian Prairie Evaporate salt edge (Figure 4.17). These major structural forms have antecedents that exerted influence in the depositional basin of the Second White Specks formation. Different colours in Figure 4.16 highlight different topographies of the area.

Commonly referred to as shale or limestone, the Second White Specks formation is a combination of bituminous, bioclastic, and calcarenitic limestone and marlstone, and calcareous grey and black shale (Christopher, 2003). The Keld and Assiniboine members, recognizable in outcrops and in eastern Saskatchewan, lose their differences westward because of depositional thinning, facies change, and truncation under the Morden Member of the Carlile Formation. Even in the

eastern region, the characteristic contact between the two members may be lacking, so picking the member boundary on geophysical logs tends to be based on an arbitrary interpretation of the resistivity signature, the Keld being the more resistive lower unit (Christopher, 2003).

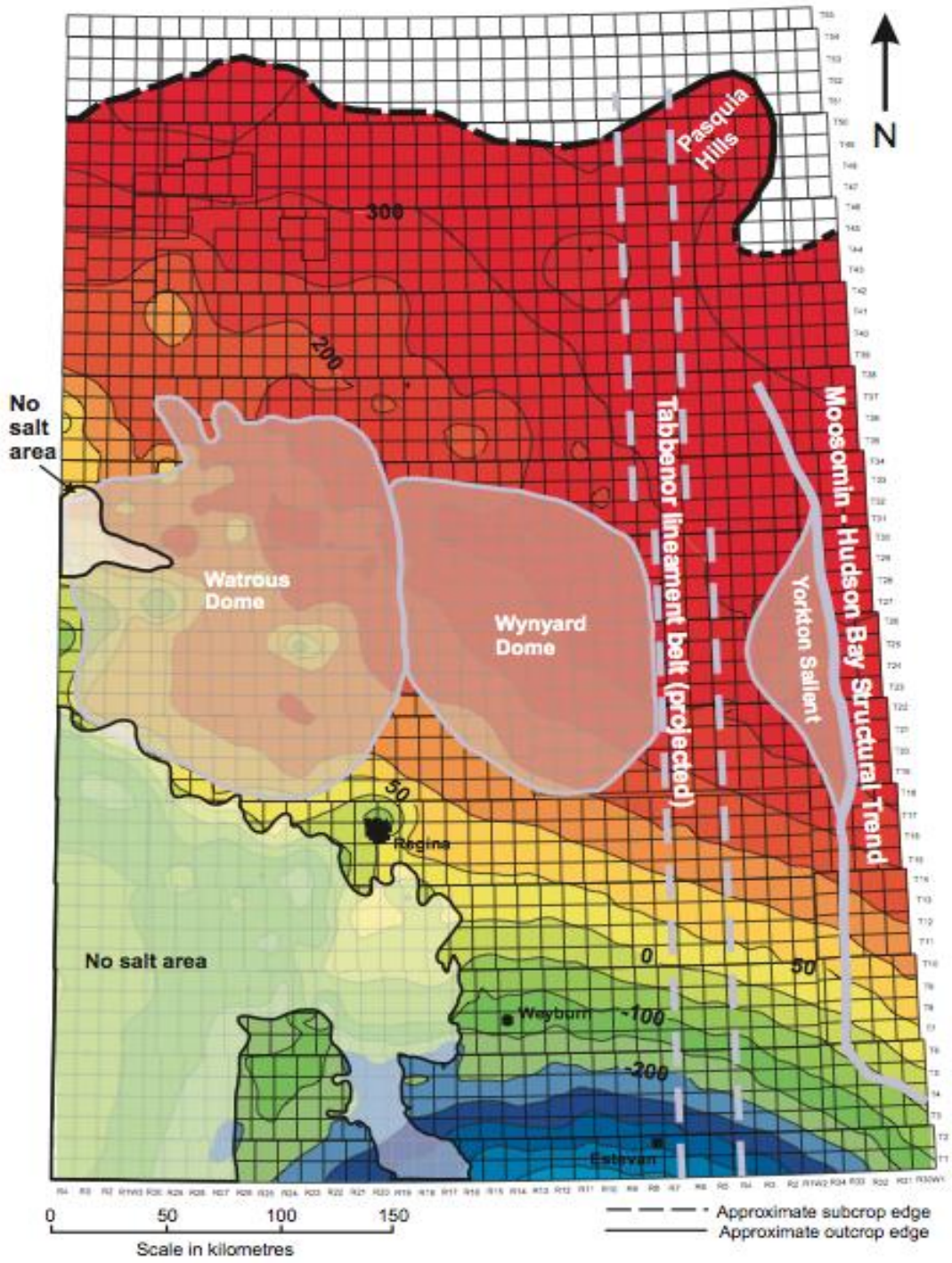

Figure 4.17: The Second White Specks formation in eastern Saskatchewan (Christopher, 2003)

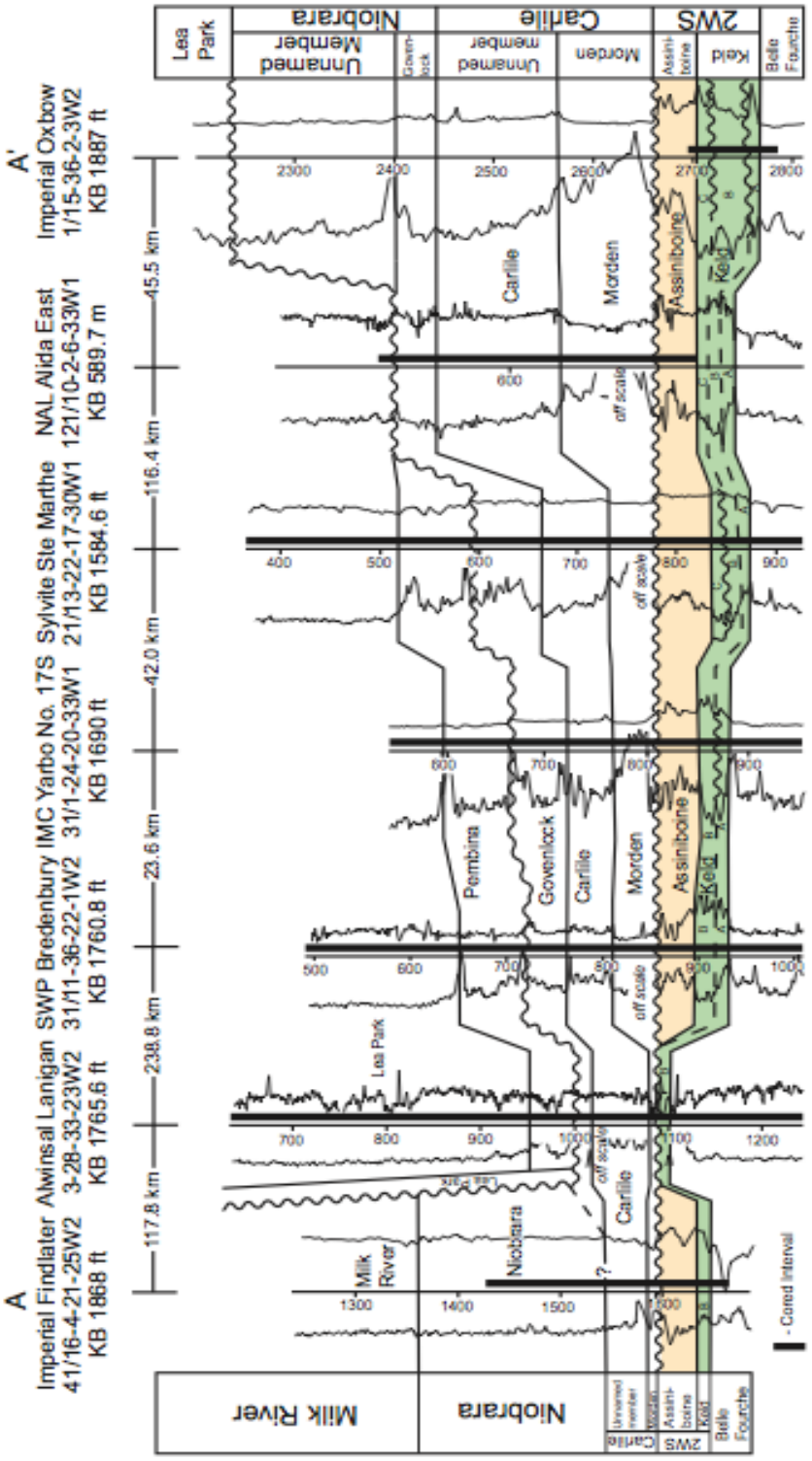

Figure 4.18: Cross section of Upper Cretaceous units in the SWS area (Wagoner *et al.*, 1987)

The composition of the calcarenite was exhaustively investigated by Bloch *et al.* (1999) and Schröder-Adams *et al.* (2001). These researchers found that, at Bainbridge Creek in the northern front of the Pasquia Hills, the calcarenite is dominated by comminuted pelecypod shell material and foraminiferal tests, and that some 54 nannofossil species make up the coccolithic white specks. The upper contact of the Second White Specks formation with the Morden Member of the Carlile Formation, where intersected in the cores of this study, is seen to be erosional at all sites except IMC Yarbo No. 17S, where the material representing the contact zone is apparently lost. The lower contact of the formation is on the so-called “X Bentonite”, which is the defined top of the Belle Fourche Shale, though it should be noted that the bentonite intersects the transition from noncalcareous black shales typifying the Belle Fourche to calcareous speckled shales characteristic of the Second White Specks.

The descriptions of the stratigraphic sections of the seven wells identified on Figure 4.18 are therein generalized, largely on the basis of their bedding cycle sequences, which generally are thin, and number as many as 17. Bedding is generally cyclic, from deeper water, greyish black shale upward to shallower water calcarenite and bioclastic limestone, or the reverse. Bedding cycles of the Assiniboine Member represent a deeper water phase of the Keld. The bedding cycles apparently represent far-ranging clinoforms. Those of the Keld Member in the study area belong to three southwesterly down lapping sequence sets (Wagoner *et al.*, 1987), here named units A, B, and C. The sequences of the Assiniboine, apparently represent distal tongues of submarine banks in the adjacent region of Manitoba;

thus they attenuate and increase in number westward. Toward the northwest near longitude 106^{O}W in south-central Saskatchewan, the Assiniboine is truncated under the sub-Morden disconformity. Samples from SWS formation have been used by several researchers to carry out a laboratory-scale investigation of hydraulic fracturing in the following sections (Wagoner *et al.*, 1987).

4.7.3 Experimental Verification

A triaxial system was employed by Mohamadighanatghestani (2015) to simulate the hydraulic fracturing process in the laboratory. In order to minimize leak-off rate a viscos fracturing fluid was chosen. The internal pressure distribution was assumed constant.

It should be noted that laboratory tests may not attain the research aims due of the following reasons: the uncertainties of specimen properties caused by environment temperature during sample drying, the complexity to estimate the accuracy of the fracture toughness under confining pressure [Zhao and Roegiers, 1993], uncemented interface between simulated borehole and specimen, complexities in sample preparation and conducting hydraulic fracturing experiments [Haimson, 1981]. The results from the triaxial tests were chosen to compare with the numerical values.

The permeability of an intact rock sample is usually computed using the Darcy equation:

$$k = \frac{2Qp_0\mu L}{A(p_i^2 - p_0^2)} \qquad (4.12)$$

where Q is the flow rate, μ is the viscosity of the injection fluid, p_o is the downstream pressure, p_i is the upstream pressure, A is the cross-sectional area of the specimen, L is the mean specimen length and k is the permeability of the specimen (Wanniarachchi, et al, 2017).

4.7.4 Experimented material

The specimens used in this work were acquired from the SWS area, which is one of the three important oil-sand deposits situated in Alberta, Canada (Fig. 4.19).

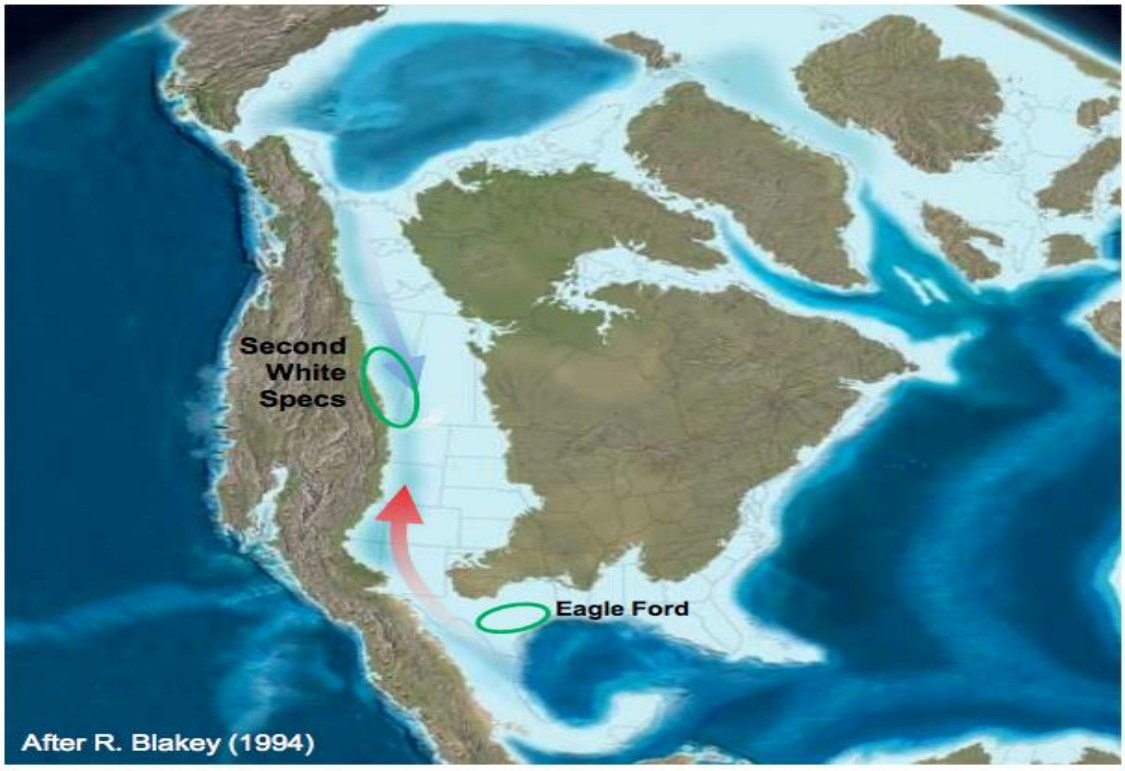

Figure 4.19: Location and stratigraphy of the SWS area (Malcolm Lamb Shale Petroleum Ltd, Americas Denver, CO - October 2013)

Conventional double-barrel coring was carried out by Mohamadighanatghestani (2015) in the vertical direction, direction of material deposition, to recover cores from the Second White Specks formation.

Table 4.2: Physical properties of the tested shale according to ASTM standard (Mohamadighanatghestani, 2015)

Formation	Tube No	Depth (m)	Natural Water Content (%)	Specific Gravity (kg/m3)	Plastic Limit (%)	Liquid Limit (%)
SWS	75	245.1-246.6	16.9	2.735	32	64
SWS	77	248.1-249.6	17.7	2.742	43	88

The range of bulk density and porosity of core specimens as acquired from borehole logs were 2150 − 2230 kg/m^3 and 0.32 − 0.34, respectively. At least two specimens were selected by Mohamadighanatghestani (2015) from each tube for calculation of index properties (average natural water content, specific gravity, plastic limit and liquid limit), the results of which are presented in Table 4.2.

4.7.5 Testing apparatus and results

A high-pressure triaxial apparatus (as shown schematically in Fig. 4.20) was used to test all the specimens (Mohamadighanatghestani, 2015). The cell's internal diameter and height were respectively, 203 mm and 406 mm, which renders it plausible to test cylindrical specimens of 3.5" (88.9 mm) in diameter and 7" (177.8mm) in height. Table 4.3 shows the initial conditions of the tested shale.

Table 4.3: Testing program and initial conditions of the tested shale (Mohamadighanatghestani, 2015)

Sample ID	Test ID	Sample Height (mm)	Sample Diameter (mm)	Dry Density (kg/m^3)	Initial Porosity
T75 S1	TC-3-25	180.2	86	1861.2	0.319
T75S2	TC-1-25	179.2	86.2	1834.8	0.329
T75 S3	CMS-3-25	180.8	86.6	1819	0.335
T75 S4	CMS-5-25	180.2	86.2	1841.5	0.327
T75 S5	TC-1-85	180.2	86.3	1844.4	0.326
T77 S1	TC-3-135	181.1	84.8	1879.5	0.315
T77 S2	TC-3-85	179.8	84.1	1856.5	0.323
T77 S4	TC-1-135	180.7	86.2	1891.9	0.310
T77 S8	TC-5-85	180.7	86.1	1888	0.311
T114 S3	TC-5-25	179.4	86.9	1885.4	0.312

Axial load was measured using a 100,000 lbf (444.8 kN) load cell. Also a displacement-measuring device was used to allow both conventional triaxial compression and extension experiments in either load-controlled or displacement-controlled modes. The cell and backpressures from pressure intensifier systems could attain values as high as 3000 psi (20.7 MPa) (Mohamadighanatghestani, 2015). For greater accuracy in the range of lower pressures, the device was also equipped with a segment that only permitted applications of pressures up to 1 MPa (Mohamadighanatghestani, 2015). To attain near-incompressibility conditions, two pressure transducers were set up as close as possible to the bottom and top of the

cell employing thick-walled stainless steel tubing's (Mohamadighanatghestani, 2015).

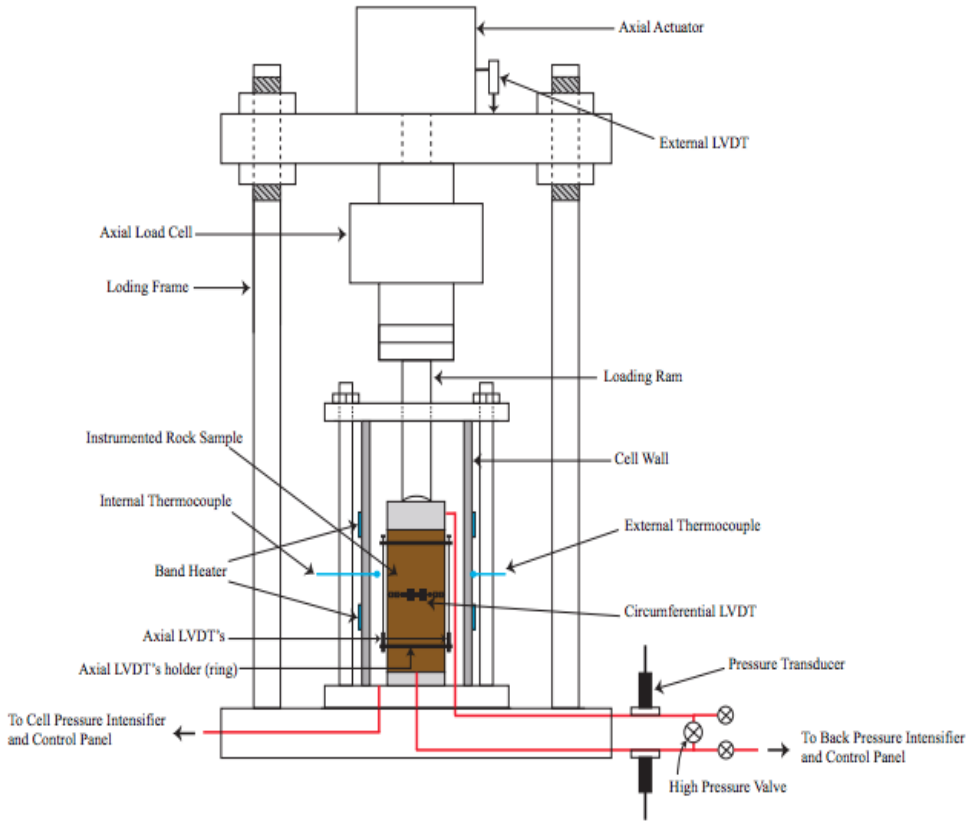

Figure 4.20: Triaxial apparatus (Mohamadighanatghestani, 2015).

Tables 4.4 and 4.5 show physical properties and mechanical properties and experimental data of the shale samples.

Table 4.4: Physical and Mechanical Properties of the Samples (Jin, Shah, Roegiers, 2013)

Parameter	Value
Young's Modulus (GPa)	15-35
Poisson Ration	0.23
Uniaxial Compressive Strength (MPa)	48.5
Permeability (md)	0.05
Borehole Diameter (m)	0.2

Table 4.5: Experimental data (Jin, Shah, Roegiers, 2013)

Number	1	2	3	4	5	6	7
Min In-situ Stress (MPa)	1	1	1	1	1	1	1
Max In-situ Stress (MPa)	4	4	4	4	6	6	6
Breakdown Pressure (MPa)	7.4	8.5	9.3	9.8	10.4	10.5	15.6

The resulting breakdown pressure values of SWS shale are plotted in Figure 4.21 versus the confining pressure. The results show that as the confining pressure increases, the fracture initiation pressure also increases (Wanniarachchi, et al, 2017).

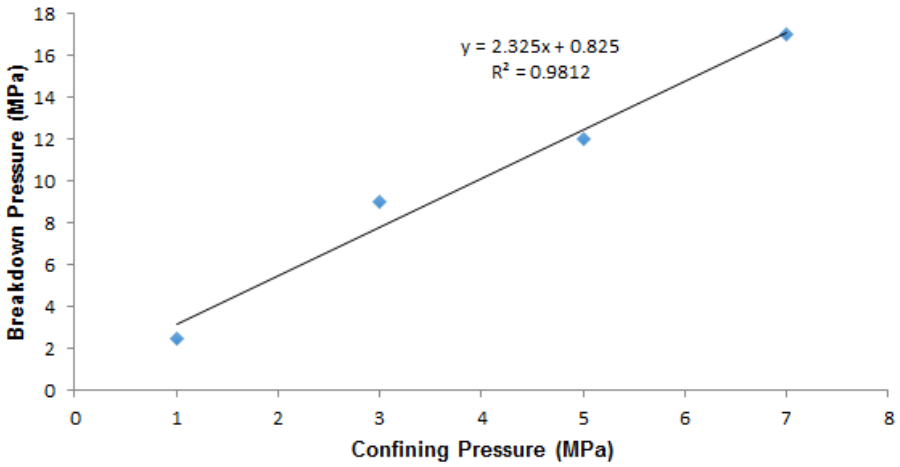

Figure 4.21: Variation of breakdown pressure with confining pressure (Wanniarachchi, et al, 2017)

Figure 4.22 shows the stress-strain behaviour of vertically aligned core specimens. The figure shows loading and unloading curve in the tests. All the specimens show higher stiffness during the stress reversal (unloading) than during loading.

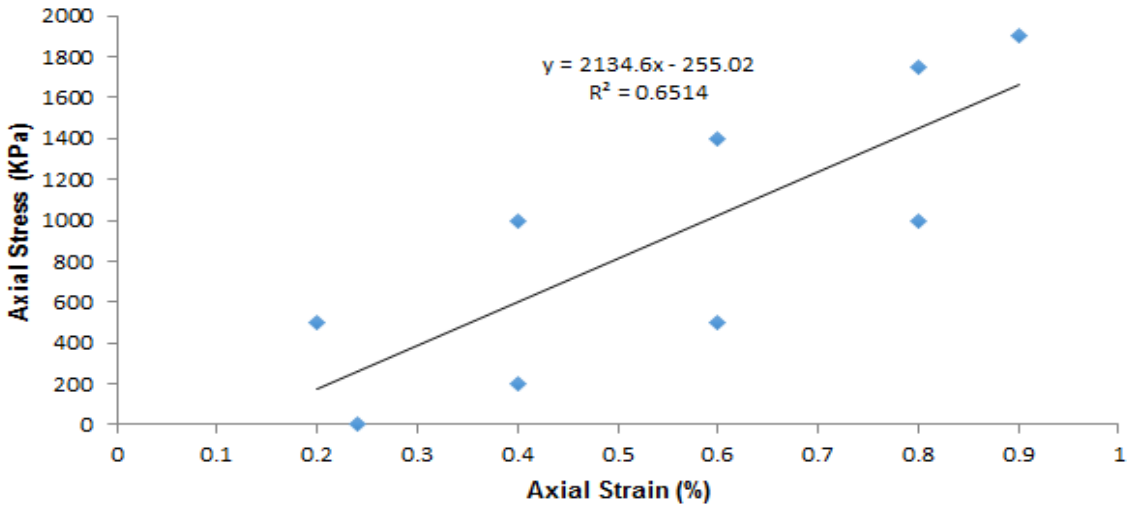

Figure 4.22: Stress-strain behaviour in SWS shale (Gatum and Wong, 2006)

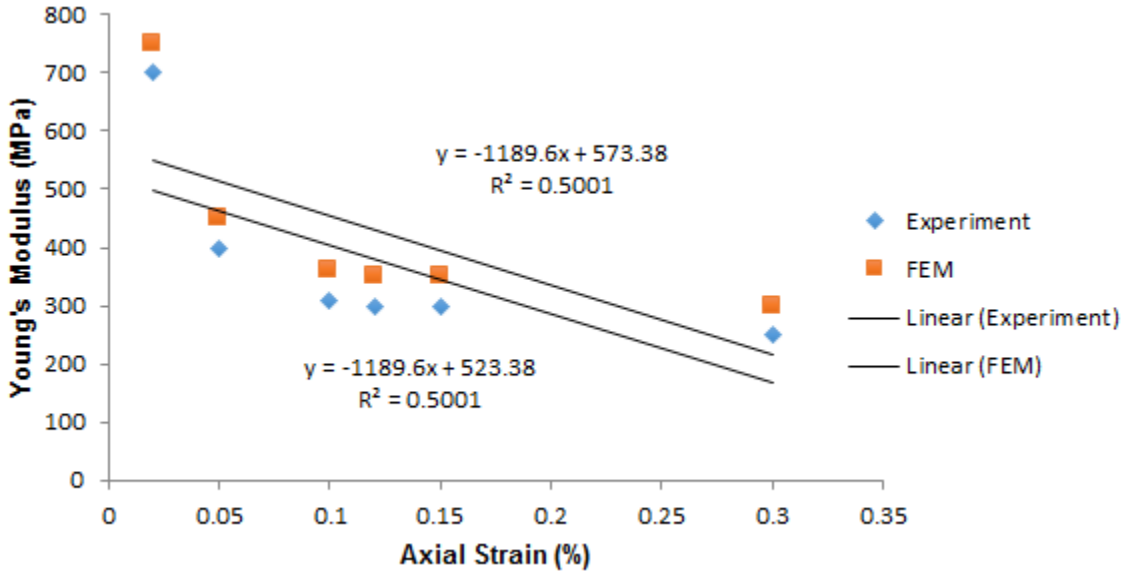

Figure 4.23: Young's Modulus vs Axial Strain in SWS shale (Gatum and Wong, 2006)

Figure 4.23 shows the variation of Young's modulus with axial strain at constant effective radial stress for Wavertically oriented SWS core specimens.

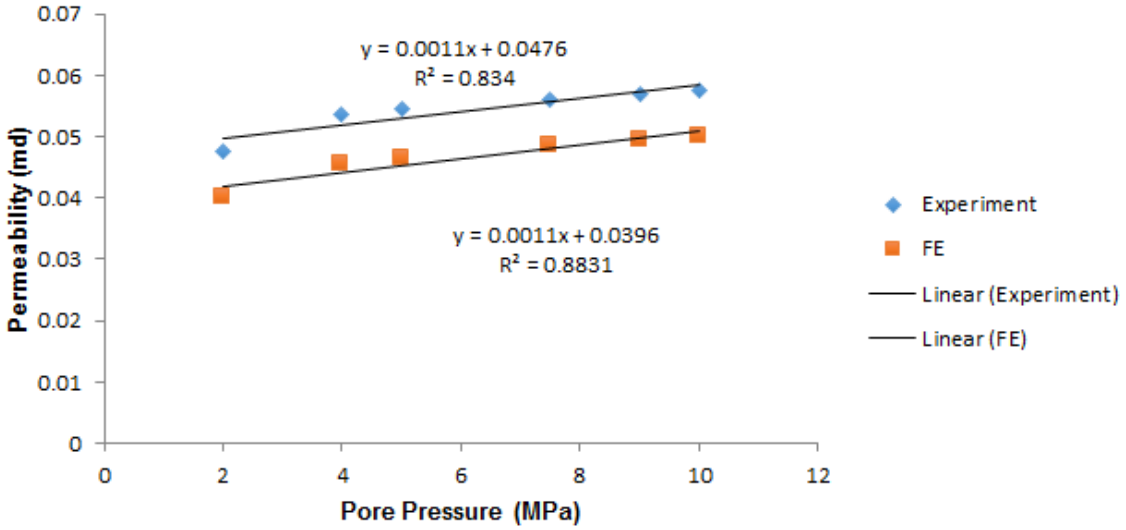

Figure 4.24: Variations of Permeability with Pore Pressure (Liu, et al. 2014; Guo, et al. 2017)

Figure 4.24 shows, variation of rock permeability with pore pressure at a fixed effective confining pressure (P_c-P_P=3 MPa, P_c is the confining pressure and P_p is the pore pressure). The rock permeability increases with the increase of pore pressure and the curve becomes relatively flatter when the pore pressure exceeds 4 MPa. Deformation occurs under the pore pressure at weak zone, which finally leads to the increase of rock permeability.

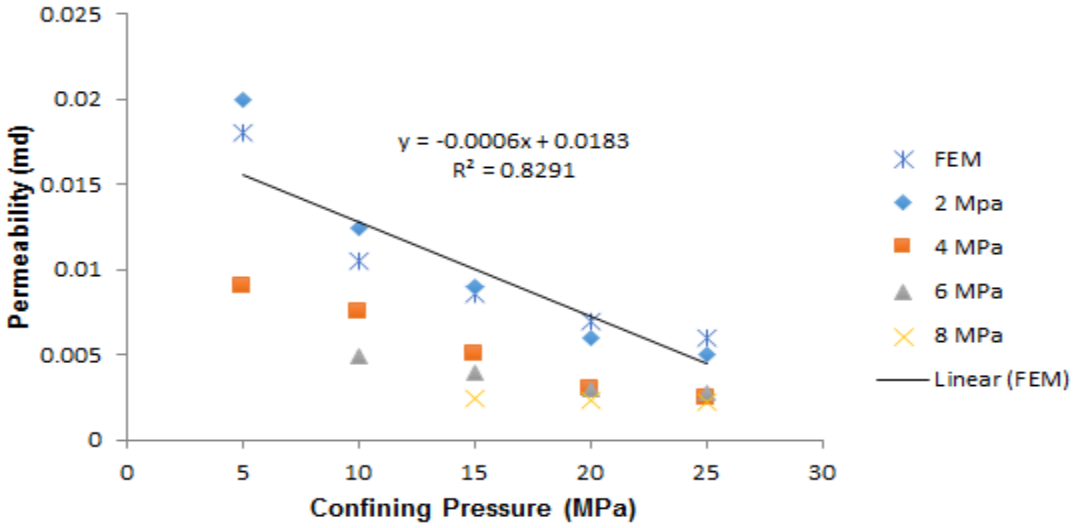

Figure 4.25: Variation of permeability with confining pressure (Wanniarachchi, et al, 2017 and Liu, et al., 2014)

Permeability tests were conducted by Wanniarachchi (2017) on intact and fractured samples to determine the variations of flow characteristic upon fracturing of the reservoir. Permeability was tested under a series of confining pressures (5, 10, 15, 20 and 25 MPa) and injection pressures (2–8 MPa). The effect of confining pressure on fractured SWS shale permeability was studied and the results are shown in Figure 4.25. The results show that the permeability decreases with increasing the confining pressure and this variation is independent of the injection pressure. Under higher confining pressures such as 20 MPa, the fracture opening can be smaller and this can greatly influence the permeability of the rock specimen regardless of the propagated fracture. The use of proppants is necessary to keep open the cracks after releasing the fluid pressure otherwise, the confining stress will close or decrease the fracture opening which will also result in a decrease in permeability. The crack will grow until the maximum stress level is reached in the specific area.

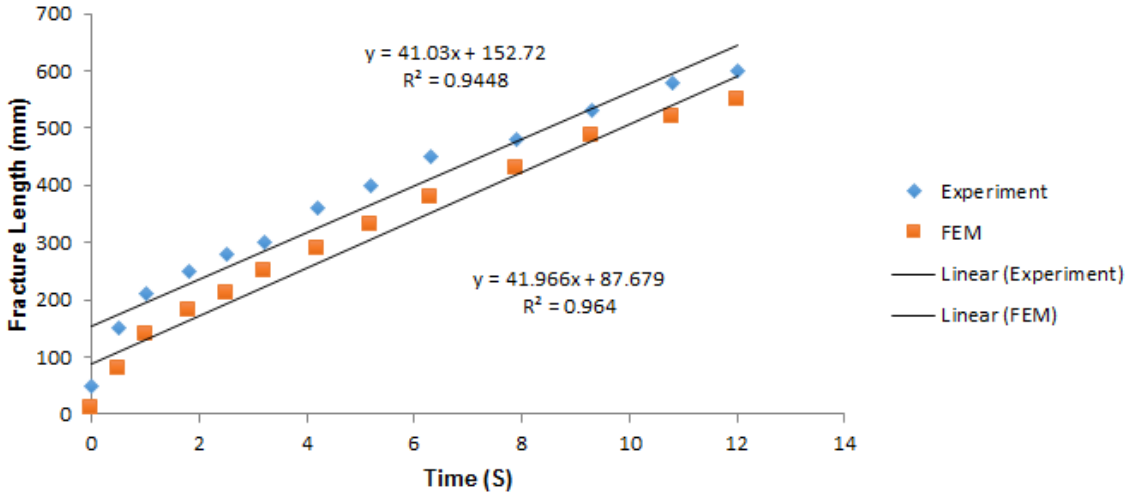

Figure 4.26: Variation of fracture length with time (Gorjian and Hawkes, 2014)

Figure 4.26 shows the predicted progress of fractured zone as a function of time during stimulation. Once such predictions have been calibrated, these outputs can be utilized to calculate when to stop injection to avoid vertical propagation into the water-bearing layer overlying the SWS formation.

4.8 Discussion and Conclusions

Hydro-mechanical coupling is crucial in order to account for the effect of fluid injection on hydraulic fracture propagation. A two-way coupling of hydraulic and mechanical processes was presented in this study. Two-way coupling is somehow simple to implement like one-way coupling, but it holds promise for capturing much more of the complex nonlinear physics, thus is closer to a fully coupled method. The hydraulic fracturing has been investigated numerically through a FEM-based model in different stress intensity factors, J-Integral, considering the effects of elastic modulus, Poisson's ratio, fluid pressure and fluid viscosity. The model couples the fluid flow with fracture propagation while damage initiation and

evaluation criteria are also presented. The results show that increasing stress intensity factor and J-Integral would increase crack propagation.

The variation of critical pressure of crack propagation with crack length growth in different pressures was studied. By increasing crack length, the critical crack propagation pressure decreases. This shows that the bottom hole pressure drops with time while the fracture length increases. The mechanical properties of reservoir including elastic modulus and Poisson's ratio, would affect hydraulic fracturing directly. The results from the model suggest that increasing elastic modulus and Poisson's ratio of rock increases the crack propagation as the stress intensity factor also increases. In general, increasing the fracturing fluid viscosity in injection operation can considerably increase the fracture stress intensity factor. A higher fluid viscosity leads to increase in net wellbore pressure that acts on the fracture surface area, which results in further opening of the fracture. The results from this work can be applied in the analysis and optimization of hydraulic fracturing especially where formation modulus contrast is a challenge such as fracturing in multi-layer reservoirs or shale formations.

Numerical simulations were carried out and the results were compared with analytical solutions. A good degree of agreementis observed which indicates the validity of the model. In the KGD model, the net pressure gradient drops rapidly with fracture length and reaches almost a constant value. The fracture mechanics solution of Rummel and Winter (1982) was used to calculate the stress intensity factor. The variation of stress intensity factor as a function of the crack length in the reservoir domain showed a good agreement between the analytical and FEM

results.

A laboratory-scale study of hydraulic fracturing in SWS shale was presented. The numerical model was used to simulate the triaxial laboratory experiments. The comparison of numerical with experimental results showed the followings:

- As the confining pressure increases, the fracture initiation pressure also increases.
- The stress-strain behaviour of vertically aligned core specimens indicated higher stiffness during the stress reversal (unloading) than during loading.
- Increasing pore pressure will increase permeability.
- Increasing Young's modulus of vertically oriented core samples decreases the axial strain.
- The results can be used in practice to prevent over-injection of fluid in order to avoid extra propagation of the fracture into the water-bearing layer in the SWS formation.

Chapter 5. Conclusion and Recommendations

5.1. Review of the Completed Work

The parameters affecting hydraulic fracturing in unconventional reservoirs were studied in this work. In general, the process of hydraulic fracturing can be defined as initiation and propagation of fractures due to the pressurization of fluid flow within existing fractures. The difference between a conventional and unconventional reservoir is migration. The unconventional reservoir has hydrocarbons that were formed within the rock and never migrated. The conventional reservoir is a porous rock formation that contains hydrocarbons that have migrated from a source rock.

The main scope of this work is the investigation of geological parameters in modelling of hydraulic fracturing.

During hydraulic fracturing in unconventional reservoirs, high conductivity channels are created. Gas and water drainage is stimulated by the conductive channel by bypassing near borehole damage and creating a low-pressure drain in the reservoir, hence increasing the gas drainage rate. In the present study, the effects of the most crucial parameters on the viability of HF of coal seams were presented in terms of seam gradient and thickness, geological disturbances, seam floor conditions and seam roof conditions. The PARVADEH 4 Tabas coalmine, one of the largest coal reserves in the Tabas coal basin, was used as a case study. The Tabas coal mine consists of C1, C2, B1, B2 and D seams (see Figure 3.2). By using the fuzzy logic, membership functions and fuzzy rule-bases were

generated and finally, the potential for HF was studied. Seam dip, thickness and uniformity variables, which are the most effective structural parameters of coal seam in one side and roof, floor and coal quality, which are strength parameters in the other side, were classified separately. The coal reserve was also classified separately as an economical parameter. The potential for HF of the PARVADEH 4 Tabas coalmine in Iran was investigated. The results of the fuzzy model are as follow:

- There is a high potential for HF in B2 and C1 seams and low potential of HF for B1, C2 and D seams of the PARVADEH 4 Tabas coalmine.
- The developed fuzzy model can be used as a pre-production model in hydraulic fracturing.
- The fuzzy model predicts efficiency of hydraulic fracturing by considering seam gradient, seam thickness, seam geological disturbance, seam floor conditions, seam roof conditions, seam strength and seam reserve.

Moreover in this study, a three-phase hydro-mechanical model was developed for simulating hydraulic fracturing. The three phases include: porous solid, fracturing fluid and reservoir fluid. Two numerical simulators (ANSYS Fluent for fluid flow and ANSYS Mechanical for geomechanical analysis) were coupled together to model multiphase fluid flow in hydraulically fractured rock undergoing deformations. The two solvers were coupled, using system coupling in ANSYS Workbench.

The finite element and finite volume methods were used to solve the governing equations of fluid flow and geomechanical deformation in an unconventional reservoir intercepted by a horizontal wellbore. The effects of fluid pressure,

viscosity and rock permeability, Young's modulus, Poisson ratio and stress intensity factor in unconventional reservoirs caused by a non-compressible fluid were investigated.

Developing a fully coupled model for a multi-phase flow and large nonlinear inelastic mechanical deformation is expensive and time-consuming. An alternative is to use the two-way coupling method to simulate flow and mechanical responses in the hydraulic fracturing problem. Staggered-in-time coupling, and two-way passage of information allow accurate modelling of a range of reservoir conditions. The staggered-in-time two-way coupling scheme alternates between flow and mechanical models. The mechanical simulator generates updated reservoir parameters, which are employed by the flow simulator in the next time step. The advantage of this approach is that the simulation domains for flow and mechanics can be significantly different.

Results from a set of triaxial experiments and also an analytical model were used for validation of the two-way coupling scheme. Good agreement was achieved between the developed numerical model, the KGD model and the triaxial test results. The KGD analytical solution was presented by Geertsma and de Klerk (1969) for a two-dimensional fracture with a Newtonian fluid. In this solution, the fracture length, fracture opening at the wellbore, and net pressure can be predicted.This study revealed little difference between the coupled solution, the analytical solution and the experimental results. The following conclusions can be drawn from the results of the coupled model:

- The results show that increasing stress intensity factor and J-Integral would increase crack propagation.
- By increasing crack length, critical crack propagation pressure decreases.
- Increasing elastic modulus and Poisson's ratio of rock increases the crack propagation as the stress intensity factor also increases.
- Generally, increasing the fracturing fluid viscosity in injection operation can considerably increase the fracture stress intensity factor.
- A higher fluid viscosity leads to increasing net wellbore pressure that acts on the fracture surface area, which results in further opening of the fracture.
- Minimum value of J-integral indicates that the crack has reached its final propagation phase and after that, by increasing fluid injection, the crack does not propagate and causes an increase in elastic strain energy in the rock that increases the potential energy.
- The variation of stress intensity factor as a function of the crack length in the reservoir domain shows a good agreement between the analytical and FEM results.
- The results show that as the confining pressure increases, the fracture initiation pressure also increases.
- Increasing pore pressure will increase permeability.

- Increasing Young's modulus of vertically oriented core samples decreases the axial strain.
- The results can be used in practice to prevent over-injection of fluid in order to avoid extra propagation of the fracture into the water-bearing layer in the SWS formation.

The outcome of this research can be useful in describing various aspects of behaviour of hydraulic fracturing in unconventional reservoirs. The fuzzy model gives the ability to estimate the potential and efficiency of hydraulic fracturing in unconventional reservoirs. The finite element and finite volume models can be used to determine appropriate fluid and solid parameters and associated design.

5.2 Recommendations for Future Research

The current fuzzy model does not include the effect of fluid on the hydraulic fracturing process. Hence, it only represents the solid part. To complete this study the fluid parameters can be added into the developed fuzzy model. Since in most cases, fracturing treatments are done in multi-layered systems, a more practical model requires to include multiple layers. Therefore, one of the major feasible lines for future study is to develop the present model to make the above achievable.

Multi-phase fluid flow for the coupling analysis is strongly recommended in order to model the injectivity of a realistic fracturing fluid and proppant transport along the fracture rather than just water, since proppant transport is an important parameter to prevent fracture closure and facilitate successful production.

The two-way coupling scheme was implemented in the FEM model in this thesis.

A fully coupled model would require further study and may be able to deliver more accurate simulation results.

The current FEM model does not include the effect of fracturing fluid leak-off to the reservoir's surrounding rock masses. Integrating this information into the coupled FEM model would improve the numerical analysis results.

References:

Aadnoy, B. S., and Chenevert, M. E. 1987. Stability of Highly Inclined Boreholes. SPE Drilling Engineering, 2(04):364–374.

Aadnoy, B. S. 1988. Inversion Technique To Determine the In-Situ, Stress Field From Fracturing Data. In SPE Annual Technical Conference and Exhibition. Society of Petroleum Engineers.

Adachi J., Siebrits E., Peirce A., and Desroches J., 2007, Computer simulation of hydraulic fractures, Int. J. Rock Mech. Min. Sci., 44, pp. 739–757.

Adeeb S., 2010. Introduction to Finite Element Analysis, Course notes, University of Alberta.

AGL. 2011. AGL Hunter Gas Project: Hydraulic Fracturing Fact sheet. Available at:http://www.agl.com.au/about-agl/how-we-source-energy/natural-coal-seam-gas/hunter-gas-project.

Andrson, T.L., 1994, Fracture Mechanics: Fundamentals and Applications, second edition, CRC.

APLNG, 2011. Summary of Chemical found in Australia Pacific LNG's hydraulic fracturing fluid. Available at: http://www.originenergy.com.au/files/Fraccing_chemical_summary.pdf. Accessed 2 November 2012.

APLNG, 2013b. Hydraulic fracture stimulation: A safe way to extract coal seam gas. Fact sheet. Available at: http://www.aplng.com.au/pdf/factsheets/Factsheet_Fraccing-APLNG.pdf, Accessed on 12 December 2013.

Arrow Energy. 2012b. What fraccing fluids are used by Arrow? Available at: http://www.arrowenergy.com.au/page/Community/FAQs/General_FAQs/What_fraccing_fluids_are_used_by_Arrow. [Accessed 2 November 2012].

Asadi, S., Javan, M., Bohloli, B., Mutabashiani, S., 2013, Experimental, Numerical and Analytical Investigation theInitiation and Propagation of Hydraulic Fracturing (Case Study: Sarvak Lime Stone), World Applied Sciences Journal 22 (5): 637-646, DOI: 10.5829/idosi.wasj.2013.22.05.1696.

Ataee M, 2005, Underground Mining, Shahrood University Publication.

Ataee, M., Khalokakaei, R., Hosseini, M., 2009, Determination of coal mine mechanization using fuzzy logic, Journal of Mining Science and Technology, 19(2):

149-154.

Bao, J.Q. Fathi, E. Ameri, S. 2014, A coupled finite element method for the numerical simulation of hydraulic fracturing with a condensation technique, Engineering Fracture Mechanics 131, 269–281.

Barsom, John M. and Rolfe, Stanley T., 1999, Fracture and Fatigue Control in Structures: Application of Fracture Mechanics, Philadelphia.

Barsoum, R.S., 1976. On the Use of Isoparametric Finite Elements in Linear Fracture Mechanics. International Journal for Numerical Methods in Engineering, 10: 25-37.

Beck, L.S. 1974, Geological Investigations in the Pasquia Hills Area; Sask. Dep. Miner. Resour., Rep. 158, 16p.

Beckwith, R. 2010. Hydraulic fracturing: the fuss, the facts, the future. Society of Petroleum Engineers Report.

Benra, F.K., Dohmen, H.J., pei, J., Schuster, F., Wan, B., 2011, A comparison of one- way and two-way coupling methods for numerical analysis of fluid structure interactions, Journal of applied mathematics, ID 853560.

Blandford, G.E., Ingraffea, A.R. and Ligget, J.A., 1981. Two-Dimensional Stress Intensity Factor Computations Using the Boundary Element Method. International Journal for Numerical Methods in Engineering, 17: 387-404.

Bloch, J.D., Schröder-Adams, C.J., Leckie, D.A., Craig, J., and McIntyre, D.J. 1999: Sedimentology, Micropaleontology, Geochemistry and Hydrocarbon Potential of Shale from the Cretaceous Lower Colorado Group in Western Canada; Geol. Surv. Can., Bull. 531, 185p.

Bobet A, Fakhimi A, Johnson S, Morris J, Tonon F and Ronald Yeung M, 2009. “Numerical Models in Discontinuous media: Review of advances for rock mechanics applications”. Journal of Geotechnical and Geoenvironmental Engineering, ASCE, November, 1547.

Bochkarev, O., and A.Grekov, M. 2014. Local instability of a plate with a circular nano-hole under uniaxial tension. Doklady Physics, 59(7):330–334.

Boone, T.J. and Ingraffea, A.R., 1990. A numerical Procedure for Simulation of Hydraulically Driven Fracture propagation in Poroelastic Media. International Journal for Numerical Methods in geomechanics, 14: 27-47.

Bradley, W. B. 1979. Failure of inclined borehole. J. Energy Resour. Technol., Trans. ASME 101: 233–239.

Bui, H.D, Leblond, J.B, Stalin-Muler, N, 2011, Handbook of materials behaviour, Volume II, Pages 549-557.

Çelikyilmaz, A., I.B. Turksen, 2009, Modeling uncertainty with fuzzy logic with recent theory and applications, Springer-Verlag, Berlin Heidelberg.

Chan, S. K, Tuba, I. S, and Wilson, W. K. 1975. On the finite element method in linear fracture mechanics. Engineering Fracture Mechanics, 2-1.

Chen and Pham, 2000, Introduction to Fuzzy Sets, Fuzzy Logic, and Fuzzy Control Systems.

Chen, Y. M. 1975, Numerical computation of dynamic stress intensity factors by a Lagrangian finite-difference method (the HEMP code). Engineering Fracture Mechanics, 7(4): 653- 660.

Christopher, J.E. 2003: Jura-Cretaceous Success Formation and Lower Cretaceous Mannville Group of Saskatchewan; Sask. Industry Resources, Rep. 223, CD-ROM.

Clifton, R.J. and Abou-Sayed, A.S., 1979. On the computation of the three-dimensional geometry of hydraulic fractures, SPE 7943. Low Permeability Gas Reservoirs.

Cotterell, B., Rice, J.R., 1980, Slightly curved or kinked cracks, International Journal of Fracture, Volume 16, Pages 155-169.

Couch, G. 2009, Underground Coal Gasification, IEA clean coal centre, ISBN 978-92-9029-471-9.

Courtin, S., C. Gardin, G. Bezine and H. Ben Hadj Hamouda, 2005. “Advantages of the J-integral approach for calculating stress intensity factors when using the commercial finite element software ABAQUS.” Engineering Fracture Mechanics, 72(14): 2174-2185.

Crittendon, B.C., 1959, The mechanics of design and interpretation of hydraulic fracture treatments, Journal of Petroleum Technology, (October), pages: 21–9.

Croft, G.A. 1980, Summary of Research into Incremental Hydraulic Fracturing of Coal Seams at the M.W. Haenke Colliery, Ipswitch, The Research Section of the Queensland Dept of Mines, Report, Feb. 21, 1980.

Dahi-Taleghani A. 2009, Analysis of hydraulic fracture propagation in fractured reservoirs: an improved model for the interaction between induced and natural fractures, PhD dissertation, Austin,Texas: The University of Texas at Austin.

Deily, F. H., and Owens, T. C. 1969, Stress around a wellbore. SPE 2557, in Proceedings of the 44th SPE Annual Fall Meeting, AIME, Denver, CO, USA Sep. 28–Oct. 1.

Detourney, E. and Cheng, A.H.D., 1991. Plane Strain Analysis of a Stationary Hydraulic Fracture in a Poroelastic Medium. International Journal of Solids and Structures, 27: 1645-1662.

Delorenzi HG, 1982, On the energy release rate and the J-integral for 3-D crack configurations, Int. J. Fract. 19, 183–193.

Devloo PRB et al. 2006, A finite element model for three dimensional hydraulic fracturing. Math Comput Simul; 73:142–55.

Dhir, R., Dern, R. R., & Mavor, M. J. 1991, Economic and reserve evaluation of coal bed methane reservoirs. Texas, USA: Society of petroleum engineers, Paper No. 22024.

Diamond, W.P., and Oyler, D.C. 1987, Effects of Stimulation Treatments on Coalbeds and Surrounding Strata, RI 9083 US Dept of the Interior, Bureau of Mines, 48 pages.

Discacciati , and Quarteroni , 2009, Navier-Stokes/Darcy Coupling: Modeling, Analysis, and Numerical Approximation, Revista Mathematica Complutense, vol. 2, Pages, 315-426.

Dubois, D. and H. Prade, 2010 “Gradualness, uncertainty and bipolarity: making sense of fuzzy sets, fuzzy sets and systems,” Fuzzy Sets and Systems, (Article in press, corrected proof) doi: 10.1016/j.fss.2010.11.007.

Dos Santos, J.S., T.P. Ballestero and E. Da Silva Pitombeira, 2011, An Analytical Model for Hydraulic Fracturing in Shallow Bedrock Formations, Ground Water, 49(3): 415-425.

Economides, M.J. and Martin, T. 2007. Modern Fracturing: Enhancing Natural Gas Production. ET Publishing, Houston, Texas.

Economides, M.J. and Nolte, K.G. 2000, Reservoir Simulation. John Wiley and Sons, LTD, 3, 9-3.

Edward A. Beaumont and Norman H. Foster, 1988. Treatise of Petroleum Geology/Handbook of Petroleum Geology: Exploring for Oil and Gas Traps, Pages 6-1 - 6-41.

Erdogan, F. and Sih, G.C. 1963, On the crack extension in plates under plane loading and transverse shear. Journal of Basic Engineering, 85:519-527.

Fredrich, J., Deitrick, G., Arguello, J., de Rouffignac, E., 1998, Reservoir compaction, surface subsidence, and casing damage: a geomechanics approach to mitigation and reservoir management. Proceeding of SPE/ISRM EUROCK 1998, No. 47284. SPE and ISRM.

Garagash D, Detournay E. JAppl Mech 2005, Plane-strain propagation of a fluid-driven fracture: small toughness solution ;72:916–28.

G.Boyle, B.Everett, S.Peake, J.Ramage, 2015. Energy Systems and Sustainability: Power for a Sustainable Future, 2nd Ed. Oxford, UK: Oxford University Press, 2012.

Golder Associates. 2010b. Response to the Coordinator-General requirements for coal seam gas operations in the Surat and Bowen Basins Queensland. Report produced for Santos Ltd. Available at: http://www.santos.com/library/Roma_Shallow_Gas_East_EMP_AppD.pdf [Accessed on 16 December 2013].

Gorjian, M. Hawkes, C.D. 2014. simulation of hydraulic fracturing in the Bakken Formation, Sotheast Saskatchewan, Canada, DFNE 2014-258.

Grekov, M., Morozov, N., and Yazovskaya, A. 2014. Effect of Surface Stress on Strength of a Plate with Elliptical and Triangular Nanoscale Holes. Procedia Materials Science, 3: 1669–1674.

Griffith, A.A., 1920. The Phenomena of Rupture and Flow in Solids. Phil. Trans.Royal Soc., Ser. A. 221: 163-198.

Griffith, A.A., 1924. The Theory of Rupture, First International Congress in Applied Mechanics, Delft, pp. 55-63.

Guanrong Chen, Trung Tat Pham, 2000, Introduction to fuzzy sets, fuzzy logic, and fuzzy control systems, CRC Press, University of Huston Texas.

Haimson, B. C. 1981, Large scale laboratory testing of hydraulic fracturing, Geophysical Research Letters, 8(7), 715-718.

Hasanpour,R.andN.Choupani, 2009. “Mixed-Mode Study of Rock Fracture Mechanics by using the Modified Arcan Specimen Test.” International Journal of Mathematical, Physical and Engineering Sciences, 3: 1.

Hossain, M. M., Rahman, M. K. and Rahman, S. S. 2000, Hydraulic fracture initiation and propagation: roles of wellbore trajectory, perforation and stress regimes. Journal of Petroleum Science and Engineering 27.3: 129-149.

Henshell, R.D. and Shaw, K.G., 1975. Crak Tip Finite Elements Are Unnecessary. International Journal for Numerical Methods in Engineering, 9: 495-507.

Hoek, E. and Martin, C.D. 2014. Fracture initiation and propagation in intact rock – A review.

Hartman, H.L., 1987, Introductory Mining Engineering, John Wiley & sons.

Holditch, S. A. 1989. Enhanced recovery of coal bed methane through hydraulic fracturing. In SPE annual technical conference and exhibition. Houston, Texas: Pub: Society of Petroleum Engineers.

Harrison, E., Kieschnick, W.F., McGuire, W.J., 1954, The mechanics of fracture induction and extension, Petroleum Trans AIME, Vol. 201 pages: 252–63.

Hubbert, M.K., Willis, D.G., 1957, Mechanics of hydraulic fracturing, Journal of Petroleum Technology, 9(6), pages: 153–168.

Ingraffea, A.R., 1977a. Discrete Fracture Propagation in Rock, University of Colorado, Colorado, U.S.A.

Ingraffea, A.R. and Manu, C., 1980. Stress-Intensity Factor Computation in Three Dimensions with Quarter Point Element. Int. J. Numer. Meth. in Eng., 15: 1427-1445.

Irwin, G. R. 1957. Relation of stresses near a crack to the crack extension force. in Proceedings of the 9th Cong. App. Mech., Brussels. Journal of Rock Mechanics and Geotechnical Engineering, 6(4): 287–300.

Iran Minerals Production and Supply Company (IMPASCO), Dec 2005, Parvadeh 4 Tabas coal mine exploration report.

Jeffrey, RG. 2012, Hydraulic Fracturing for Coal Seam Gas (CSG) Stimulation in NSW. CSIRO, Australia. Report EP122949, 15 pages.

Jeffrey, R.G., Enever, J.R., Henning, A., Meaney, K.T.A., and Doyle, R. 1997, The Impact of Structure and Stress on Permeability and Gas Drainage as Measured at a Vertical Well Drainage Site at Dartbrook Mine, proceedings of the Symposium on Safety in Mines: The Role of Geology, Newcastle, NSW, p 91-104.

Jeffrey, R.G., Vlahovic, W. Doyle, R.P., and Wood, J.H. 1998, Propped Fracture Geometry of Three Hydraulic Fractures in Sydney Basin Coal Seams, paper SPE 50061, proceedings of the 1998 SPE Asia Pacific Oil & Gas Conference and Exhibition, Perth, p 191-201.

Jeffrey, R.G. 1999, Stimulation of Gas Make from Horizontal In-Seam Drain Holes

by Hydraulic Fracturing, CSIRO Petroleum Confidential Report No 99-061, 37 pages.

Jing L, Hudson J.A, 2002. Numerical Methods in Rock Mechanics. International Journal of Rock Mechanics & Mining Science 39 409-427.

Jing L, 2003. A review to techniques, advances and outstanding issues in numerical modeling for rock mechanics and rock engineering. International Journal of Rock Mechanics & Mining Science 40 283-353.

John Williams Scientific Services Pty Ltd. 2012, An analysis of coal seam gas production and natural resource management in Australia, A report prepared forThe Australian Council of Environmental Deans and Directors.

Kendall, P. F., & Briggs, H. 1993. The formation of rock joints and the cleats of coal. Royal Society of Edinburgh, 53, 164e187.

Kriesi, 2018, Ozen Engineeering and Ansys- Enfold WordPress Theme.

Kirsch, E.G. 1898. Die Theorie der Elastizität und die Bedürfnisse der Festigkeitslehre. Zeitschrift des Vereines deutscher Ingenieure, 42:797-807.

Kravits, S.J. 1993, Evaluation of Hydraulically-fractured In-Mine Horizontal Wells as a Completion Approach for Coalbed Methane Recovery Independent of and in Conjunction with Coal Mine Operations, REI Underground Exploration Draft Report, October 1993.

Lee, C.C. 1990. Fuzzy logic in control systems: fuzzy logic controller, part II, IEEE Transactios on Systems, Man, and Cybernerics, 20(2), 419–435.

Lewis, R., Sukirman, Y. Finite element modelling for simulating the surface subsidence above a compacting hydrocarbon reservoir. Int. J. Numer. Anal. Methods Geomech. 18, 619 – 639, 1993a.

Lewis, R., Sukirman, Y., 1993b, Finite element modelling of three- phase flow in deforming saturated oil reservoirs. Int. J. Numer. Anal. Methods Geomech. 17, 577–598.

Lewis, R., Ghafouri, H., 1997, A novel finite element double porosity model for multiphase flow through deformable fractured porous media. Int. J. Numer. Anal. Methods Geomech. 21, 789 – 816.

MacDonald, G. J. 1990. The future of methane as an energy resource (Vol. 15). Annual Review of Energy. Virginia, USA.

Mahabadi, O.K., Lisjak, A., Munjiza. A., and Grasselli. G., 2012, New Combined Finite-Discrete Element Numerical Code for Geomechanical Applications, International Journal of Geomechanics, 12, 676-88.

Malcolm Lamb Shale Petroleum Ltd, Americas Denver, CO - October 2013.

McNeil, D. and Caldwell, W.G.E. 1981: Cretaceous Rocks and their Foraminifera in the Manitoba Escarpment; Geol. Assoc. Can., Spec. Pap. 21, 439p.

Mendel. J., 1995, Fuzzy logic systems for engineering: a tutorial. Proceedings of the IEEE, 83(3):345–377.

Mohamadighanatghestani, M., 2015, Experimental and Constitutive Investigation of the Thermo-Hydro-Mechanical Behavior of Shales: A Case Study of the Colorado Clay Shale PhD Thesis, University of Calgary.

Murti, V. and Valliappan, S., 1986. A Universal Optimum Quarter Point Element. Engineering Fracture Mechanics, 25(2): 237-258.

Nuismer, R., 1975, An energy release rate criterion for mixed mode fracture, International Journal of Fracture 11, pages 245-250.

Oden, J.T., 1991, Finite elements: An Introduction in: Handbook of Numerical Analysis II (North-Holland,Amsterdam) 3-15.

Osorio, J., Chen, H., Teufel, L., Numerical simulation of the impact of flow-induced geomechanical response on the productivity of stress-sensitive reservoirs. Proceedings of the 15th Reservoir Simulation Symposium, No. 51929. SPE, Richardson, TX, pp. 373–387, 1999.

Owen, D.R.J. and Fawkes, A.J., 1983. Engineering Fracture Mechanics; Numerical Methods and Applications. Pineridge Press Limited, Swansea, U.K.

Pande G.N., Beer G., 1990. Williams J.R, Numerical Methods in Rock Mechanics, John Wiley & Sons Ltd, England.

Peng, S., Chiang, H., 1984, Longwall Mining, John Wiley & sons, New York. Queensland Gas Company Pty Ltd (QGC). 2011. Fact Sheet No. 4, Hydraulic fracturing. Available at: http://www.qgc.com.au/media/100557/04--hydraulic_fracturing.pdf. [Accessed 2 November 2012].

Perkins, T.K. and Kern, L.R. Widths of Hydraulic Fractures, Journal of Petroleum Technology, 9, 937–949, 1961.

Rajeeb Gatum and Ron C.K. Wong, 2006. Transversely isotropic stiffness parameters and their measurments in Colorado shale, Can. Geotech. J. 43: 1290-1350.

Reddy, J. N. 1984, An introduction to the finite element method, McGraw-Hill

Robert, M., 2002, "Coal bed methane (CBM) and mine methane (CMM) in North America where and why", Norwest Mine Services, www.ipec.utulsa.edu.

Rummel, F. and R.B. Winter, 1982, Application of laboratory fracture mechanics data to hydraulic fracturing field tests. 1st Japan-USA Symp on Fracture Mechanics Approach, Hydraulic Fracture and Geothermal Energy, Sendai, Japan. pp: 495-501 in Proc.

Sayma, A. 2009, Coputational Fluid Dynamics.

Schreurs, P.J.G., 2012, Fracture Mechanics, Eindhoven University of Technology.

Schröder-Adams, C.J., Cumbaa, S.L., Bloch, J., Leckie, D.A., Craig, J., Seif El Dein, S.A., Simons, D., and Kenig, F. 2001: Late Cretaceous (Cenomanian to Campanian) paleoenvironmental history of the eastern Canadian margin of the Western Interior Seaway: Bonebeds and anoxic events; Palaeogeo. Palaeoclim. Palaeoecol., v170, p261-289.

Schmitt, D.R. and Zoback, M.D. 1989. Laboratory tests of the effects of pore pressure on tensile failure, Rock at Great Depth, Maury & Fourmaintraux, eds., Balkema, Rotterdam.

Singiresu S.R, 2004. The Finite Element Method in Engineering, Fourth Edition. Elsevier Science & Technology Books, December.

Smith, R.N.L. and Mason, J.C., 1982. A Boundary Element Method for Curved Crack Problems in Two Dimensions. Boundary Element Methods in Engineering. Springer-Verlag, Berlin.

Santos. 2011. Submission No. 337 to the General Purpose Standing Committee No. 5 inquiry into coal seam gas, New South Wales Parliament, Sydney, Australia.

Sereshki, F., Aziz, N., & Porter, I. 2003. Impact of coal permeability on gas sorption and coal volume change. In Proceedings of the 7th annual environ- mental engineering research event conference, Marysville, Victoria, Australia (pp. 333e342).

Soeder, D. J. 1991. The effects of overburden stress on coal bed methane production. Tec book, Geology in Coal Resources Utilization.

Settari, A., Mourits, F., 1994, Coupling of geomechanics and reservoir simulation models. In: Siriwardane, Zaman (Eds.), Computer Methods and Advances in Geomechanics. Balkema, Rotterdam, pp. 2151–2158.

Settari, A., Walters, D., 1999, Advances in coupled geomechanical and reservoir modeling with applications to reservoir compaction. Proceedings of the 15th Reservoir Simulation Symposium, No. 51927. SPE, Richardson, TX, pp. 345–357.

Shih, C. F. B. Moran, and T. Nakamura, 1986, Energy Release Rate Along a Three-Dimensional Crack Front in a Thermally Stressed Body, International

Journal of Fracture, 30, pp 79-102.

Sih, G.C, 1974, Strain energy density factor applied to mixed mode problems, International Journal of Fracture 10, 305-321.

Sun, C.T. and Jin, J.H. 2012, Fracture Mechanics, ISBN: 978-0-12-385001-0.

Taleghani, A.D. 2009. Analysis of hydraulic fracture propagation in fractured reservoirs: an improved model for the interaction between induced and natural fractures. PhD Thesis. University of Texas at Austin.

Unrug K, Szwilski B. 1982, Methods of roof cavability prediction. State of the Art of Ground Control in Longwall Mining and Mining Subsidence, AIME,13–29.

Valko, P., and Economides, M. J. 1995. Hydraulic Fracture Mechanics. Chichester, England: John Wiley & Sons.

Versteeg, H.K. and Malalasekara, W. 1995, An Introduction to Computational Fluid Dynamics: The Finite Volume Method, Prentice-Hall.

Wang, J., Wu, R., & Zhang, P. 2015. Characteristics and applications of gas desorption with excavation disturbances in coal mining. International Journal of Coal Science & Technology, 2, 30e37.

Wagoner, J.E., Mitchum, R.M., Posamentier, H.W., and Vail, P.R. 1987: Part 2: Key definitions of seismic stratigraphy; in Bally, A.W. (ed.), Atlas of Seismic Stratigraphy, Amer. Assoc. Petrol. Geol., Tulsa, OK, p11- 14.

Wanniarachchi, W.A.M,.Gamage, R.P,.Perera, M.S.A,. Rathnaweera, T.D, Gao, M and Padmanabhan, E,. 2017, Investigation of Depth and Injection Pressure Effects on Breakdown Pressure and Fracture Permeability of Shale Reservoirs: An Experimental Study, Applied Science, MDPI.

Warpinski, N.R., Mayerhofer, M.J., Bridges, A.C., and Du, J. 2012. Hydraulic Fracture Geomechanics and Microseismic Source Mechanisms. In SPE Annual Technical Conference and Exhibition. Society of Petroleum Engineers.

Warpinski, N.R., Schmidt, R.A. and Northrop, D.A. 1982. In-Situ Stresses: The Predominant Influence on Hydraulic Fracture Containment. Journal of Petroleum Technology, 34(03): 653–664.

Wei Guo, Zhiming Hu, Xiaowei Zhang, Rongze Yu and Li Wang, 2017. Shale gas adsorption and desorption characteristics and its effects on shale permeability. Energy Exploration and Exploitation, Vol 35(4) 436-481.

Wickenden, R.T.D. 1945: Mesozoic Stratigraphy of the Eastern Plains, Manitoba and Saskatchewan; Geol. Surv. Can., Mem. 239, 87p.

Wilkes, J.O.1999, Fluid Mechanics for Chemical Engineers, Prentice Hall.

Xiaochun Jin, Subhash N. Shah, Jean-Claude Roegiers. 2013. Breakdown Pressure Determination - A Fracture Mechanics Approach**,** The University of Oklahoma; and Bing Hou, China University of Petroleum (Beijing).

Yoffe, E.H., 1951. The Moving Griffith Crack. Philosophical Magazine, 42: 739-750.

Zadeh, L. A. 1973. Outline of a new approach to the analysis complex systems and decision processes, IEEE Trans Syst. Man Cibern SMC(3): 28–44.

Zadeh, L.A. 1992. Knowledge representation in fuzzy logic, An introduction to Fuzzy Logic Applications in Intelligent Systems, R.R. Yager and L.A. Zadeh, eds, Kluwer Academic Publishers, Boston, pp. 1–26.

Zhao, H., Tannat, D., Ma, F., Guo, J., and Feng, X. 2019. Investigation of Hydraulic Fracturing Behavior in Heterogeneous Laminated Rock Using a Micromechanics-Based Numerical Approach, Energies, 12, 3500, doi: 10.3390/en12183500.

Zhao, X., and J.-C. Roegiers 1993, Determination of in situ fracture toughness, International journal of rock mechanics and mining sciences & geomechanics abstracts, 30(7), 837-840.

Zimmermann, H.J. 1991 Fuzzy set theory and its applications (Second ed.), Boston: Kluwer Academic Publishers.

Z.Yun, Y.Hui, Coupled fluid structure flutter analysis of a transonic fan, Chinese Journal of Aeronautics, vol.24, 258-264, 2011.